

SYNTHESIS OF LAYERED DOUBLE HYDROXIDES TO SEQUESTER HALIDES
FROM FLUE GAS DESULFURIZATION WASTEWATER CONCENTRATE

by

Abhisek V. Manikonda

A dissertation submitted to the faculty of
The University of North Carolina at Charlotte
in partial fulfillment of the requirements
for the degree of Doctor of Philosophy in
Infrastructure and Environmental Systems

Charlotte

2020

Approved by:

Dr. Vincent O. Ogunro

Dr. John L. Daniels

Dr. James D. Bowen

Dr. Haitao Zhang

Dr. John M. Stogner

©2020
Abhisek V. Manikonda
ALL RIGHTS RESERVED

ABSTRACT

ABHISEK V. MANIKONDA. Synthesis of Layered Double Hydroxides to Sequester Halides from Flue Gas Desulfurization Wastewater Concentrate. (Under the direction of DR. VINCENT O. OGUNRO)

An emerging strategy for the management of flue gas desulfurization wastewater involves volume reduction of the wastewater by concentrating to brine and then mixing the brine with fly ash and other chemical additives to form a paste suitable for landfill disposal. This process, termed as paste encapsulation technology, has not achieved the same level of success in immobilizing halides as achieved in sequestering heavy metals, because of the high solubility and elevated concentrations of halides in the brines. Hypersaline brines like flue gas desulfurization wastewater concentrate are also difficult to treat because of high halide concentration and currently, there are a lack of cost-effective and energy-efficient technologies for removal of halides. This research explored the feasibility of removing halides from high-salinity brines through the precipitation of layered double hydroxides. Parameters that affect the reduction of concentration of halides including, the initial molar concentration of halides, the calcium to aluminum ratio, and reaction temperature were evaluated. The stability of the layered double hydroxide products at various prevailing solutions and environmental conditions were investigated and an optimal calcium to aluminum ratio for the effective removal of the halides were established. Experimental results confirmed that the initial halide concentration, rather than the calcium to aluminum ratio, highly influenced the mass of halides sequestered in the structure of the layered double hydroxide samples. It was also observed that the layered double hydroxide samples undergo congruent dissolution when mixed in water or solutions at basic pH, while

dissolution rate of all the samples in acidic solution was high with little residues remaining. Based on the analyses from characterization using various instrumentation and also the statistical analyses, it could be hypothesized that the synthesis of layered double hydroxides using a calcium to aluminum ratio of 3:1 will be optimal for effective removal of halides from hypersaline solutions. The optimal condition of Ca:Al ratio of 3:1 was employed to remove halides from simulated FGD wastewater brines. X-ray diffraction and thermogravimetric analysis showed that the structure of the precipitate after treatment of the simulated brine is similar to a layered double hydroxide, especially Friedel's salt, with chloride ions mainly in the interlayers. The optimal conditions that were determined in this research will provide a framework to treat field samples such as an actual FGD wastewater concentrate. These optimal conditions can also be employed to treat other sources of wastewater with high salinity and TDS, including RO reject water from desalination, produced water from oil and gas fracking, and rejects from industrial cooling towers. In addition, the results suggest that this process is a simple and effective method to treat high-salinity brines. This research will lead to a better understanding of the formation of layered double hydroxides while contributing to the evaluation of variables that influence the long-term sequestration of halides in the cementitious systems like fly ash-brine paste.

DEDICATION

To my Mom, for fiercely supporting me and irrevocably believing in me, even when I kept giving you multiple reasons not to. Thank you for your unwavering faith in me. This dissertation is dedicated to you.

ACKNOWLEDGMENTS

I would like to express my gratitude to my advisor, Dr. Vincent O. Ogunro, for taking me on as one of his graduate students and for his guidance, encouragement, and insightful contributions throughout my time here at UNC Charlotte. I would also like to thank Dr. John L. Daniels, Dr. James D. Bowen, Dr. Haitao Zhang, and Dr. John M. Stogner for serving on my dissertation committee and also for their valuable contributions and review of my dissertation. A special thanks to Dr. William Langley, who although was not on my committee, helped me with my research and also for employing me as a teaching assistant. I would like to acknowledge EPRI and Duke Energy for their partial funding of this project and also the CEE Dept and the Graduate School at UNC Charlotte for their financial assistance. I am also thankful to the INES program, Dr. Jay Wu, and UNC Charlotte for providing me with the resources to conduct this research.

To all my friends, getting to know the other graduate students was certainly the highlight of this program. There was rarely a dull moment, and I am so glad to have been part of such a vibrant community of students and researchers. Special recognition to Rui He, Akpovona Ojaruega, and Dr. Livingstone Dumenu, who contributed both intellectually and emotionally to my scientific journey and I could not have asked for better lab mates and friends. I would also like to thank the other members of ‘Wolves of EPIC’ – Vivek Francis, Babatunde Adeyeye, Manohar Seetharamu; for their friendship which made this journey much easier. I am also grateful to other graduate students in the CEE department, like Fateme, Babak, and others, for filling my time in grad school with cherished memories! I especially need to thank Dr. Abhispa Sahu, without whom, I

would not have been able to complete this dissertation. You supported me with your friendship, words of encouragement, and you believed in me when I didn't believe in myself at times. This accomplishment would not have been possible without you. Thank you!

To my parents. Without you I would not exist, and without your care, guidance, and support I would not be where I am today, so thank you from all my heart! To my sister, Dr. Shravanthi Manikonda, and brother-in-law, Dr. Purushothaman Srinivasan, thank you for all your support over the years as well! I would also like to dedicate this dissertation to my nephew, Sujay, and niece, Roshini.

TABLE OF CONTENTS

LIST OF TABLES	xiii
LIST OF FIGURES	xv
LIST OF ABBREVIATIONS	xix
CHAPTER 1: INTRODUCTION	1
1.1. Paste Encapsulation Technology	3
1.2. Layered Double Hydroxides	7
1.2.1. AFm and AFt Phases	9
1.2.1.1. Friedel's Salt	11
1.2.1.2. Kuzel's Salt	18
1.2.1.3. Ettringite	21
1.2.2. Stability of the CaO-Al ₂ O ₃ -CaCl ₂ -H ₂ O system	26
1.3. Dissertation Aims and Objectives	27
References	30
CHAPTER 2: EFFECT OF REACTION TEMPERATURE ON THE STRUCTURE OF FRIEDEL'S SALT	38
Abstract	38
2.1. Introduction and Background	39
2.2. Motivation and Strategy	41
2.3. Experimental Investigation	44

2.3.1. Reagents	44
2.3.2. Preparation of Friedel's Salt	45
2.3.3. Characterization and Purification of Friedel's Salt	46
2.4. Results and Discussion	47
2.4.1. Microstructure of Friedel's Salt	47
2.5. Conclusions and Future Work	51
References	53
CHAPTER 3: ASSESSMENT OF HIGH CONCENTRATION CHLORIDE REMOVAL PERFORMANCE BY PRECIPITATION OF FRIEDEL'S SALT	56
Abstract	56
3.1. Introduction	57
3.2. Materials and Methods	59
3.2.1. Synthesis and Characterization of Friedel's Salt	60
3.2.2. Variation of Protocol Variables	62
3.2.3. Solubility and Stability	63
3.3. Results and Discussion	64
3.3.1. Selection of Optimum Protocol	64
3.3.2. Variation of Ca:Al ratio and Initial Cl ⁻ Concentration	69
3.3.3. Variation of Atmospheric Conditions	76
3.3.4. Variation of Environmental Conditions	78

3.3.5. Solubility of Friedel's Salt	80
3.4. Conclusions	82
References	83
CHAPTER 4: BROMIDE ION REMOVAL FROM HYPERSALINE BRINES BY CA- AL LAYERED DOUBLE HYDROXIDES	86
Abstract	86
4.1. Introduction	87
4.2. Materials and Methods	90
4.2.1. Synthesis of Bromide Substituted LDHs	91
4.2.2. Characterization of Bromide Substituted LDHs	92
4.2.3. Variation of Protocol Parameters	92
4.2.4. Stability and Solubility of Bromide Substituted LDHs	93
4.3. Results and Discussion	94
4.3.1. Characterization of Synthesized Bromide Substituted LDHs	94
4.3.2. Effect of Variation of Protocol Parameters on Bromide Removal	102
4.3.3. Stability of Br-LDHs in Varying Environmental Conditions	105
4.3.4. Solubility of Bromide Substituted LDHs	108
4.4. Conclusions	109
References	110
Supplementary Information	115

CHAPTER 5: LAYERED DOUBLE HYDROXIDE PRECIPITATION FOR MANAGING SULFATE AND CHLORIDE RICH BRINES: FEASIBILITY AND PARAMETER ASSESSMENT	116
Abstract	116
5.1. Introduction	117
5.2. Materials and Methods	120
5.2.1. Synthesis of Ca-Al LDH Synthesis	121
5.2.2. Characterization of Ca-Al LDH Samples	122
5.2.3. Variation of Protocol Parameters	122
5.2.4. Stability and Solubility of Ca-Al LDH Samples	124
5.3. Results and Discussion	124
5.3.1. Effect of Variation of Protocol Parameters on Structure of Ca-Al LDHs	124
5.3.2. Stability and Solubility of Ca-Al LDH Samples	133
5.4. Conclusions	135
References	137
CHAPTER 6: OVERALL CONCLUSIONS AND RESEARCH CONTRIBUTIONS	142
6.1. Overall Conclusions	142
6.2. Research Contributions	145
APPENDIX A: PRACTICAL APPLICATION OF LAYERED DOUBLE HYDROXIDES PRECIPITATION METHOD FOR REMOVAL OF HIGH CONCENTRATION HALIDES FROM SIMULATED BRINE	148

A.1. Introduction	148
A.2. Experimental Setup	149
A.3. Results and Discussion	151
A.4. Conclusions	156
References	157

LIST OF TABLES

Table 1.1. Average Pollutant Concentrations in FGD Wastewater (USEPA 2015)	3
Table 1.2. Solubility product constants of AFm phases and common salts	11
Table 1.3. Description of quantities used in making mix samples (Pretorius et al. 2017)	12
Table 2.1. Comparison of the % mass lost over the three different temperatures ranges	50
Table 3.1. Levels of the factors tested in the two-factorial ANOVA design	63
Table 3.2. Comparison of % mass lost recorded using TGA for samples synthesized using protocols P1, P2, and P3	65
Table 3.3. Comparison of % mass lost recorded using TGA for samples synthesized using protocol P2 while Ca:Al ratio and $[Cl^-]$ was varied	72
Table 3.4. Analysis of variance (ANOVA) results	75
Table 3.5. Solubility of Friedel's salt samples	81
Table 4.1. Levels of parameters tested in the two-factorial ANOVA design along with the identifiers for each sample	93
Table 4.2. Comparison of % mass lost recorded using TGA for Br-LDH samples synthesized while Ca:Al ratio and $[Br^-]$ were varied	96
Table 4.3. Influence of bromide concentration and Ca:Al ratio parameters on the mass of bromide sequestered	103
Table 4.4. Molar compositions of synthesized Br-LDH samples	105
Table 4.5. Solubility product constants of synthesized Br-LDH samples at various pH conditions	109
Table S4.1. Analysis of variance (ANOVA) results when Br/Ca is the dependent variable	115

Table S4.2. Regression statistic results when Br/Ca is the dependent variable	115
Table 5.1. Levels of parameters tested in the Latin square design, where C_{Sulfate} is the molar concentration of SO_4^{2-}	123
Table 5.2. Comparison of % mass lost recorded using TGA for Ca-Al LDH samples synthesized with Ca:Al ratio, $[\text{Cl}^-]$, and $[\text{SO}_4^{2-}]$ varied	126
Table 5.3. Solubility product constants of for Ca-Al LDH samples at various pH conditions	135
Table A.1. Composition of Simulated FGD Brines	150
Table A.2. Comparison of % mass lost recorded using TGA for LDH samples synthesized using simulated brine	152

LIST OF FIGURES

Figure 1.1. Proposed “Closed-Loop” FGD Wastewater Management Process (Dr. Vincent Ogunro, personal communication, June 2018)	6
Figure 1.2. Schematic diagram of a LDH structure (Goh et al. 2008)	9
Figure 1.3. Schematic representation of Friedel's salt structure (Li et al. 2017)	12
Figure 1.4. Combined TGA and DSC curves for Friedel's salt (Grishchenko et al. 2013)	15
Figure 1.5. X-ray Diffractogram of Friedel's salt (Grishchenko et al. 2013)	15
Figure 1.6. IR spectrum of Friedel's salt (Grishchenko et al. 2013)	16
Figure 1.7. Raman spectra of Friedel's salt (Yue et al. 2018)	17
Figure 1.8. Schematic representation of Kuzel's salt structure (Mesbah et al. 2011)	18
Figure 1.9. TGA curve of Kuzel's salt (Mesbah et al. 2011)	19
Figure 1.10. Raman spectra of Kuzel's salt (Mesbah et al. 2011)	20
Figure 1.11. Schematic representation of structure of Ettringite (Zhang and Reardon 2003)	22
Figure 1.12. TG and DTG curves for Ettringite (Antao et al. 2002)	23
Figure 1.13. XRD of ettringite (McMurdie et al. 1986)	24
Figure 1.14. FTIR spectra for ettringite (Perkins and Palmer 1999)	24
Figure 1.15. Raman spectra of ettringite (Renaudin et al. 2007)	25
Figure 1.16. Phase development depending on varying chloride to aluminate ratios (2Cl/Al ₂ O ₃) with fixed initial sulfate ratio of 1 (Balonis et al. 2010)	27
Figure 2.1. Illustration of experimental set-up of synthesis of Friedel's salt	46

Figure 2.2. Comparison of DSC curves recorded for samples synthesized using protocols P1 (—), P2 (-.-), and P3 (···) at a reaction temperature of 50 °C	49
Figure 2.3. Comparison of weight loss data recorded by TGA for samples synthesized using protocols P1 (—), P2 (-.-), and P3 (···) at a reaction temperature of 50 °C	49
Figure 2.4. X-ray pattern of a) P1 b) P2 C) P3 at 25 °C and 50 °C	51
Figure 3.1. Comparison of (A) TGA and (B) DSC analysis for FS samples synthesized using protocols P1 (-), P2 (-.-), and P3 (···)	66
Figure 3.2. FTIR spectra of Friedel's salt samples synthesized using protocols (A) P1, (B) P2, and (C) P3	67
Figure 3.3. X-ray pattern of P2CA31CL1	69
Figure 3.4. Comparison of DSC curves recorded for samples synthesized using protocol P2 with Ca:Al ratio and [Cl ⁻] varied	71
Figure 3.5. Comparison of weight loss data recorded by TGA for samples synthesized using protocol P2 with Ca:Al ratio and [Cl ⁻] varied	71
Figure 3.6. FTIR spectra of Friedel's salt samples synthesized using protocol P2 with Ca:Al ratio and [Cl ⁻] varied	73
Figure 3.7. Influence of chloride concentration (1 M – 2 M) and Ca:Al ratio (2:1 – 4:1) variables on the mass of chloride sequestered	75
Figure 3.8. FTIR spectra for FS samples synthesized at (A) ambient atmosphere (B) inert atmosphere, and (C) carbon dioxide rich atmosphere	78
Figure 3.9. Comparison of (A) TGA and (B) DSC analysis for P2CA31CL1 samples dispersed in pH natural (-.-) and pH 13 (...) with initial P2CA31CL1 sample (-)	79

Figure 4.1. Comparison of DSC curves recorded for Br-LDH samples synthesized with Ca:Al ratio and [Br ⁻] varied	97
Figure 4.2. Comparison of weight loss data recorded by TGA for Br-LDH samples synthesized with Ca:Al ratio and [Br ⁻] varied	97
Figure 4.3. FTIR spectra for Br-LDH samples synthesized with Ca:Al ratio and [Br ⁻] varied	99
Figure 4.4. Powder XRD patterns for Br-LDH samples synthesized with Ca:Al ratio and [Br ⁻] varied, where F: Br-LDH, C: Ca(OH) ₂ , and B: NaBr	101
Figure 4.5. Comparison of (A) TGA and (B) DSC analysis for FSCA21BR25 samples dispersed in pH natural (---) and pH 13 (···) compared to initial FSCA21BR25 sample (-)	106
Figure 4.6. Comparison of FTIR spectrum for FSCA21BR25 samples dispersed in (B) pH natural and (C) pH 13 compared to (A) initial FSCA21BR25 sample	107
Figure 5.1. Comparison of DSC curves recorded for Ca-Al LDH samples synthesized with Ca:Al ratio, [Cl ⁻], and [SO ₄ ²⁻] varied	127
Figure 5.2. Comparison of weight loss data recorded by TGA for Ca-Al LDH samples synthesized with Ca:Al ratio, [Cl ⁻], and [SO ₄ ²⁻] varied	127
Figure 5.3. Raman spectra in the range 400–1200 cm ⁻¹ for Ca-Al LDH samples synthesized with Ca:Al ratio, [Cl ⁻], and [SO ₄ ²⁻] varied	129
Figure 5.4. Powder XRD patterns for Ca-Al LDH samples synthesized with Ca:Al ratio, [Cl ⁻], and [SO ₄ ²⁻] varied where K: Kuzel's salt and F: Friedel's salt	131
Figure 5.5. Comparison of TGA for KSCA21CL01SO75 samples dispersed in (A) pH natural and pH 13 (B) pH 2 compared to initial KSCA21CL01SO75 sample	134

Figure A.1. Summary of the Optimal Conditions for LDH Precipitation	149
Figure A.2. Illustration of experimental set-up for treatment of simulated brine	151
Figure A.3. Comparison of (A) TGA and (B) DSC analysis for LDH samples synthesized using simulated brine	153
Figure A.4. Powder XRD patterns for LDH samples synthesized using simulated brine, where F denotes Friedel's salt	154
Figure A.5. Percentage removal efficiency of Cl^- , Br^- , and SO_4^{2-} ions from simulated brines	155

LIST OF ABBREVIATIONS

AFm	Alumina or ferric oxide, monosulfate
AFt	Alumina or ferric oxide, trisulfate
ANOVA	Analysis of variance
APCDs	Air pollution control devices
Br-LDHs	Bromide substituted Friedel's salt
C ₃ A	Tricalcium aluminate
Ca-Al/Ca:Al	Calcium-aluminum
CCR	Coal combustion residuals
CFA	Coal fly ash
CSH	Calcium silicate hydrate
DBP	Disinfection byproduct
DI	Deionized
DSC	Differential scanning calorimetry
DSEMF	Dynamic shear enhanced membrane filtration
ELGs	Effluent Limitation Guidelines
FGD	Flue gas desulfurization
FGDWW	Flue gas desulfurization wastewater
FO	Forward osmosis
FS	Friedel's salt
FTIR	Fourier-transform infrared spectroscopy
IC	Ion chromatography
ICP-OES	Inductively coupled plasma optical emission spectrometry
KS	Kuzel's salt
K _{sp}	Solubility product
LDHs	Layered double hydroxides
MD	Membrane distillation
Mg-Al	Magnesium-aluminum
OPC	Ordinary Portland cement

ppm	Parts per million
PTFE	Polytetrafluoroethylene
RO	Reverse osmosis
SEM	Scanning electron microscope
SO _x	Sulfur Oxides
S/S	Solidification/Stabilization
%T	Transmittance
TDS	Total dissolved solids
TE	Thermal evaporators
TGA	Thermogravimetric analysis
USEPA	United States Environmental Protection Agency
XRD	X-ray diffraction
ZLD	Zero-liquid discharge

CHAPTER 1: INTRODUCTION

Disposal of wastewater from wet flue gas desulfurization (FGD) systems is a major concern for the coal-fired power plant industry. According to a U.S. Environmental Protection Agency (USEPA) report, most of the high concentrations of metals (Ca, Na, As, Cr) and halides (Cl, Br) encountered in waste from coal-fired power plants occur in FGD systems and hydraulic coal fly ash (CFA) transportation systems. The major source of halides and heavy metals is from coal, while additives like calcium chloride (CaCl_2) and calcium bromide (CaBr_2), which are added as dust suppressants and emission control measures to increase mercury capture, are minor sources. Flue gas in the wet FGD system is sprayed into or bubbled through Ca or Ca-Mg slurries in order to remove sulfur oxides (SO_x). However, along with the SO_x removal, metals and halides partition from the gas phase (flue gas) to the aqueous phase and accumulate in the FGD slurry (Gingerich et al. 2018). Table 1.1 presents the average pollutant concentrations in the FGD wastewater. FGD wastewater generally contains high concentrations of total dissolved solids (TDS). Chloride (Cl) and sulfate (SO_4^{2-}) are the dominant anions in FGD wastewater. Calcium (Ca), Magnesium (Mg), and Sodium (Na) are the dominant cations in the wastewater. FGD wastewater also has significant concentrations of heavy metals like Arsenic (As), Selenium (Se), and Mercury (Hg) (USEPA 2009). Factors like the mineralogy of coal and the nature of air pollution control devices (APCDs) can influence the composition of FGD wastewater (Gingerich et al. 2018). The distribution of heavy metals and halides in coal and FGD wastewater can depend on the source of coal, since the peat beds that formed the coal can vary depending on the atmosphere, particulate matter, groundwater, surface water and other factors. Location of air pollution control devices (APCDs) upstream of the FGD

system can also influence the FGD wastewater composition, since the APCDs can remove heavy metals and halides before they enter the FGD system (Gingerich et al. 2018).

Other than the FGD wastewater, coal-fired power plant industries can produce other types of brines with high salt concentrations. Brines generated during desalination and raw water recovery from cooling towers are a concern for the industry (Mahlaba et al. 2011). Some plants also discharge water that was used to remove fly ash and bottom ash from the particulate removal systems and boilers, respectively. Similar to FGD wastewater, untreated ash transport waters contain high concentrations of total solids and metals (USEPA 2015). Other sources of wastewater with high total dissolved solids (TDS) concentration include discharges from coal mines (Cravotta and Brady 2015), effluent from plastics and textile manufacturing (Mctigue et al. 2014), wastewater during oil and gas extraction (Landis et al. 2016), and coal combustion residue wastewater (Ruhl et al. 2012).

Discharge of high TDS wastewaters like FGD wastewater, brines from desalination or cooling towers and ash transport water can have negative environmental impacts including, promotion of pitting corrosion, increased metal leaching from sediments, and formation of disinfection byproducts (Boelter et al. 1992). The heavy metals can bioaccumulate in fishes, impairing fish reproduction. It can also lead to negative impacts in human health when humans consume fish contaminated with high TDS wastewaters. Therefore, USEPA released the proposed final revision to the Steam Electric Power Effluent Limitation Guidelines (ELGs) which regulate FGD wastewater and other processed water (USEPA 2015), including discharge limits for many pollutants. One potential pathway being explored to manage FGD wastewater is the zero-liquid discharge (ZLD) strategy. The principle of the ZLD strategy involves reducing the volume of FGD

wastewater to concentrated brine using technologies such as thermal evaporators (TE) or advanced membrane processes such as dynamic shear enhanced membrane filtration (DSEMF), forward osmosis (FO), and membrane distillation (MD).

Table 1.1. Average Pollutant Concentrations in FGD Wastewater (USEPA 2015)

Element/Component	Unit	Average Total Concentration
Chloride	mg/L	7,180
Bromide	mg/L	75
Sulfate	mg/L	13,300
Total Dissolved Solids	mg/L	33,300
Total Suspended Solids	mg/L	14,500
Aluminum	µg/L	331,000
Arsenic	µg/L	507
Boron	µg/L	242,000
Cadmium	µg/L	127
Calcium	µg/L	3,290,000
Chromium	µg/L	1,270
Magnesium	µg/L	3,250,000
Mercury	µg/L	289
Selenium	µg/L	3,130
Sodium	µg/L	2,520,000

1.1. Paste Encapsulation Technology

However, volume reduction approaches using evaporators or advanced membrane processes still result in rejects such as residual brine or salt that must be managed. Logically, this concentrated brine will contain higher concentrations of the pollutants. The concentrations shown in Table 1.1. could be increased by a factor of 10 – 100 and the final TDS concentration could increase to 100,000 – 300,000 mg/L. Through the process, termed as “paste encapsulation technology”, brine is mixed in cementitious matrices of fly ash and hydraulic chemical binder to form a solidified and stabilized paste. While this approach

provides a material that is suitable for landfill disposal, its primary goal is to provide for long term sequestration of constituents from the FGD wastewater and coal fly ash.

Paste encapsulation technology is similar to the solidification/stabilization (S/S) typically used to treat and remediate hazardous wastes into an environmentally acceptable form. The USEPA has identified S/S as the best demonstrated available technology for 57 hazardous sites (Shi and Spence 2004). Traditional applications of S/S use ordinary Portland cement (OPC) as the primary binder and has been shown to be a viable treatment process for sequestering heavy metals in the solid form (Batchelor 2006). However, the availability of coal fly ash (CFA) at facilities producing FGD wastewater provides a unique opportunity. According to a report by the American Coal Ash Association in 2017, nearly 40 million tons of fly ash are produced annually in the United States, with similar amounts produced in western Europe and throughout the world. Most types of fly ashes are considered to be pozzolanic in nature, and its geotechnical properties and lime-binding capacity makes it suitable for use in the solidification and stabilization of FGD wastewater (Ahmaruzzaman 2010). Traditional S/S approaches involve design mixes to be compacted close to its maximum dry density at the optimum moisture content. Those mixes are then transported via truck or conveyor to the landfill. However, this approach has several drawbacks. The liquid-to-solid ratio is limited by what can be safely transported by truck (typically 15-18%). This range of moisture content limits the magnitude of hydration and falls short of the adequate moisture required to form stable mineral phases in the cementitious mixture. Also, this approach introduces significant environmental concerns, safety issues and increased risk associated with moving of high-volume material by trucks,

considering that in most cases, it does not solve the zero water balance requirements at the coal power plant.

However, the paste encapsulation technology, which transports material via pipeline, allows material to be pumped directly into a landfill. This technology allows for increase of the liquid-to-solid ratio, which means higher volumes of wastewater can be disposed with the fly ash as well as providing enough moisture to allow adequate hydration reactions. Pastes mixture can contain 30% or more wastewater in the mix design while maintaining a non-segregating grout-like consistency that is distinct from a wet slurry. Additionally, since it can be designed to targeted rheological properties, the material can be pumped via pipeline over significant distances. Upon deposition and over time the paste sets and cures into a hardened dense cementitious material gaining in compressive strength and decreasing in permeability (Ellison 2015). One challenge that advocates the use of this technology is that it meets the paint filter regularity limit, used in traditional landfill operation to minimize introduction of free water in landfill (Ellison 2015).

Due to the potential benefits of this approach and the regulatory requirement of disposing dry coal combustion residuals (CCR) in landfills, paste encapsulation technology is being investigated as a feasible option for the integrated disposal of fly ash and FGD wastewater. A conceptual illustration of paste technology as a key component of the “closed-loop” iterative FGD wastewater management process in steam electric power facilities is presented in Figure 1.1. The overarching goal of this process is to develop an optimized and sustainable wastewater treatment processes in terms of overall cost, concentrated brine-fly ash mass balance, landfill management, and environmental contamination prevention.

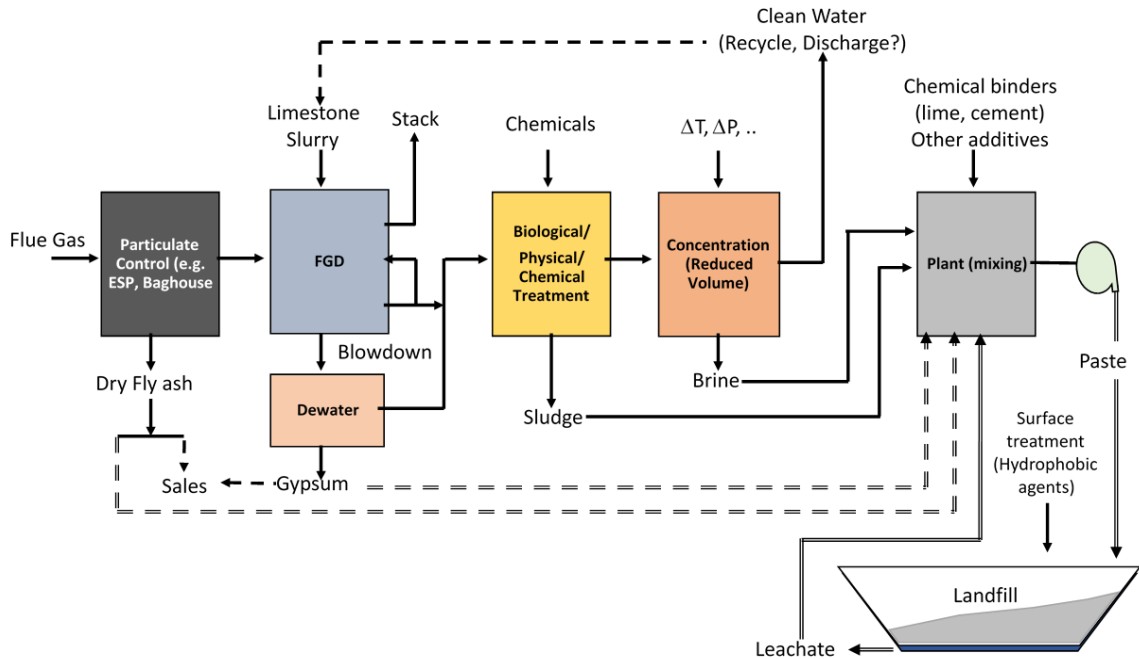


Figure 1.1. Proposed “Closed-Loop” FGD Wastewater Management Process (Dr. Vincent Ogunro, personal communication, June 2018)

However, studies have identified some challenges that have limited the implementation of this “closed-loop” iterative FGD wastewater management process. The cost for volume reduction of wastewater to brine and the additives to enhance encapsulation is still economically unfavorable compared to other treatment approaches (Ellison 2015). The characteristics of fly ash mineralogy and FGD brine affect the behavior of the paste material and vary from site to site, rendering the creation of a universal mix design to be challenging (Longo et al. 2017).

Leaching studies on paste technology specimens have shown that heavy metals are encapsulated in the system. Renew et al. (2016), Zhang et al. (2020), and Zhang et al. (2019) studied co-disposal of FGD brine with fly ash Portland cement and achieved 68 – 90% retainment of As, Cd, Hg, and Se in the paste system. Fatoba et al. (2011) and Fatoba

et al. (2017) modeled the interactions of fly ash and brine and showed that species like Na, As, Co, and Ni were immobilized in the fly ash and brine system. Ellison (2015) determined that the addition of a binder like lime to the fly ash and brine mixture decreased the leachate of the heavy metals from the paste. However, studies by Oza et al. (2015) and Fatoba et al. (2011) show that the halides in the paste encapsulation are still mobile. Fatoba et al. (2011) observed that less than 30% of the chloride from the brine was immobilized in the fly ash-brine system. Oza et al. (2015) indicated that even though the increase in lime content in the system moderately decreased the leaching of chloride and bromide from the paste, the cumulative mass release of halides at the end of the testing period was still high. Therefore, the overarching goal of this research proposal is to enhance the sequestration of halides and prevent them from leaching out into the groundwater or surface waters. This can be achieved by targeting the microstructure of the paste to preferentially form layered double hydroxides. These layered double hydroxides will encapsulate the halides in the paste system.

1.2. Layered Double Hydroxides

Layered Double Hydroxides (LDHs) are a class of two-dimensional lamellar compounds based on the structure of brucite, $Mg(OH)_2$. They consist of positively charged octahedral layers with a negatively charged interlayer consisting of water and anion molecules (Goh et al. 2008). Layered double hydroxides have the ability to be good adsorbents and ion-exchangers of contaminant ions due to the presence of a significant number of exchangeable anions in the interlayer and the availability of large interlayer spaces (Yang et al. 2005). This has led to considerable interest in using LDHs to remove environmental contaminants from drinking water or wastewater. Yang et al. (2005) used

calcined LDHs to adsorb arsenic and selenium from aqueous solutions simulating power-plant effluent streams. Similarly, Loganathan et al. (2014) characterized the sorption of phosphate from wastewater onto LDHs while Sheng et al. (2016) used LDHs to sequester hexavalent chromium via adsorption. Hourri et al. (1999) reported that ZnAl-, MgAl-, and ZnCr-Cl-LDHs can adsorb 1.0 mmol of Cr (VI) per gram of layered double hydroxide.

Layered double hydroxides are generally represented by the formula $[M_1-x^{2+}M_x^{3+}(\text{OH})_2]^{X+}(\text{A}^{n-})_{X/n} \cdot m\text{H}_2\text{O}$ where M^{2+} and M^{3+} are divalent (e.g. Ca, Mg) and trivalent (e.g. Al, Fe) cations, respectively; A is an interlayer anion of charge n^- ; and x is equal to the molar ratio of $M^{3+}/(M^{2+} + M^{3+})$. The structure of LDHs is composed of octahedral units of M^{2+} and M^{3+} . These octahedral units share edges in order to form infinite sheets. The infinite sheets made of octahedral units of M^{2+} and M^{3+} are stacked on top of each other and are bound together by hydrogen bonding (Goh et al. 2008). A schematic representation of a LDH structure is shown in Figure 1.2. Anionic species like halides, oxy-anions, anionic complexes and others can be positioned among the hydroxide ions, between the sheets of M^{2+} and M^{3+} ions. The interactions in the interlayer of LDHs are controlled by coulombic forces between the positively charged M^{2+} and M^{3+} sheets and the anions in the interlayer, and hydrogen bonding between the water molecule and the anions in the interlayer with the hydroxyl groups of the sheet (Palmer et al. 2009).

Section 1.2.1 introduces some examples of LDHs like Friedel's salt (Section 1.2.1.1) and Kuzel's salt (Section 1.2.1.2), which are also known as AFm phases. The synthesis and characterization of the AFm phases are discussed in detail, while the solubility product constants of the phases are also provided. The solubility product constants can be used to determine the stability of the AFm phase as a precipitate or as part

of a paste system. Section 1.2.1.3 provides details about ettringite, a sulfate mineral belonging to AFt group. Section 1.2.2 discusses the thermodynamic stability of an AFm system in presence of chloride and sulfate. The stability of the system can determine the binding affinity of chloride and other halides in the paste material.

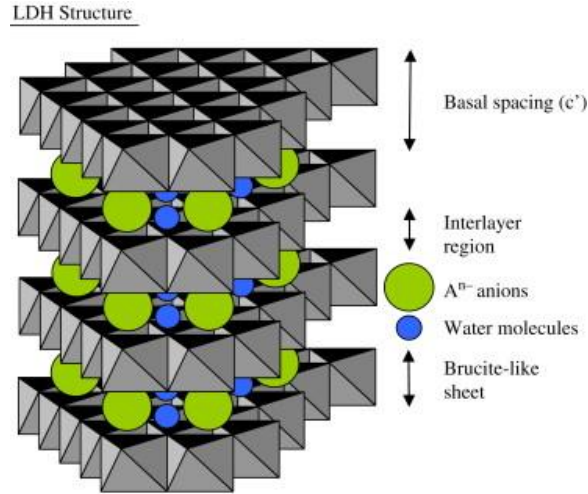


Figure 1.2. Schematic diagram of a LDH structure (Goh et al. 2008)

1.2.1. AFm and AFt Phases

AFm (alumina or ferric oxide, monosulfate) phases belong to the family of LDHs. The general formula of an AFm phase is $[Ca^{2+}_4(Al^{3+}_xFe^{3+(1-x)})_2(OH)_{12}] \cdot A \cdot nH_2O$, where $A \cdot nH_2O$ represents the hydrated exchangeable interlayer anions (Marty et al. 2018). The well-known family of AFm phases include: hydroxy-AFm, monosulfoaluminate, monocarboaluminate, hemicarboaluminate, Friedel's salt $[Ca_2Al(OH)_6Cl \cdot 2H_2O]$, and Kuzel's salt $[3CaO \cdot Al_2O_3 \cdot 1/2CaCl_2 \cdot 1/2CaSO_4 \cdot \sim 11H_2O]$. AFt (alumina or ferric oxide, trisulfate) phases represent a group of calcium sulfoaluminate hydrates. The general formula of an AFt phase is $3CaO \cdot (Al,Fe)_2O_3 \cdot 3CaX_2 \cdot nH_2O$, where X represents an anion

(Champenois et al. 2012). The AFt family of phases includes ettringite $[\text{Ca}_6\text{Al}_2(\text{SO}_4)_3(\text{OH})_{12}\cdot 26\text{H}_2\text{O}]$ with carbonate, sulfate, and chloride as substituents.

Halides can be sequestered in the fly ash-brine paste by substituting halides and sulfate in high aluminate cementitious materials to form AFm phases. These phases can form in hydrated cementitious systems when alumina combines with water, calcium, and substituents including hydroxide, carbonate, sulfate, and halides. High concentrations of chloride and other halides in the FGD wastewater brine can be sorbed or exchanged to form the AFm phases, thereby encapsulating them in the paste. Calcium and aluminum are also essential elements to form AFm and AFt phases. FGD wastewater brine has high concentrations of calcium, which is further supplemented by the addition of chemical additives like lime. Most types of fly ashes have high aluminum content and can be released due to the pozzolanic activity of the fly ash. Therefore, the essential elements for the formation of AFm and AFt phases are already available in the fly ash-brine paste. Most importantly, Friedel's salt, Kuzel's salt, ettringite, and other cementitious mineral phases are significantly more stable and relatively insoluble compared to common salts like NaCl, CaCl_2 , AlCl_3 and cement minerals like portlandite and calcium silicate hydrate (CSH) phases as illustrated with their solubility product constant values in Table 1.2 (Manikonda et al. 2019).

Table 1.2. Solubility product constants of AFm phases and common salts

Phase	Compound	K_{sp}	Temperature	Reference
AFm	Friedel's salt	7.94×10^{-28}	20 °C	Birnin-Yauri and Glasser (1998)
	Kuzel's salt	4.37×10^{-29}	25 °C	Balonis et al. (2010)
AFt	Ettringite	1.26×10^{-45}	25 °C	Lothenbach (2010)
Cement	Portlandite	6.61×10^{-6}	25 °C	Duchesne and Reardon (1995)
	Jennite-type C-S-H	6.76×10^{-14}	25 °C	Lothenbach (2010)
	Tobermorite-type C-S-H	1×10^{-8}	25 °C	Lothenbach (2010)
Other Salts	Sodium chloride	36	25 °C	PubChem Substance and Compound databases
	Calcium chloride	1210	20 °C	
	Aluminum chloride	20400	20 °C	

1.2.1.1. Friedel's Salt

Friedel's salt [$\text{Ca}_2\text{Al}(\text{OH})_6\text{Cl}\cdot 2\text{H}_2\text{O}$] (Figure 1.3), is an anion-exchange mineral belonging to the layered double hydroxides (LDHs) family (Birnin-Yauri and Glasser 1998). It is composed of hydroxide layers with Ca^{+2} and Al^{+3} octahedral units and an interlayer of Cl^- ions. Although the natural occurrences of Friedel's salt (FS) are rare, they have been studied in a wide range of synthetic examples and are important constituents of cement-based materials subjected to high halide concentration environment (Mills et al. 2012). Furthermore, semi-quantitative XRD analysis conducted by Pretorius et al. (2017) on the two mixes in Table 1.3 recorded the occurrence of trace amounts (0-3%) of FS mineral in hardened paste encapsulation samples. Table 1.3 presents the mix recipes of the samples made using brine (Cl^- conc.: 180000 mg/L), fly ash (ASTM class F), and quick lime. Similarly, Zhang et al. (2020) detected the presence of FS in FGD wastewater and sub-bituminous coal fly ash co-disposed solids and concluded that the formation of FS was key component in the retainment of heavy metals in the solids.

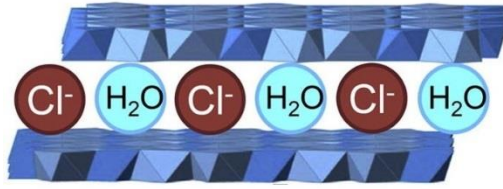


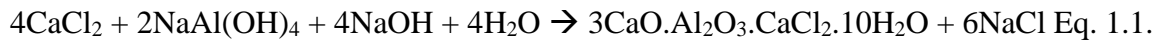
Figure 1.3. Schematic representation of Friedel's salt structure (Li et al. 2017)

Table 1.3. Description of quantities used in making mix samples (Pretorius et al. 2017)

Mix	Description	Concentrated Brine %	Ash Mass %	Quick Lime Mass %	Total Mass %
#5	Dry, no cake	29.3	66.5	4.3	100
#9	Flowable, no cake	37.4	58.1	4.5	100

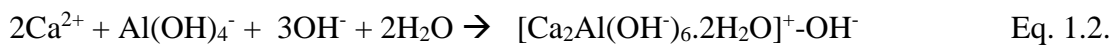
Friedel's salt is widely used in environmental remediation, particularly dealing with heavy metals from wastewater because of its high adsorption efficiency (Ma et al. 2015). Zhang and Reardon (2003) showed that the uptake of boron, chromium, molybdenum, and selenium into FS was very high and concentrations in the fly ash leachate were reduced to below drinking water standards. Dai et al. (2009) removed Cr (VI) from wastewater with a removal efficiency of 99%. Zhang et al. (2011) found that FS has high adsorption capacity for arsenic. Zhang et al. (2013) determined that FS could be used to remove cadmium from water. Zhang et al. (2013) and Zhang and Reardon (2003) proposed two possible mechanisms for the uptake of the contaminants by Friedel's salt: surface adsorption and complexation, and ion-exchange. Zhang and Reardon (2003) reported that borate, chromate, molybdate, and selenate substitute directly for OH⁻ in the interlayers of Friedel's salt, while Zhang et al. (2013) concluded that the removal of Cd²⁺ occurs mainly through the complexation of cadmium with the Ca-Al layers.

Friedel's salt was synthesized in various ways in literature using starting materials such as CaCl_2 , $\text{Al}(\text{OH})_3$, NaOH , NaAlO_2 , AlCl_3 , and $3\text{CaO}\cdot\text{Al}_2\text{O}_3$. Ma et al. (2015) and Zhang et al. (2011) synthesized FS by dropwise addition of NaAlO_2 to CaCl_2 under constant stirring and at constant temperature. After the addition was complete, the precipitate was filtered, washed and dried in an oven. Equation 1.1 gives the reaction for the formation of Friedel's salt.



Vieille et al. (2003) and Guo and Tian (2013) prepared FS using a coprecipitation method where a mixed solution of CaCl_2 and AlCl_3 was added dropwise to NaOH at $\text{pH} = 11.5$. After the completion of addition of the salts, the precipitate was centrifuged and then dried in vacuum at room temperature. Birnin-Yauri and Glasser (1998) added $3\text{CaO}\cdot\text{Al}_2\text{O}_3$ in portions to a solution of CaCl_2 under vigorous stirring. Tricalcium aluminate ($3\text{CaO}\cdot\text{Al}_2\text{O}_3$) was prepared by baking CaCO_3 and Al_2O_3 (3:1 molar ratio) at 1470–1670 K. After the addition of $3\text{CaO}\cdot\text{Al}_2\text{O}_3$ was complete, precipitate was collected by filtration and dried in a desiccator at room temperature.

Ma et al. (2015) proposed two possible mechanisms for the formation of Friedel's salt: via adsorption or via an anion-exchange. In the anion-exchange mechanism, the first step is the formation of Ca-Al-OH layers, shown in Equation 1.2. The free Cl^- ions in the solution then exchange with OH^- in the interlayer to form Friedel's salt (Equation 1.3).



In the adsorption mechanism, Ma et al. (2015) state that the principle layer $[\text{Ca}_2\text{Al}(\text{OH})_6 \cdot 2\text{H}_2\text{O}]^+$ is formed first (Equation 1.4). The free chloride in the solution then directly adsorb in the interlayers of the principle layer, leading to the formation of Friedel's salt (Equation 1.5).



The structure and morphology of Friedel's salt was characterized using thermogravimetric analysis-differential scanning calorimetry (TGA-DSC), x-ray diffraction (XRD), scanning electron microscope (SEM), fourier-transform infrared spectroscopy (FTIR), and Raman spectroscopy. Grishchenko et al. (2013), Ma et al. (2009) and Vieille et al. (2003) performed TGA-DSC on Friedel's salt. According to Vieille et al. (2003), Friedel's salt has three main weight losses over the temperature ranges 150 – 180 °C (removal of interlayer water), 250 – 400 °C (dehydroxylation of hydroxide layers), and 400 - 1000 °C (recombination of hydroxyl groups and carbonate decomposition). The mass loss between 150 – 180 °C should be 12.8%, in the second step (250 – 400 °C) should be 19.2%, and in the last step (400 - 1000 °C) is less than 1%. The total mass loss should be 32.1% (Grishchenko et al. 2013). Figure 1.4 shows the TGA and DSC plots of Friedel's salt.

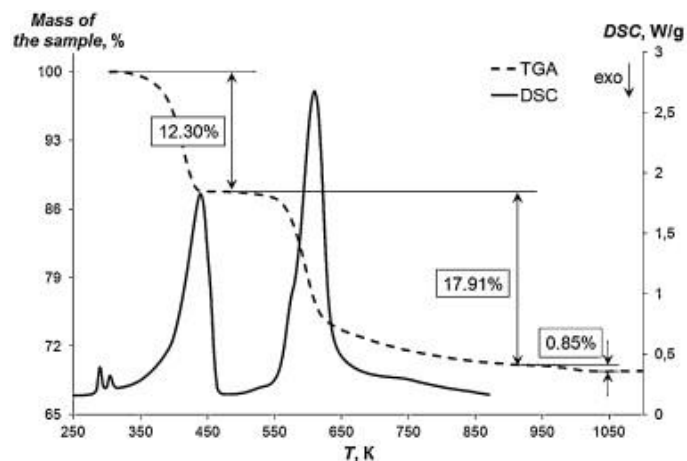


Figure 1.4. Combined TGA and DSC curves for Friedel's salt (Grishchenko et al. 2013)

Grishchenko et al. (2013) state that the XRD patterns (Figure 1.5) of Friedel's salt should index a monoclinic phase at temperature below 35 °C, with lattice parameters $a=9.979 \text{ \AA}$, $b=5.751 \text{ \AA}$, $c=16.320 \text{ \AA}$, $\beta=104.53^\circ$ and space group $C2/c$ (Terzis et al. 1987). At temperatures above 35 °C, Renaudin et al. (1999) state that structure of Friedel's salt transforms to rhombohedral phase with lattice parameters $a=5.736 \text{ \AA}$, $c=46.849 \text{ \AA}$, $\beta=104.53^\circ$ and space group $R-3c$.

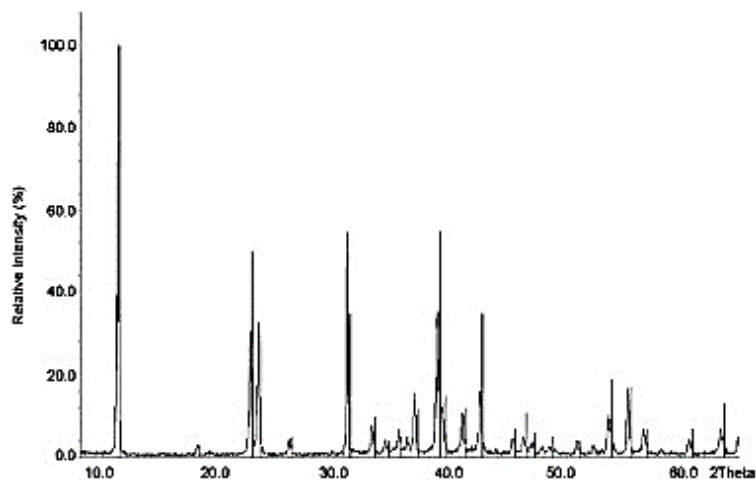


Figure 1.5. X-ray Diffractogram of Friedel's salt (Grishchenko et al. 2013)

Birnin-Yauri and Glasser (1998), Grishchenko et al. (2013) and Yue et al. (2018) recorded the infrared spectrum for Friedel's salt (Figure 1.6) using a FTIR spectrometer. They state that the bands at $\sim 532 - 787 \text{ cm}^{-1}$ are due to Al-OH stretching vibration mode. The band at $\sim 1620 \text{ cm}^{-1}$ is due to the water bending vibration mode, while the broad bands at $\sim 3484 \text{ cm}^{-1}$ is due to the vibration due to OH stretching in water and metal-OH.

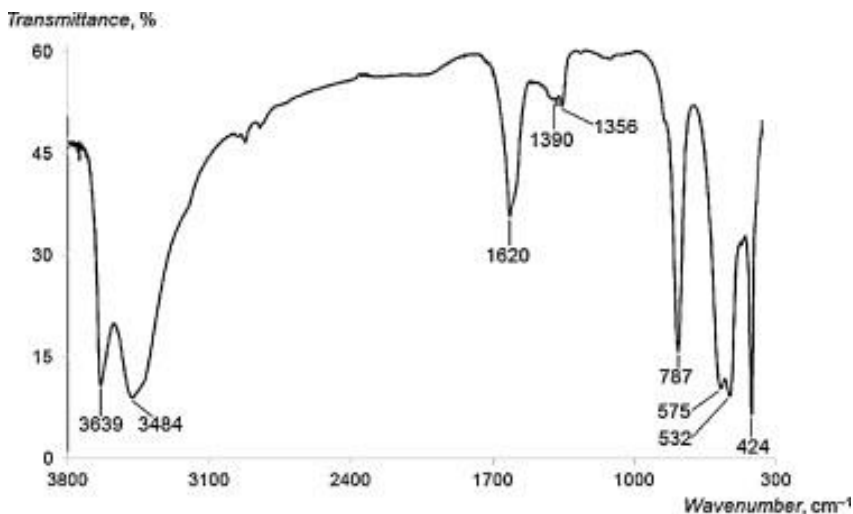


Figure 1.6. IR spectrum of Friedel's salt (Grishchenko et al. 2013)

Yue et al. (2018) recorded a Raman spectrum (Figure 1.7) for Friedel's salt using a Raman spectrometer. The Raman bands of FS, according to the authors, were mostly located in two frequency ranges, at $200 - 1200 \text{ cm}^{-1}$ and at $3200 - 3800 \text{ cm}^{-1}$. The bands at $200 - 1200 \text{ cm}^{-1}$ are because of the vibrations of the $\text{Al}(\text{OH})_6$ functional group, while the bands at $3200 - 3800 \text{ cm}^{-1}$ are due to mostly due to the vibrations in the water and hydrogen bond network.

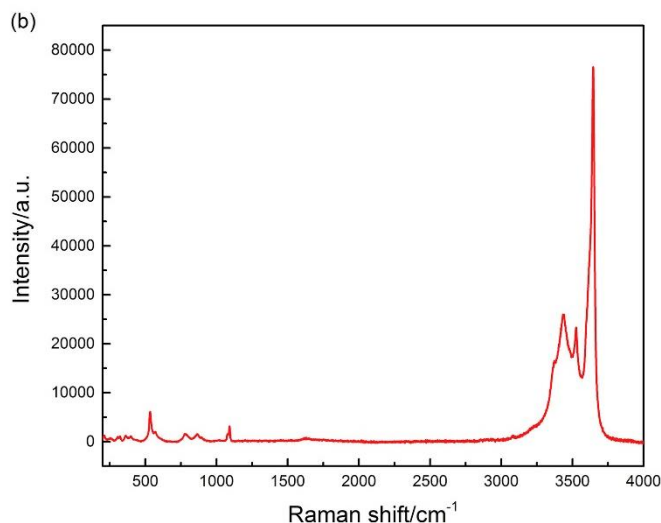


Figure 1.7. Raman spectra of Friedel's salt (Yue et al. 2018)

Birnin-Yauri and Glasser (1998) measured the solubility product (K_{sp}) of Friedel's salt in water at 20 °C. The K_{sp} was calculated from the relationship defined in Equation 1.6 and was determined to be -27.10 at 20 °C. Balonis et al. (2010) measured the value of $\log K_{sp}$ between -27.78 and -27.87 at 25 °C, while Bothe and Brown (2004) calculated the solubility product of FS to be within the range -28.8 and -27.6.

$$K_{sp} = [\text{Ca}]^4[\text{Al}(\text{OH})_4]^2[\text{Cl}]^2[\text{OH}]^4 \quad \text{Eq. 1.6.}$$

Studies like Fang et al. (2018) and Ma et al. (2015) have investigated the effects of initial CaCl_2 concentration, calcium to aluminum molar ratio, reaction time, and reaction temperature on the structure of Friedel's salt. Ma et al. (2015) state that the structure of FS was not affected for reaction temperatures below 100 °C, however, Fang et al. (2018) say that the removal efficiency of chloride from solution decreased as the reaction temperature increased from 25 °C to 60 °C because of the change in phase of FS above 35 °C. Other studies have synthesized FS at a reaction temperature of 50 °C, which is not practical for field relevant scenarios. Ma et al. (2015) report that the initial concentration of CaCl_2 did

not influence the structure of FS but changed the morphology of FS particles. Ma et al. (2015) and Fang et al. (2018) report that the optimum range of Ca:Al molar ratio is 2-3:1. However, none of the studies investigated the interactions between initial chloride concentration and the Ca:Al molar ratio and its effect on the structure of Friedel's salt.

1.2.1.2. Kuzel's Salt

Kuzel's salt is a chloride and sulfate ordered compound belonging to the AFm phase of the LDH family. Kuzel's salt (KS) has a composition of $3\text{CaO}\cdot\text{Al}_2\text{O}_3\cdot 1/2\text{CaCl}_2\cdot 1/2\text{CaSO}_4\cdot n\text{H}_2\text{O}$, ideally with a $[\text{Cl}]/[\text{SO}_4]$ molar ratio of 2:1 (Balonis et al. 2010). The main layer of KS consists of aluminum-oxygen-calcium (Al-O-Ca) bonds (Mesbah et al. 2011). Kuzel's salt has a staging AFm structure (Figure 10), with succession of interlayer populated with $[\text{Cl}\cdot 2\text{H}_2\text{O}]^-$ followed by interlayer filled with $[(\text{SO}_4)_{0.5}\cdot 3\text{H}_2\text{O}]^-$.

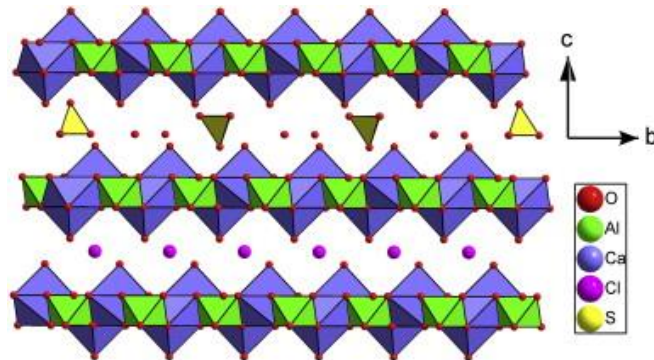


Figure 1.8. Schematic representation of Kuzel's salt structure (Mesbah et al. 2011)

Balonis et al. (2010) and Glasser et al. (1999) synthesized Kuzel's salt by first heating a 3:1 molar mixture of CaCO_3 and Al_2O_3 at $1400\text{ }^\circ\text{C}$ to prepare C_3A . The C_3A powder was then mixed with CaCl_2 and CaSO_4 in water and agitated for three months. The

precipitate was then filtered, dried in a desiccator and the resulting solid was determined to be Kuzel's salt.

Mesbah et al. (2011) characterized the structure and morphology of Kuzel's salt using thermogravimetric analysis (TGA), x-ray diffraction (XRD) and Raman spectroscopy. Similar to Friedel's salt, Kuzel's salt also has three main weight losses over the temperature ranges 25 – 300 °C (dehydration of water molecules), 450 – 900 °C (release of chloride), and 1000 – 1200 °C (decomposition of sulfate). The mass loss at 25 – 300 °C should be 34.08%, in the second step (450 – 900 °C) should be 7.53%, and in the last step (1000 - 1200 °C) is 6.94%. Figure 1.9 shows the TGA curve of Kuzel's salt.

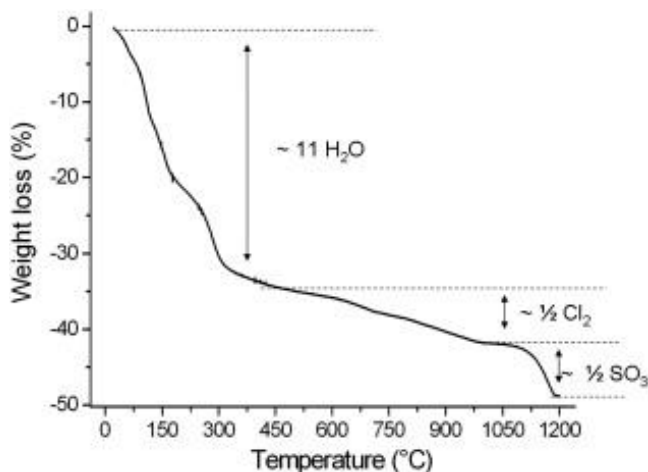


Figure 1.9. TGA curve of Kuzel's salt (Mesbah et al. 2011)

Balonis et al. (2010) and Mesbah et al. (2011) state that the XRD patterns of Kuzel's salt should index a rhombohedral phase at 20 °C, with lattice parameters $a=5.751 \text{ \AA}$, $c=50.418 \text{ \AA}$, space group $R\bar{3}$ -, and basal spacing $d = 8.32 \text{ \AA}$. Mesbah et al. (2011) recorded the Raman spectra for Kuzel's salt (Figure 1.10). The bands at 453, 616, 981 and 1098

cm^{-1} are due to SO_4 stretching vibration mode, while the band at 531 cm^{-1} is due to the vibration mode in $\text{Al}(\text{OH})_6$ according to the authors.

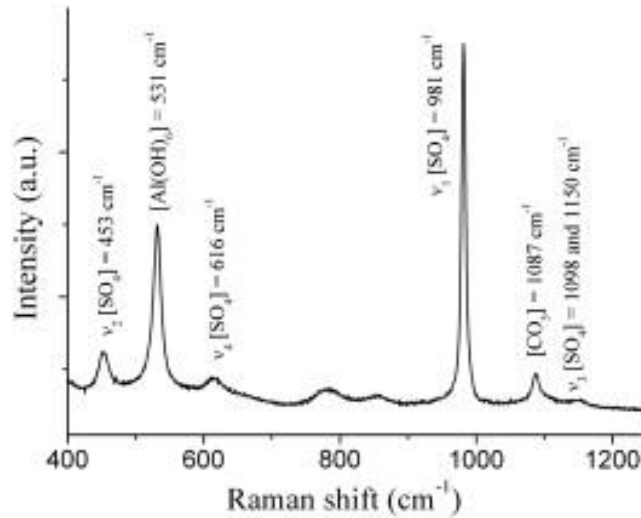
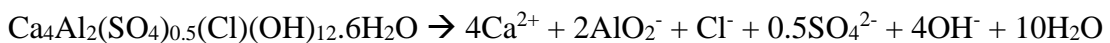


Figure 1.10. Raman spectra of Kuzel's salt (Mesbah et al. 2011)

Balonis et al. (2010) measured the solubility product at $25 \text{ }^\circ\text{C}$ of Kuzel's salt to be in the range -28.25 to -28.53 . The solubility product was measured using the dissolution reaction defined in Equation 1.7. Glasser et al. (1999) estimated the solubility product of Kuzel's salt to be -28.54 .



Eq. 1.7.

Unlike Friedel's salt, there are lack of studies investigating the effects of initial concentrations of chloride and sulfate and the Ca:Al molar ratio on the structure of Kuzel's salt. Balonis et al. (2010) and Glasser et al. (1999) synthesized KS by agitating the mixture of C_3A , CaCl_2 and CaSO_4 for three months, which is not feasible for field scenarios. Therefore, alternative synthesis methods for KS needed to be investigated.

1.2.1.3. Ettringite

Ettringite is a hydroxy calcium alumino-sulfate mineral belonging to the AFt phase family and is represented by $[\text{Ca}_6\text{Al}_2(\text{SO}_4)_3(\text{OH})_{12}\cdot 26\text{H}_2\text{O}]$. Ettringite is an important product formed during the hydration of Portland cements and special binders such as calcium sulfoaluminate cements and calcium aluminate cements blended with calcium sulfates. It is also formed in other alkaline materials like cement based waste solidification byproducts, alkaline fly ashes and mine spoils (Perkins and Palmer 1999). Ettringite consists of $\{\text{Ca}_6[\text{Al}(\text{OH})_6]_2\cdot 24\text{H}_2\text{O}\}^{6+}$ columns with the inter-column space being occupied by $[\text{SO}_4^{2-}]_3$, and water molecules between the $[\text{SO}_4^{2-}]_3$ molecules and the columns (Figure 1.11).

The channel structure in ettringite enables the replacement of sulfate with oxyanions such as chromate, arsenate, selenate (Chrysochoou 2006). Several studies have investigated the oxyanionic substitution in ettringite. Myneni et al. (1997) performed adsorption and coprecipitation experiments to determine the extent of uptake of arsenate into ettringite and found that substitution of arsenate was the preferred mechanism compared to surface adsorption. Similarly, Poellmann et al. (1993) studied the incorporation of borate and chromate into ettringite.

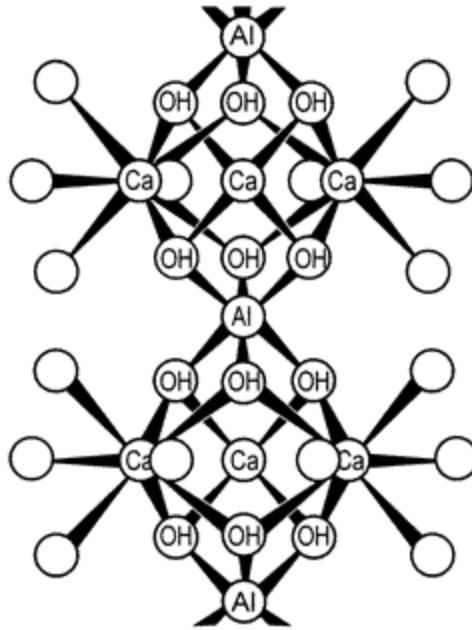


Figure 1.11. Schematic representation of structure of Ettringite (Zhang and Reardon 2003)

Many synthesis methods reported in the literature are based on using 10% sucrose solution as the reaction medium. Myneni et al. (1998) synthesized ettringite by mixing $\text{Al}_2(\text{SO}_4)_3$ and CaO in a 10% sucrose solution under constant stirring. The precipitate was separated by centrifugation and dried in a desiccator. Other synthesis methods have followed the same process without the addition of sucrose. The precipitating solids was determined to be ettringite. Zhang and Reardon (2003) synthesized ettringite by the addition of $\text{Ca}(\text{OH})_2$ to $\text{Al}_2(\text{SO}_4)_3$ as presented in Equation 1.8. Chrysochoou (2006) states that addition of sucrose resulted in short needle like structures being formed in ettringite while absence of sucrose resulted in elongated structures.



Antao et al. (2002) characterized the structure and morphology of ettringite using thermogravimetric analysis (TGA). They state that during the TGA analysis of ettringite, mass loss occurs over three distinct temperature intervals (Figure 1.12). The water between the columns is lost between 100 °C and 180 °C, corresponding to 33%. The loss of mass from the dehydroxylation of aluminum hydroxide and the loss of the remaining water molecules occurs between 200 and 900 °C. The loss due to dehydroxylation of aluminum hydroxide and the loss of the remaining water molecules corresponds to 12.3%. The final interval of mass loss between 900 °C and 1200 °C is due to the decomposition of sulfate molecules (15.4%). The total mass loss corresponding to the chemical formula of ettringite should be 60.7%.

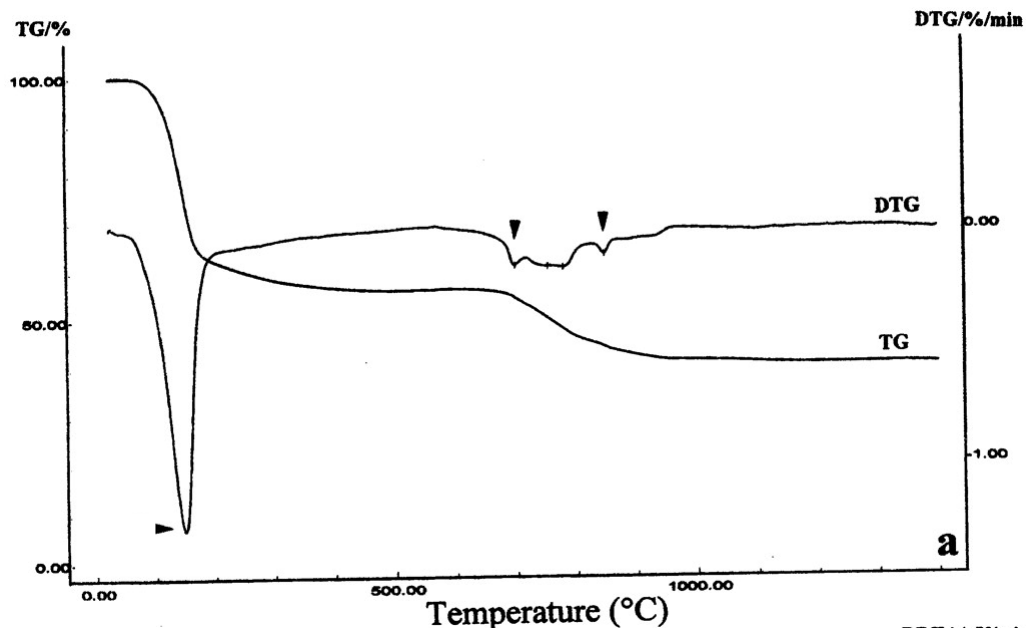


Figure 1.12. TG and DTG curves for Ettringite (Antao et al. 2002)

Myneni et al. (1998) and Perkins and Palmer (1999) studied the structure of ettringite using XRD and FTIR. The XRD diffractogram of ettringite is shown in Figure

1.13. The cell parameters are $a=11.225 \text{ \AA}$, $c=21.467 \text{ \AA}$ and unit cell volume of 2342.5 \AA^3 , with a space group P63/mmc (McMurdie et al. 1986).

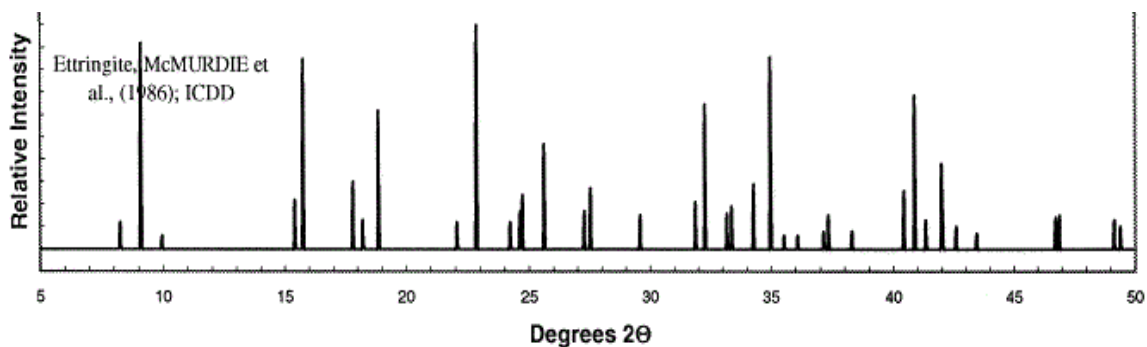


Figure 1.13. XRD of ettringite (McMurdie et al. 1986)

Figure 1.14 shows the FTIR spectra recorded for ettringite. According to Myneni et al. (1998), the strong peak at $\sim 1108 \text{ cm}^{-1}$ is due to SO_4 . The peaks at $\sim 1663 \text{ cm}^{-1}$ and 3421 cm^{-1} are due to bending and stretching vibration of water molecules. The mode at 3630 cm^{-1} is due to the OH-stretching vibration of the $\text{Al}(\text{OH})_6$ unit. Myneni et al. (1998) and Renaudin et al. (2007) recorded the Raman spectra for ettringite (Figure 1.15). The authors state that the bands at 449 , 605 , 988 and 1114 cm^{-1} are due to SO_4 stretching vibration mode, while the band at 551 cm^{-1} is due to the vibration mode in $\text{Al}(\text{OH})_6$.

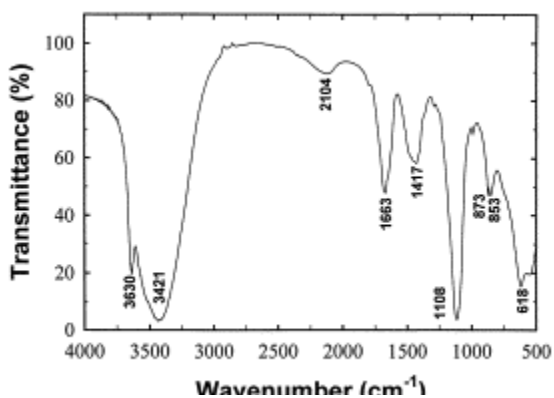


Figure 1.14. FTIR spectra for ettringite (Perkins and Palmer 1999)

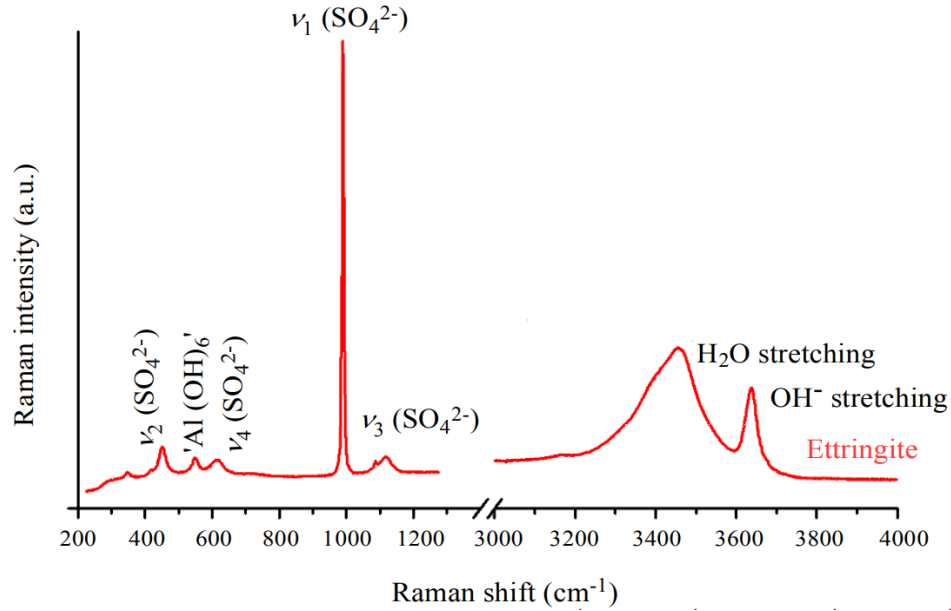


Figure 1.15. Raman spectra of ettringite (Renaudin et al. 2007)

Perkins and Palmer (1999) calculated the solubility product of ettringite at 25 °C using the dissolution relationship shown in Equation 1.9, which was solved to give the K_{sp} relationship in Equation 1.10. Perkins and Palmer (1999) measured the solubility product to be -44.9 ± 0.3 . Warren and Reardon (1994) calculated a value of -44.61 ± 0.56 at 25 °C, while Myneni et al. (1998) calculated the solubility product at 25 °C as -111.6 ± 0.8 as $\{Al^{+3}\}$, which was recalculated by Perkins and Palmer (1999) to be -45.08 as $\{Al(OH)_4^-\}$.



$$K_{sp} = \{Ca^{2+}\}^6 \{Al(OH)_4^-\}^2 \{SO_4^{2-}\}^3 \{OH^-\}^4 \{H_2O\}^{26} \quad \text{Eq. 1.10.}$$

Balonis et al. (2010) state that their attempts to synthesize chloride-ettringite at 5 °C and 25 °C was not successful and instead resulted in the formation of Friedel's salt. They postulate that chloride-ettringite occurs in a thermodynamically stable form at temperatures below 0 °C.

1.2.2. Stability of the CaO-Al₂O₃-CaCl₂-H₂O system

It is important to understand the binding power for chloride in an AFm system in presence of realistic concentrations of sulfate. FGD wastewater has high concentrations of sulfate and can interfere with the formation of AFm phases that can bind chloride. Balonis et al. (2010), Brown and Bothe (2004), and Glasser et al. (1999) modelled the thermodynamic stability of the CaO-Al₂O₃-CaCl₂-H₂O system to determine the binding affinity of AFm and AFt systems for chloride and sulfate. Figure 1.16 shows the sequence of AFm and AFt phase changes with increasing molar ratio of chloride to alumina. The initial system had no chloride present and the sulfate to Al₂O₃ ratio was fixed at one. Chloride, when introduced to the system, can displace sulfate from monosulfoaluminate (SO₄-AFm_{ss}). If the molar ratio of 2Cl/Al₂O₃ is below ~ 0.70 (low Cl⁻ concentration), monosulfoaluminate transforms to Kuzel's salt. However, at 2Cl/Al₂O₃ above 0.70 (high chloride concentration), monosulfoaluminate transforms to form Friedel's salt. The sulfate ions that have been released from monosulfoaluminate form ettringite.

Glasser et al. (1999) state that compositions of the AFm phase are sensitive to the chemistry of the solution. If the conditions are suitable, hydroxy and sulfate AFm phases readily transformed to chloride and chloride-sulfate phases. Sulfate-AFm phases are thermodynamically unstable at temperatures below 40 °C. An exception to this rule is that at approximately 20 °C, the driving force stabilizing AFt relative to AFm is very small which causes the sulfate-AFm to be persistent. AFm phases including Friedel's salt and Kuzel's salt are thermodynamically stable at ~ 20 °C (Glasser et al. 1999).

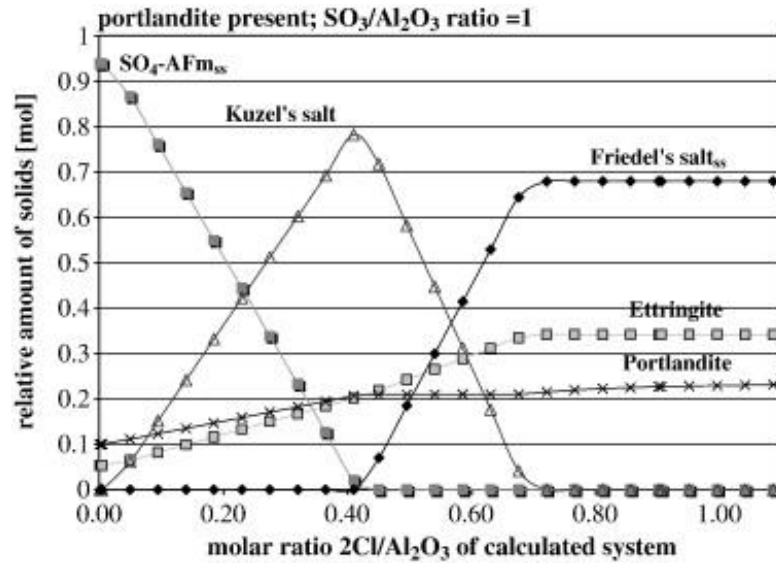


Figure 1.16. Phase development depending on varying chloride to aluminate ratios ($2Cl/Al_2O_3$) with fixed initial sulfate ratio of 1 (Balonis et al. 2010)

1.3. Dissertation Aims and Objectives

The objective of this dissertation research herein is to enhance the removal of highly mobile halides from hypersaline brines like FGD wastewater concentrate and prevent them from entering the groundwater or surface waters through preferential formation of layered double hydroxides. Coal fly ash and FGD wastewater concentrate are characterized with an extremely complex composition matrix. It would be challenging to understand the factors that will influence the formation of layered double hydroxides if synthesized using the FGD wastewater concentrate and fly ash paste. Therefore, the synthesis of LDHs were investigated using laboratory grade reagents to determine the optimum operating parameters. The purpose of this research is:

- I. Investigation of sequestration of chloride (Cl^-), the halide with the highest concentration in many of the hypersaline brines, by enhancing the formation of AFm phases

The synthesis of Friedel's salt and Kuzel's salt has been discussed in detail in the previous sections and the structures have been characterized using multiple instruments. However, in the case of Friedel's salt, there is a lack of information about the interactions between the process parameters, such as initial concentration of chloride and Ca:Al molar ratio on the structure of FS and chloride removal. For Kuzel's salt, the synthesis protocol used in literature would be challenging to use in field conditions. An alternative synthesis protocol suitable for implementation in field scenarios needed to be investigated. Also, there is little information about the effect of parameters like reaction temperature, initial concentration of chloride and sulfate and Ca:Al molar ratio on the structure of Kuzel's salt.

II. Investigation of sequestration of bromide (Br^-) from hypersaline brines by enhancing the formation of AFm phases.

Bromine is naturally present in coal in trace amounts and bromide is also added to coal to control mercury emissions. Therefore, bromide is found to be present in elevated concentrations in FGD wastewaters at some power plants. Release of bromide into surface water and groundwater may lead to the formation of brominated disinfection byproducts (bromoacetic acid, dibromoacetic acid, tribromoacetic acid etc.) which are carcinogenic and can pose health risk to humans (Good and Vanbriesen 2017). Therefore, it is important to control the release of bromide ions from the paste system. There is gap in knowledge about the ability of AFm phases to successfully sequester bromide. Renaudin et al. (2004) characterized bromide substituted Friedel's salt to understand the influence of intercalated anion on the structural phase of Friedel's salt. However, there is little information available about the solubility product constants of bromide substituted AFm phases, and therefore the stability of bromide dominated system has not been studied.

In order to evaluate the variables that influence the long-term sequestration of halides, the rest of this dissertation has been organized into four chapters: Chapter 2 assessed various synthesis protocols for Friedel's salt that were outlined in literature and characterizes the effect of temperature of the structure of Friedel's salt. Chapter 3 explored the feasibility of removing chloride from high-salinity brines through the precipitation of Friedel's salt. Factors affecting removal of chloride like the initial molar concentration of chloride, the calcium to aluminum ratio and the interactions between them were evaluated. Similarly, Chapter 4 investigated the removal of bromide from hypersaline brines through the precipitation of layered double hydroxides. The influence of initial bromide concentration and its interactions with the Ca:Al molar ratio on bromide removal performance was examined. Chapter 5 characterizes the influence of initial sulfate and chloride concentration and its interactions with the Ca:Al molar ratio on sulfate and chloride removal from sulfate and chloride rich brines through precipitation of LDHs like Kuzel's salt and Friedel's salt. Appendix A summarizes the selection criteria for the precipitation of LDHs based on the characteristics of hypersaline brines and also establishes the feasibility of employing the optimum operating parameters on simulated FGD wastewater concentrate to reduce the concentrations of halides like chloride and bromide in the wastewater.

References

- Ahmaruzzaman, M. (2010). "A review on the utilization of fly ash." *Progress in Energy and Combustion Science*, 36(3), 327-363.
- Antao, S. M., Duane, M. J., and Hassan, I. (2002). "DTA, TG, and XRD studies of sturmanite and ettringite." *Canadian Mineralogist*, GeoScienceWorld, 40(5), 1403–1409.
- Balonis, M., Lothenbach, B., Le Saout, G., and Glasser, F. P. (2010). "Impact of chloride on the mineralogy of hydrated Portland cement systems." *Cement and Concrete Research*, Pergamon, 40(7), 1009–1022.
- Batchelor, B. (2006). "Overview of waste stabilization with cement." *Waste Management*, Pergamon, 26(7), 689–698.
- Birnin-Yauri, U. ., and Glasser, F. . (1998). "Friedel's salt, $\text{Ca}_2\text{Al}(\text{OH})_6(\text{Cl},\text{OH})\cdot 2\text{H}_2\text{O}$: its solid solutions and their role in chloride binding." *Cement and Concrete Research*, 28(12), 1713–1723.
- Boelter, A. M., Lamming, F. N., Farag, A. M., and Bergman, H. L. (1992). "Environmental effects of saline oil-field discharges on surface waters." *Environmental Toxicology and Chemistry*, Wiley-Blackwell, 11(8), 1187–1195.
- Bothe, J. V., and Brown, P. W. (2004). "PhreeqC modeling of Friedel's salt equilibria at $23 \pm 1 \text{ }^\circ\text{C}$." *Cement and Concrete Research*, Pergamon, 34(6), 1057–1063.
- Brown, P., and Bothe, J. (2004). "The system $\text{CaO}-\text{Al}_2\text{O}_3-\text{CaCl}_2-\text{H}_2\text{O}$ at $23\pm 2 \text{ }^\circ\text{C}$ and the mechanisms of chloride binding in concrete." *Cement and Concrete Research*, Pergamon, 34(9), 1549–1553.
- Champenois, J.-B., Mesbah, A., Cau, C., Coumes, D., Renaudin, G., Leroux, F., Mercier, C., Revel, B., and Damidot, D. (2012). "Crystal structures of Boro-AFm and sBoro-AFt phases."
- Chrysochoou, M. (2006). "Evaluation of ettringite and hydrocalumite formation for

heavy metal immobilization: Literature review and experimental study.” *Journal of Hazardous Materials*, Elsevier, 136(1), 20–33.

Cravotta, C. A., and Brady, K. B. C. (2015). “Priority pollutants and associated constituents in untreated and treated discharges from coal mining or processing facilities in Pennsylvania, USA.” *Applied Geochemistry*, Elsevier Ltd, 62, 108–130.

Dai, Y., Qian, G., Cao, Y., Chi, Y., Xu, Y., Zhou, J., Liu, Q., Xu, Z. P., and Qiao, S. Z. (2009). “Effective removal and fixation of Cr(VI) from aqueous solution with Friedel’s salt.” *Journal of Hazardous Materials*, Elsevier, 170(2–3), 1086–1092.

Duchesne, J., and Reardon, E. J. (1995). “Measurement and prediction of portlandite solubility in alkali solutions.” *Cement and Concrete Research*, Pergamon, 25(5), 1043–1053.

Ellison, K. (2015). “Industry Perspectives on Integrating ELG and CCR Compliance through Wastewater Encapsulation: Challenges, Opportunities, and Technology Readiness.” *2015 World of Coal Ash Conference (www ...*

Fang, P., Tang, Z., Chen, X., Huang, J., Tang, Z., and Cen, C. (2018). “Chloride Ion Removal from the Wet Flue Gas Desulfurization and Denitrification Wastewater Using Friedel’s Salt Precipitation Method.” *Journal of Chemistry*, 2018, 1–9.

Fatoba, O. O., Petrik, L. F., Akinyeye, R. O., Gitari, W. M., and Iwuoha, E. I. (2017). “Geochemical Partitioning of Major Elements in Brine Impacted Coal Fly Ash Residues Geochemical Partitioning of Major Elements in Brine Impacted Coal Fly Ash.” *Energy Science and Technology*, 5(1), 45–53.

Fatoba, O. O., Petrik, L. F., Gitari, W. M., and Iwuoha, E. I. (2011). “Fly ash-brine interactions: Removal of major and trace elements from brine.” *Journal of Environmental Science and Health - Part A Toxic/Hazardous Substances and Environmental Engineering*, 46(14), 1648–1666.

Gingerich, D. B., Grol, E., and Mauter, M. S. (2018). “Fundamental challenges and engineering opportunities in flue gas desulfurization wastewater treatment at coal fired

power plants.” *Environmental Science: Water Research and Technology*, Royal Society of Chemistry, 4(7), 909–925.

Glasser, F. P., Kindness, A., and Stronach, S. A. (1999). “Stability and solubility relationships in AFm phases. Part I. Chloride, sulfate and hydroxide.” *Cement and Concrete Research*, Pergamon, 29(6), 861–866.

Goh, K.-H., Lim, T.-T., and Dong, Z. (2008). “Application of layered double hydroxides for removal of oxyanions: A review.” *Water Research*, Pergamon, 42(6–7), 1343–1368.

Good, K. D., and Vanbriesen, J. M. (2017). “Power Plant Bromide Discharges and Downstream Drinking Water Systems in Pennsylvania.” *Environmental Science and Technology*, 51(20), 11829–11838.

Grishchenko, R. O., Emelina, A. L., and Makarov, P. Y. (2013). “Thermodynamic properties and thermal behavior of Friedel’s salt.” *Thermochimica Acta*, 570, 74–79.

Guo, Q., and Tian, J. (2013). “Removal of fluoride and arsenate from aqueous solution by hydrocalumite via precipitation and anion exchange.” *Chemical Engineering Journal*, Elsevier B.V., 231, 121–131.

Houri, B., Legrouri, A., Barroug, A., Forano, C., and Besse, J.-P. (1999). “Removal of Chromate Ions from Water by Anionic Clays.” *Journal de Chimie Physique et de Physico-Chimie Biologique*, EDP Sciences, 96(3), 455–463.

Landis, M. S., Kamal, A. S., Kovalcik, K. D., Croghan, C., Norris, G. A., and Bergdale, A. (2016). “The impact of commercially treated oil and gas produced water discharges on bromide concentrations and modeled brominated trihalomethane disinfection byproducts at two downstream municipal drinking water plants in the upper Allegheny River, Pennsylvania, .” *Science of the Total Environment*, Elsevier, 542, 505–520.

Li, D., Guo, X., Tian, Q., Xu, Z., Xu, R., and Zhang, L. (2017). “Synthesis and application of Friedel’s salt in arsenic removal from caustic solution.” *Chemical Engineering Journal*.

- Loganathan, P., Vigneswaran, S., Kandasamy, J., and Bolan, N. S. (2014). “Removal and Recovery of Phosphate From Water Using Sorption.” *Critical Reviews in Environmental Science and Technology*, Taylor & Francis Group, 44(8), 847–907.
- Longo, S., Pigeon, P., and Pretorius, C. (2017). “Paste technology – not just for mining anymore.” *PASTE 2017*, University of Science and Technology Beijing, 235–242.
- Lothenbach, B. (2010). “Thermodynamic equilibrium calculations in cementitious systems.” *Materials and Structures*, Springer Netherlands, 43(10), 1413–1433.
- Ma, J., Li, Z., Jiang, Y., and Yang, X. (2015). “Synthesis, characterization and formation mechanism of Friedel’s salt (FS: $3\text{CaO}\cdot\text{Al}_2\text{O}_3\cdot\text{CaCl}_2\cdot 10\text{H}_2\text{O}$) by the reaction of calcium chloride with sodium aluminate.” *Journal Wuhan University of Technology, Materials Science Edition*, 30(1), 76–83.
- Ma, J., Li, Z., Zhang, Y., and Demopoulos, G. P. (2009). “Desilication of sodium aluminate solution by Friedel’s salt (FS: $3\text{CaO}\cdot\text{Al}_2\text{O}_3\cdot\text{CaCl}_2\cdot 10\text{H}_2\text{O}$).” *Hydrometallurgy*, Elsevier B.V., 99(3–4), 225–230.
- Mahlaba, J. S., Kearsley, E. P., and Kruger, R. A. (2011). “Effect of fly ash characteristics on the behaviour of pastes prepared under varied brine conditions.” *Minerals Engineering*, Elsevier Ltd, 24(8), 923–929.
- Manikonda, A., Ogunro, V. O., Ellison, K. M., and Moo-Young, K. (2019). “Synthesis of Friedel’s Salt for Application in Halide Sequestration Using Paste Encapsulation Technology.” *Geo-Congress 2019*, Proceedings, 167–176.
- Marty, N. C. M., Grangeon, S., Elkaïm, E., Tournassat, C., Fauchet, C., and Claret, F. (2018). “Thermodynamic and crystallographic model for anion uptake by hydrated calcium aluminate (AFm): An example of molybdenum.” *Scientific Reports*, 8(1), 1–13.
- McMurdie, H., Morris, M., Evans, E., Paretzkin, B., Wong-ng, W., and Zhang, Y. (1986). “Calcium aluminum sulfate hydroxide hydrate, $\text{Ca}_6\text{Al}_2(\text{SO}_4)_3(\text{OH})_{12}\cdot 26\text{H}_2\text{O}$.” *Powder Diff.*, 4(337), 398–413.

Mctigue, N. E., Cornwell, D. A., Graf, K., and Brown, R. (2014). "Occurrence and consequences of increased bromide in drinking water sources." *Journal - American Water Works Association*, American Water Works Association, 106(11), E492–E508.

Mesbah, A., François, M., Cau-Dit-Coumes, C., Frizon, F., Filinchuk, Y., Leroux, F., Ravaux, J., and Renaudin, G. (2011). "Crystal structure of Kuzel's salt $3\text{CaO}\cdot\text{Al}_2\text{O}_3\cdot\frac{1}{2}\text{CaSO}_4\cdot\frac{1}{2}\text{CaCl}_2\cdot 11\text{H}_2\text{O}$ determined by synchrotron powder diffraction." *Cement and Concrete Research*, Pergamon, 41(5), 504–509.

Mills, S. J., Christy, A. G., Génin, J.-M. R., Kameda, T., and Colombo, F. (2012). "Nomenclature of the hydrotalcite supergroup: natural layered double hydroxides." *Mineralogical Magazine*, De Gruyter, 76(05), 1289–1336.

Myneni, S. C. B., Traina, S. J., and Logan, T. J. (1998). "Ettringite solubility and geochemistry of the $\text{Ca}(\text{OH})_2\text{-Al}_2(\text{SO}_4)_3\text{-H}_2\text{O}$ system at 1 atm pressure and 298 K." *Chemical Geology*, Elsevier, 148(1–2), 1–19.

Myneni, S. C. B., Traina, S. J., Logan, T. J., and Waychunas, G. A. (1997). "Oxyanion behavior in alkaline environments: Sorption and desorption of arsenate in ettringite." *Environmental Science and Technology*, American Chemical Society, 31(6), 1761–1768.

Oza, S., Ogunro, V., Ellison, K. M., and Daniels, J. (2015). "Sequestration of Halides from FGD Wastewater through Lime Stabilization of Fly Ash." *2015 World of Coal Ash Conference*, 13.

Palmer, S. J., Frost, R. L., and Nguyen, T. (2009). "Hydrotalcites and their role in coordination of anions in Bayer liquors: Anion binding in layered double hydroxides." *Coordination Chemistry Reviews*, Elsevier, 253(1–2), 250–267.

Perkins, R. B., and Palmer, C. D. (1999). "Solubility of ettringite ($\text{Ca}_6[\text{Al}(\text{OH})_6]_2(\text{SO}_4)_3\cdot 26\text{H}_2\text{O}$) at 5–75°C." *Geochimica et Cosmochimica Acta*, Pergamon, 63(13–14), 1969–1980.

Poellmann, H., Auer, S., Kuzel, H. J., and Wenda, R. (1993). "Solid solution of

ettringites. Part II: Incorporation of $B(OH)_4$ - and CrO_4^{2-} -in $3CaO \cdot Al_2O_3 \cdot 3CaSO_4 \cdot 32H_2O$.” *Cement and Concrete Research*, Pergamon, 23(2), 422–430.

Pretorius, C., Hareepsad, S., and Ellison, K. (2017). “Mineralogical & Geochemical Evaluation of Brine-Encapsulated Monoliths.” *2017 World of Coal Ash Conference*, 17.

Renaudin, G., Kubel, F., Rivera, J. P., and Francois, M. (1999). “Structural phase transition and high temperature phase structure of Friedels salt, $3CaO \cdot Al_2O_3 \cdot CaCl_2 \cdot 10H_2O$.” *Cement and Concrete Research*, 29(12), 1937–1942.

Renaudin, G., Rapin, J.-P., Elkaim, E., and François, M. (2004). “Polytypes and polymorphs in the related Friedel’s salt $[Ca_2Al(OH)_6] + [X \cdot 2H_2O]$ – halide series.” *Cement and Concrete Research*, 34(10), 1845–1852.

Renaudin, G., Segni, R., Mentel, D., Nedelec, J. M., Leroux, F., and Taviot-Gueho, C. (2007). *A Raman study of the sulfated cement hydrates: Ettringite and monosulfoaluminate. Journal of Advanced Concrete Technology.*

Renew, J. E., Huang, C.-H., Burns, S. E., Carrasquillo, M., Sun, W., and Ellison, K. M. (2016). “Immobilization of Heavy Metals by Solidification/Stabilization of Co-Disposed Flue Gas Desulfurization Brine and Coal Fly Ash.” *Energy & Fuels*, American Chemical Society, 30(6), 5042–5051.

Ruhl, L., Vengosh, A., Dwyer, G. S., Hsu-Kim, H., Schwartz, G., Romanski, A., and Smith, S. D. (2012). “The Impact of Coal Combustion Residue Effluent on Water Resources: A North Carolina Example.” *Environmental Science & Technology*, American Chemical Society, 46(21), 12226–12233.

Sheng, G., Hu, J., Li, H., Li, J., and Huang, Y. (2016). “Enhanced sequestration of $Cr(VI)$ by nanoscale zero-valent iron supported on layered double hydroxide by batch and XAFS study.” *Chemosphere*, Pergamon, 148, 227–232.

Shi, C., and Spence, R. (2004). “Designing of cement-based formula for solidification/stabilization of hazardous, radioactive, and mixed wastes.” *Critical Reviews*

in Environmental Science and Technology, Taylor & Francis Group.

Terzis, A., Filippakis, S., Kuzel, H.-J., and Burzlaff, H. (1987). “The crystal structure of $\text{Ca}_2\text{Al}(\text{OH})_6\text{Cl} \cdot 2\text{H}_2\text{O}$.” *Zeitschrift für Kristallographie - Crystalline Materials*, De Gruyter Oldenbourg, 181(1–4), 29–34.

USEPA. (2009). “Particulate Matter | Air & Radiation | US EPA.”
<<http://www3.epa.gov/airquality/particlepollution/index.html>> (Jan. 19, 2016).

USEPA. (2015). “Steam Electric Power Generating Effluent Guidelines - 2015 Final Rule.” <<https://www.epa.gov/eg/steam-electric-power-generating-effluent-guidelines-2015-final-rule>> (Oct. 16, 2020).

Vieille, L., Rousselot, I., Leroux, F., Besse, J. P., and Taviot-Guého, C. (2003). “Hydrocalumite and Its Polymer Derivatives. 1. Reversible Thermal Behavior of Friedel’s Salt: A Direct Observation by Means of High-Temperature in Situ Powder X-ray Diffraction.” *Chemistry of Materials*, American Chemical Society, 15(23), 4361–4368.

Warren, C. J., and Reardon, E. J. (1994). “The solubility of ettringite at 25°C.” *Cement and Concrete Research*, Pergamon, 24(8), 1515–1524.

Yang, L., Shahrivari, Z., Liu, P. K. T., Sahimi, M., and Tsotsis, T. T. (2005). “Removal of trace levels of arsenic and selenium from aqueous solutions by calcined and uncalcined layered double hydroxides (LDH).” *Industrial and Engineering Chemistry Research*, 44(17), 6804–6815.

Yue, Y., Wang, J. J., Basheer, P. A. M., and Bai, Y. (2018). “Raman spectroscopic investigation of Friedel’s salt.” *Cement and Concrete Composites*, Elsevier Ltd, 86, 306–314.

Zhang, D., Jia, Y., Ma, J., and Li, Z. (2011). “Removal of arsenic from water by Friedel’s salt (FS: $3\text{CaO} \cdot \text{Al}_2\text{O}_3 \cdot \text{CaCl}_2 \cdot 10\text{H}_2\text{O}$).” *Journal of Hazardous Materials*, 195, 398–404.

Zhang, J., Zhao, H., Cao, H., Li, H., and Li, Z. (2013). “Removal of Cd^{2+} from water by

Friedel's salt (FS: $3\text{CaO}\cdot\text{Al}_2\text{O}_3\cdot\text{CaCl}_2\cdot 10\text{H}_2\text{O}$): Sorption characteristics and mechanisms." *Journal of Environmental Sciences (China)*, Elsevier, 25(9), 1719–1725.

Zhang, M., and Reardon, E. J. (2003). "Removal of B, Cr, Mo, and Se from wastewater by incorporation into hydrocalumite and ettringite." *Environmental Science and Technology*, American Chemical Society, 37(13), 2947–2952.

Zhang, W., Oswal, H., Renew, J. E., Gallagher, B., Ellison, K., and Huang, C. H. (2020). "Solidification/stabilization of flue gas desulfurization brine and coal fly ash for heavy metals and chloride immobilization: Effects of S/S conditions and zero-valent-iron pretreatment." *Journal of Hazardous Materials*, Elsevier B.V., 384, 121463.

Zhang, W., Oswal, H., Renew, J., Ellison, K., and Huang, C. H. (2019). "Removal of heavy metals by aged zero-valent iron from flue-gas-desulfurization brine under high salt and temperature conditions." *Journal of Hazardous Materials*, Elsevier B.V., 373, 572–579.

CHAPTER 2: EFFECT OF REACTION TEMPERATURE ON THE STRUCTURE OF FRIEDEL'S SALT

Abhisek Manikonda, Vincent O. Ogunro, Kirk M. Ellison, Keith Moo-Young

Citation

Manikonda, A., Ogunro, V. O., Ellison, K. M., and Moo-Young, K. (2019). "Synthesis of Friedel's Salt for Application in Halide Sequestration Using Paste Encapsulation Technology." *In Geo-Congress 2019: Geoenvironmental Engineering and Sustainability*, 167–176. With permission from ASCE.

Abstract

An emerging strategy for the management of flue gas desulfurization wastewater (FGDWW) involves volume reduction of the FGDWW by concentrating to brine and then mixing the brine with fly ash and other chemical additives to form a paste suitable for landfill disposal. This process, termed as paste encapsulation technology, has not achieved the same level of success in immobilizing halides as achieved in sequestering heavy metals, because of the high solubility and elevated concentrations of halides in the brines. The focus of this study is to synthesize and characterize AFm (alumina, ferric oxide, monosulfate) phases like Friedel's salt (FS) in the laboratory using reagent-grade chemicals. The formation of these AFm phases in the brine-fly ash paste can enhance the encapsulation of halides in the paste. The structure and morphology of the synthesized samples were examined using thermogravimetric analysis (TGA), and x-ray diffraction (XRD). The total mass loss of FS, calculated using TGA, was comparable to the theoretical value. The XRD patterns also showed good agreement to a monoclinic layered double-hydroxide structure. Using these optimized operating variables, preliminary results of

phase formation will be assessed using field materials such as fly ash, wastewater brine, and chemical binders.

2.1. Introduction and Background

Disposal of wastewater from wet flue gas desulfurization (FGD) systems is a major concern for the coal-fired power plant industry. According to a USEPA report, most of the high concentrations of metals (Ca, Na, As, Cr) and halides (Cl, Br) encountered in waste from coal-fired power plants occur in FGD systems and hydraulic coal fly ash (CFA) transportation systems. The major source of halides is from coal, while additives like CaCl_2 and CaBr_2 , which are added as dust suppressants and emission control measures to increase mercury capture, are minor sources. Flue gas in the wet FGD system are sprayed into or bubbled through Ca or Ca-Mg slurries in order to remove sulfur oxides (SO_x). However, along with the SO_x removal, metals and halides partition from the gas phase (flue gas) to the aqueous phase and accumulate in the FGD slurry. FGD wastewater generally contains high concentrations of total dissolved solids (TDS). Chloride (Cl) and sulfate (SO_4) are the dominant anions in FGD wastewater. Calcium (Ca), Magnesium (Mg), and Sodium (Na) are the dominant cations in the wastewater. FGD wastewater also has significant concentrations of heavy metals like Arsenic (As), Selenium (Se) and Mercury (Hg) (USEPA 2009).

Discharge of high TDS wastewaters can have negative environmental impacts including, promotion of pitting corrosion, increased metal leaching from sediments, and formation of disinfection byproducts (Boelter et al., 1992). Therefore, USEPA released the proposed final revision to the Steam Electric Power Effluent Limitation Guidelines (ELG)

which regulate FGD wastewater and other processed water (USEPA 2015), including discharge limits for many pollutants. One potential pathway being explored to manage FGD wastewater is the zero-liquid discharge (ZLD) strategy. The principle of the ZLD strategy involves reducing the volume of FGD wastewater to concentrated brine using technologies such as evaporators or advanced membrane processes such as dynamic shear enhanced membrane filtration (DSEMF), forward osmosis (FO), and membrane distillation (MD). However, such volume reduction approaches still result in a residual brine or salt that must be managed. Through the process, termed as “paste encapsulation technology”, brine is mixed in cementitious matrices of fly ash and hydraulic chemical binder to form a solidified and stabilized paste. While this approach provides a material that is suitable for landfill disposal, its primary goal is to provide for long term sequestration of constituents from the FGD wastewater and coal fly ash.

Paste encapsulation technology is similar to the solidification/stabilization (S/S) typically used to treat and remediate hazardous wastes into an environmentally acceptable form. The USEPA has identified S/S as the best demonstrated available technology for 57 hazardous sites (Shi and Spence 2004). Traditional applications of S/S use ordinary Portland cement (OPC) as the primary binder (Batchelor 2006) and has been shown to be a viable treatment process for sequestering heavy metals in the solid form (Batchelor 2006). However, the availability of coal fly ash (CFA) at facilities producing FGD wastewater provides a unique opportunity. According to a report by the American Coal Ash Association in 2015, nearly 50 million tons of fly ash are produced annually in the United States, with similar amounts produced in western Europe and throughout the world. Most types of fly ashes are considered to be pozzolonic in nature, and its geotechnical

properties and lime-binding capacity makes it suitable for use in the solidification and stabilization of FGD wastewater (Ahmaruzzaman 2010). Traditional S/S approaches involve transporting the mixed material by truck and conveyor to the landfill. However, this approach has several drawbacks. The liquid-to-solid ratio is limited by what can be safely transported by truck (typically 15-18%). This range of moisture content limits the magnitude of hydration and falls short of the adequate moisture required to form stable mineral phases in the cementitious mixture.

However, the paste technology, which transports material via pipeline, allows material to be pumped directly into a landfill. This technology allows for increase of the liquid-to-solid ratio, which means higher volumes of wastewater can be disposed with the fly ash as well as providing enough moisture to allow adequate hydration reactions. Pastes mixture can contain 30% or more wastewater in the mix design while maintaining a non-segregating grout-like consistency that is distinct from a wet slurry. Additionally, due to its thixotropic properties, the material can be pumped via pipeline over significant distances. Upon deposition, the paste transforms into a hardened dense material with low permeability (Ellison 2015). Due to the potential benefits of this approach, paste encapsulation technology is being investigated for its feasibility as an option for the integrated disposal of fly ash and FGD wastewater (Ellison 2015).

2.2. Motivation and Strategy

Paste encapsulation technology is a key component of the “closed-loop” iterative FGD wastewater management process in many steam electric power facilities. The overarching goal of this process is to develop an optimized and sustainable wastewater

treatment processes in terms of overall cost, concentrated brine-fly ash mass balance, landfill management, and environmental contamination prevention. However, the technology must also be evaluated for its ability to sequester constituents of concern such as heavy metals and halides. Leaching studies by Oza et al. (2015) have shown that the halides in the paste encapsulation are still mobile.

The motivation of this study is to enhance the sequestration of halides in the paste and prevent the halides from leaching out into the groundwater or surface waters. One strategy of sequestering halides in paste is by preferential formation of layered double hydroxides (LDHs) in the paste. The LDHs are positively charged stacked layers with hydrated charge-balancing anions in the interlayer (Marty et al. 2018, Baquerizo et al. 2015). The broad objective is to improve halide sequestration in the fly ash-brine paste by substituting halides and sulfate in high aluminate cementitious materials to form LDHs such as AFm (alumina, ferric oxide, monosulfate) and AFt (alumina, ferric oxide, trisulfate) phases. AFm and AFt are solid phases that form in hydrated cement systems when alumina combines with water, calcium, and substituents including hydroxide, carbonate, sulfate, and halides. The general formula of an AFm phase is $[Ca^{2+}_4(Al^{3+}_xFe^{3+(1-x)})_2(OH)_{12}] \cdot A \cdot nH_2O$, where $A \cdot nH_2O$ represents the hydrated exchangeable interlayer anions (Marty et al. 2018). The well-known AFm family of phases include: hydroxy-AFm, monosulfoaluminate, monocarboaluminate, hemicarboaluminate, Friedel's salt $[Ca_2Al(OH)_6Cl \cdot 2H_2O]$, and Kuzel's salt $[3CaO \cdot Al_2O_3 \cdot 1/2CaCl_2 \cdot 1/2CaSO_4 \cdot \sim 11H_2O]$. The AFt family of phases includes ettringite $[Ca_6Al_2(SO_4)_3(OH)_{12} \cdot 26H_2O]$ with carbonate, sulfate, and chloride as substituents. Some of the properties that influence the formation of AFm phase over the AFt phase include the available Al_2O_3/SO_4 molar ratio, pH, and

temperature (Renew et al. 2016). The AFm phase is generally promoted over the AFt phase formation when the $\text{Al}_2\text{O}_3/\text{SO}_4^{2-}$ molar ratios is greater than 1.0.

Friedel's salt or hydrocalumite (Figure 1.3), is an anion-exchange mineral belonging to the layered double hydroxides (LDHs) family (Birnin-Yauri and Glasser 1998). Although the natural occurrences of hydrocalumite are rare, they have been studied in a wide range of synthetic examples and are important constituents of cement-based materials subjected to high halide concentration environment (Mills et al. 2012). Furthermore, semi-quantitative XRD analysis conducted by Pretorius et al. (2017) on two mixes made using brine (Cl^- conc.: 180000 mg/L), fly ash (ASTM class F), and quick lime recorded the occurrence of trace amounts (0-3%) of hydrocalumite mineral in hardened paste encapsulation samples.

Friedel's salt is widely used in environmental remediation, particularly dealing with heavy metals from wastewater because of its high adsorption efficiency (Ma et al. 2015). Various studies have shown that Friedel's salt can be used for the removal of boron and chromium (Zhang and Reardon 2003), and arsenic (Li et al. 2017) from wastewater. However, not many studies have investigated the capability of halide sequestration by enhancing the formation of AFm and AFt phases in fly ash-brine cementitious paste systems. High concentrations of chloride in the FGD wastewater brine can be used to form the LDHs, thereby encapsulating them in the paste. Calcium and aluminum are also essential elements to form LDHs. FGD wastewater brine has high concentrations of calcium, which is further supplemented by the addition of chemical additives like lime. Most types of fly ashes have high aluminum content and can be released due to the pozzolonic activity of the fly ash. Therefore, the essential elements for the formation of

LDHs are already available in the fly ash-brine paste. Most importantly, Friedel's salt, Kuzel's salt, ettringite, and other cementitious mineral phases are significantly more stable and relatively insoluble compared to common salts like NaCl, CaCl₂, AlCl₃ and cement minerals like portlandite and CSH as illustrated with their solubility product constant values in Table 1.2.

The formation of LDHs is important to the chemical stabilization and long-term sequestration of halides in cementitious matrices. This paper presents some preliminary results about the synthesis and characterization of Friedel's salt. The variables (like reaction temperature, calcium/aluminum ratio, atmospheric conditions, and molar concentrations) that influence the formation of Friedel's salt in field relevant scenarios will be investigated. The optimized operating variables will be used to assess the phase formation when field materials such as fly ash, wastewater brine, and chemical binders are used.

2.3. Experimental Investigation

2.3.1. Reagents

The starting materials CaCl₂, Al(OH)₃, NaOH, NaAlO₂, and AlCl₃ for the preparation of Friedel's salt (FS) were of analytical grade and were used without further purification. Ultrapure deionized water (18 MΩ) was used for solution preparation and washing.

2.3.2. Preparation of Friedel's Salt

Friedel's salt was prepared using three different protocols in order to determine the most appropriate protocol that can be implemented in field conditions. Each protocol was carried out at three different temperatures (25 °C, 50 °C, 75 °C) to determine the effect of the temperature of the FS structure. All the experiments were carried out in ambient atmospheric conditions.

- Protocol 1 (P1): Friedel's salt was prepared according to procedure followed in Ma et al. (2015). Aluminum hydroxide ($\text{Al}(\text{OH})_3$) was dissolved in 2 M NaOH to form $\text{NaAl}(\text{OH})_4$, and the reaction solution was heated to the desired temperature while continuously stirring. When the solution reached the desired temperature, 1.5 M CaCl_2 was added dropwise. When CaCl_2 addition was completed, stirring was continued for an additional one hour.

- Protocol 2 (P2): Protocol 2 is similar to P1, but instead of using $\text{Al}(\text{OH})_3$ and NaOH to prepare $\text{NaAl}(\text{OH})_4$, reagent grade NaAlO_2 was dissolved directly in 18 MΩ water to form $\text{NaAl}(\text{OH})_4$ (Zhang et al. 2011). The reaction solution was heated to the desired temperature, and 2 M CaCl_2 was then added dropwise under continuous stirring. When CaCl_2 addition was completed, stirring was continued for an additional one hour.

- Protocol 3 (P3): The synthesis was done by the procedure outlined by Vieille et al. (2003). A mixed solution of 1.32 M CaCl_2 and 0.66 M AlCl_3 was added dropwise to the reactor containing 2 M NaOH under continuous stirring. NaOH was heated to the desired reaction temperature prior to the addition. Similar to P1 and P2, stirring was continued for an additional hour after the completion of the addition procedure.

In the case of all three protocols, the white precipitate was collected at the end of the stirring period by filtration using a 0.45 μm PTFE filters. The precipitate was then washed with 18 M Ω water three time to remove any remaining ions, and finally dried in an oven at 100 $^{\circ}\text{C}$ for 24 hours. An example of the experimental test setup for the synthesis of Friedel's salt is shown in Figure 2.1.

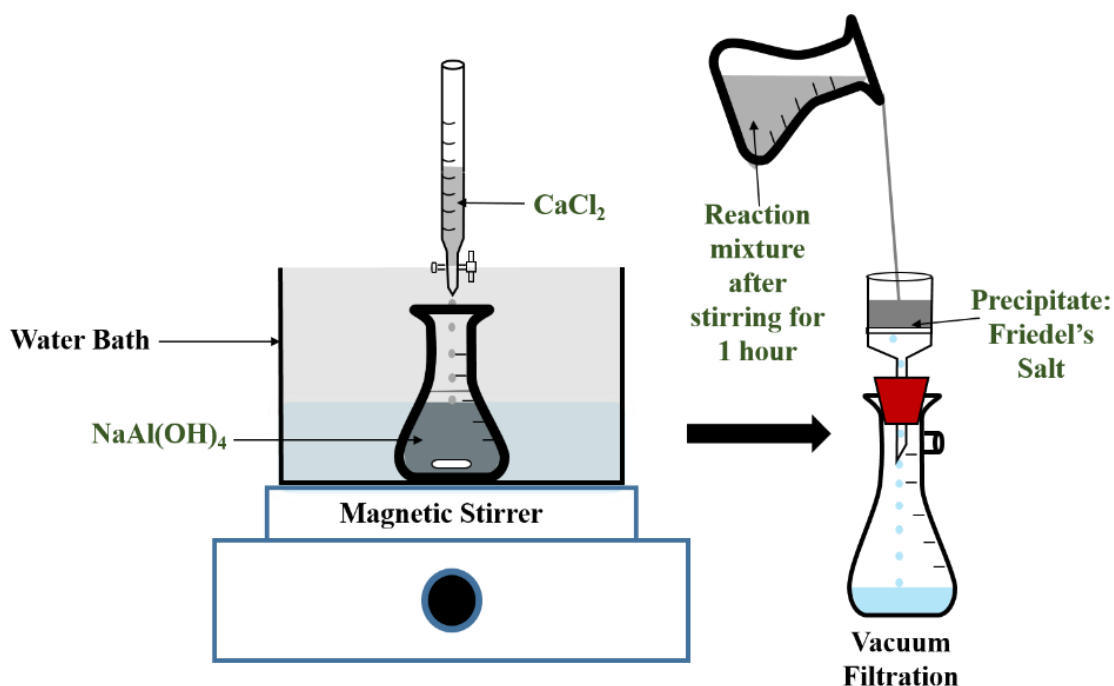


Figure 2.1. Illustration of experimental set-up of synthesis of Friedel's salt

2.3.3. Characterization and Purification of Friedel's Salt

The microstructure of the synthesized samples were characterized using thermogravimetric analysis and differential scanning calorimetry (TGA-DSC), and X-ray powder diffraction (XRD). The TGA-DSC analysis was performed using a SDT Q600 (TA Instruments, Delaware) by heating the specimen from room temperature to 1000 $^{\circ}\text{C}$ in a

nitrogen atmosphere at a rate of 20 °C/min. X-ray powder diffraction patterns were recorded using a PANalytical (Netherlands) X'Pert PRO diffractometer ($2\theta = 5-70^\circ$, stepsize 0.02° with 0.5 s/step). The supernatant obtained from the filtration of the precipitate was analyzed for concentrations of Cl^- , using an ICS-3000 ion chromatography system (Dionex, California), and for Al^{+3} , Ca^{+2} , and Na^+ , using a 5100 ICP-OES instrument (Agilent, California).

The synthesized samples were also purified in two different methods; immersion in 18 M Ω water at liquid-to-solid ratio of 20:1 and kept stationary for 24 hours, and immersion in 18 M Ω water at liquid-to-solid ratio of 20:1 followed by continuous tumbling at 28 rpm for 24 hours. The precipitate was filtered after the end of the tumbling period and dried in an oven at 100 °C for 24 hours. The dried sample was characterized using TGA-DSC and XRD. The supernatant from the filtration was analyzed for concentrations of Cl^- , Al^{+3} , and Ca^{+2} ions.

2.4. Results and Discussion

2.4.1. Microstructure of Friedel's Salt

Thermogravimetric analysis of the samples synthesized at a reaction temperature of 50 °C are shown in Figure 2.3 (TGA) and Figure 2.2 (DSC). According to Vieille et al. (2003), Friedel's salt has three main weight losses over the temperature ranges 150 – 180 °C (removal of interlayer water), 250 – 400 °C (dehydroxylation of hydroxide layers), and 400 - 1000 °C (recombination of hydroxyl groups and carbonate decomposition). The percent mass loss over the three temperature ranges for the samples from the three

protocols are given in Table 2.1. The theoretical total mass loss for FS is 32.09% (Vieille et al. 2003).

Although the percent total mass loss for the samples from the three protocols is comparable to the theoretical total mass loss, the mass loss between each temperature range varies from the theoretical values for all the samples. Comparing the TGA (Figure 2.3) and DSC (Figure 2.2) curves for P1 and P2 samples and values in Table 2.1, it is observed that there is a higher percentage of mass loss between temperature range of 250 – 400 °C than 0 – 250 °C. However, this percent mass loss is less than the theoretical mass. Also, P1 samples had a 10% mass loss in 400 - 1000 °C range but the theoretical loss should have been less than 1%. Sample P3 had a higher mass loss in the temperature range between 0 – 250 °C than 250 – 400 °C. Since the TGA-DSC analysis was performed on unpurified samples, the speculation is that there is still presence of impurities in the samples. Impurities like CaCl_2 and AlCl_3 are hygroscopic and they absorb moisture during storage though were oven dried at 100 °C. This could be the reason there is mass loss for temperatures less than 100 °C in the TGA, particularly for sample P3 (Figure 2.3). The above interpretations indicate that the samples from the three protocols did not yield a well-ordered structure of Friedel's salt.

The influence of reaction temperature was not significant in the case of protocols P1 and P2. The major difference was that the percent loss of interlayer water at 150 – 180 °C was less for sample synthesized at 25 °C compared to the samples at 50 °C and 75 °C. However, in the case of P3, the DSC and TGA profiles were different for reaction at 25 °C compared to 50 and 75 °C. The total mass loss (27.5%) was less an anecdotal evident that

the FS formation increased with temperature, but the loss of mass due to dehydroxylation of hydroxide layers at 250 – 400 °C was higher.

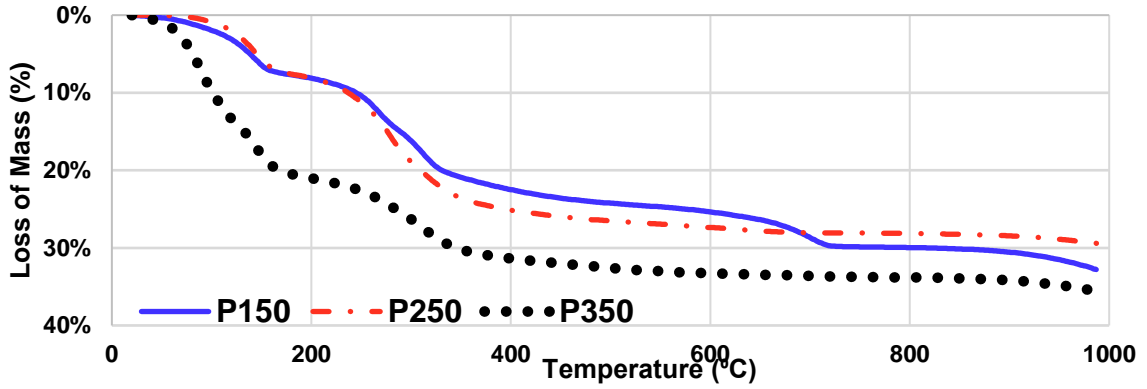


Figure 2.3. Comparison of weight loss data recorded by TGA for samples synthesized using protocols P1 (—), P2 (-·-), and P3 (···) at a reaction temperature of 50 °C

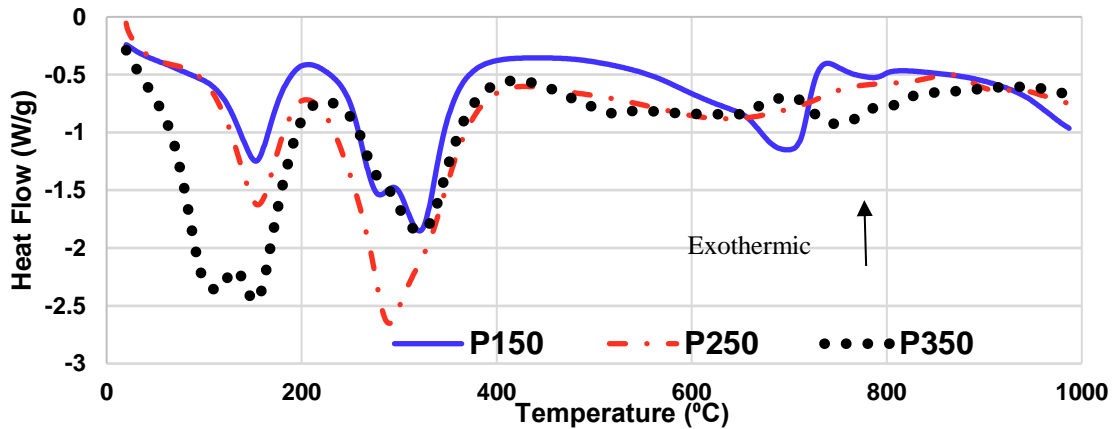


Figure 2.2. Comparison of DSC curves recorded for samples synthesized using protocols P1 (—), P2 (-·-), and P3 (···) at a reaction temperature of 50 °C

Table 2.1. Comparison of the % mass lost over the three different temperatures ranges

Protocol	Reaction Temperature (°C)	Mass of the Sample Lost (%)			Total Mass Lost (%)
		T < 250 °C	250 °C < T < 400 °C	400 °C < T < 1000 °C	
Vieille et al. (2003)		12.8	19.2	0.9	32.9
P1	25	8.74	13	10.10	31.84
	50	10.29	12.13	10.36	32.78
	75	10.48	11.96	10.77	33.21
P2	25	7.14	14.28	4.67	26.09
	50	11.17	13.95	4.26	29.38
	75	11.57	13.89	4.33	29.79
P3	25	8.14	14.25	5.13	27.52
	50	22.60	8.79	4.27	35.65
	75	23.57	8.68	4.31	36.56

The XRD pattern of P1, P2, and P3 samples at 25 °C and 50 °C are shown in Figure 2.4. It can be observed that the FS samples synthesized from the three protocols show a typical layered structure with sharp peaks at $2\theta = 11.25^\circ$ (0 0 2), 22.66° (0 0 4), 23.49° (2 0 2), 31.09° (0 2 0). Sample P1 has an additional sharp peak at $2\theta = 29.45^\circ$. The XRD diffractogram of the P1, P2, and P3 samples at 75 °C closely resembled the diffractogram when the reaction temperature was 25 °C or 50 °C. Similar to the TGA-DSC analysis, it was observed from the XRD patterns that the reaction temperature did not have a significant effect on the structure of the final product for all three synthesis protocols. Samples P2 and P3 display a good agreement with the profile of the monoclinic LDH structure (PDF 00-044-0616 (ICDD, 2010)), with a chemical formula of $\text{Ca}_4\text{Al}_2\text{H}_{0.34}\text{O}_{6.34}\text{Cl}_{1.67}$. Sample P1 showed a good agreement with the profile of a different monoclinic LDH structure (PDF 00-019-0202 (ICDD, 2010)) with the chemical formula $\text{Ca}_4\text{Al}_2\text{O}_6\text{Cl}_2 \cdot 10\text{H}_2\text{O}$, but the additional sharp peak at 29.45° could not be matched with the

diffraction data file. The XRD patterns further strengthen the argument that the samples from the three protocols did not yield a well-ordered structure of Friedel's salt.

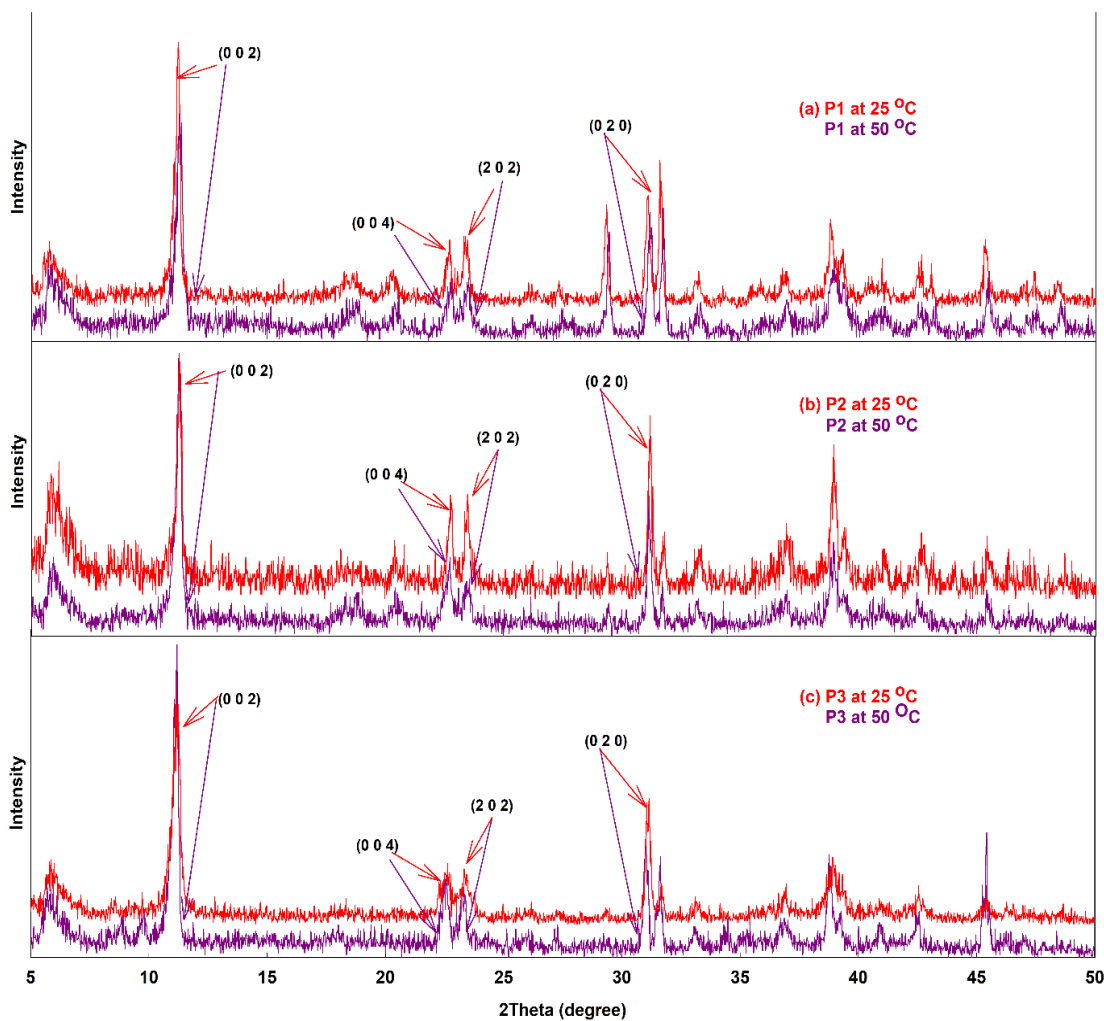


Figure 2.4. X-ray pattern of a) P1 b) P2 C) P3 at 25 °C and 50 °C

2.5. Conclusions and Future Work

Friedel's salt was synthesized using three different protocols. These protocols followed the synthesis methods outlined in various studies. The synthesized samples were characterized using XRD and TGA-DSC.

Samples from protocols P1, P2, and P3 had a total mass loss comparable to the theoretically calculated value. However, the profile of mass loss in the three main temperature ranges is different than the profile described by Vieille et al. (2003). The influence of the reaction temperature was not significant for P1 and P2 samples, but the P3 sample at 25 °C had a different TGA-DSC profile compared to samples at 50 °C and 75 °C. The XRD patterns for the three protocols showed good agreement to a profile of a monoclinic LDH structure. The diffractograms recorded for the three reaction temperatures were similar. Therefore, it can be concluded that the reaction temperature does not alter the structure of the final product. This is significant in field conditions since the synthesis would be carried out at ambient outdoor temperature.

Although the above interpretations indicate that the samples from the three protocols did not yield a well-ordered structure of Friedel's salt, nevertheless significant mass of chloride has been sequestered. The next step is to vary the Ca:Al ratio and repeat the synthesis and characterization of Friedel's salt. The effect of the atmospheric conditions on the formation of the phases will also be evaluated by performing the reactions under carbon-rich and nitrogen-rich atmospheres. The stability and the solubility of the final product for long-term sequestration of halides will be investigated under various pH conditions. The optimized operating conditions obtained from the various experiments will be employed to synthesize FS using field raw materials such as fly ash and brine to establish the realistic formation potential in field relevant scenarios. Outcomes of this study will be used to improve paste mix design and will provide solubility constant (K_{sp}) values for thermodynamic modeling of halide sequestration in paste.

References

- Ahmaruzzaman, M. (2010). "A review on the utilization of fly ash." *Progress in energy and combustion science*, 36(3), 327-363.
- ACAA (American Coal Ash Association). (2015) *Production and Use of Coal Combustion Products in the U.S.* Retrieved from <https://www.aaa-usa.org/Portals/9/Files/PDFs/ReferenceLibrary/ARTBA-final-forecast.compressed.pdf>.
- Balonis, M., Lothenbach, B., Le Saout, G., and Glasser, F. P. (2010). "Impact of chloride on the mineralogy of hydrated Portland cement systems." *Cement and Concrete Research*, 40(7), 1009-1022.
- Baquerizo, L. G., Matschei, T., Scrivener, K. L., Saeidpour, M., and Wadsö, L. (2015). "Hydration states of AFm cement phases." *Cement and Concrete Research*, 73, 143-157.
- Batchelor, B. (2006). "Overview of waste stabilization with cement." *Waste management*, 26(7), 689-698.
- Boelter, A. M., Lamming, F. N., Farag, A. M., and Bergman, H. L. (1992). "Environmental effects of saline oil-field discharges on surface waters." *Environmental Toxicology and Chemistry*, 11(8), 1187-1195.
- Birnin-Yauri, U. A., and Glasser, F. P. (1998). "Friedel's salt, $\text{Ca}_2\text{Al}(\text{OH})_6(\text{Cl}, \text{OH}) \cdot 2\text{H}_2\text{O}$: its solid solutions and their role in chloride binding." *Cement and Concrete Research*, 28(12), 1713-1723.
- Duchesne, J., and Reardon, E. J. (1995). "Measurement and prediction of portlandite solubility in alkali solutions." *Cement and Concrete Research*, 25(5), 1043-1053.
- Ellison, K. (2015). "Industry Perspectives on Integrating ELG and CCR Compliance through Wastewater Encapsulation: Challenges, Opportunities, and Technology Readiness." *2015 World of Coal Ash Conference*. Retrieved from <http://www.flyash.info/2015/065-ellison-2015.pdf>.

- Li, D., Guo, X., Tian, Q., Xu, Z., Xu, R., and Zhang, L. (2017). "Synthesis and application of Friedel's salt in arsenic removal from caustic solution." *Chemical Engineering Journal*, 323, 304-311.
- Lothenbach, B. (2010). "Thermodynamic equilibrium calculations in cementitious systems." *Materials and Structures*, 43, 1413–1433
- Ma, J., Li, Z., Jiang, Y., and Yang, X. (2015). "Synthesis, characterization and formation mechanism of friedel's salt (FS: $3\text{CaO} \cdot \text{Al}_2\text{O}_3 \cdot \text{CaCl}_2 \cdot 10\text{H}_2\text{O}$) by the reaction of calcium chloride with sodium aluminate." *Journal of Wuhan University of Technology. Materials Science Edition*, 30(1), 76.
- Marty, N. C., Grangeon, S., Elkaïm, E., Tournassat, C., Fauchet, C., and Claret, F. (2018). "Thermodynamic and crystallographic model for anion uptake by hydrated calcium aluminate (AFm): an example of molybdenum." *Scientific reports*, 8(1), 7943.
- Mills, S. J., Christy, A. G., Génin, J. M., Kameda, T., and Colombo, F. (2012). "Nomenclature of the hydrotalcite supergroup: natural layered double hydroxides." *Mineralogical Magazine*, 76(5), 1289-1336.
- Oza, S., Ogunro, V., Daniels, J., and Ellison, K. M. (2015). "Sequestration of Halides from FGD Wastewater through Lime Stabilization of Fly Ash." 2015 *World of Coal Ash Conference*. Retrieved from <http://www.flyash.info/2015/064-ogunro-2015.pdf>.
- Pretorius, C., Hareeparsad, S., and Ellison, K. (2017). "Mineralogical & Geochemical Evaluation of Brine-Encapsulated Monoliths." 2017 *World of Coal Ash Conference*. Retrieved from <http://www.flyash.info/2017/231-Pretorius-woca2017p.pdf>.
- Renew, J. E., Huang, C. H., Burns, S. E., Carrasquillo, M., Sun, W., and Ellison, K. M. (2016). "Immobilization of heavy metals by solidification/stabilization of co-disposed flue gas desulfurization brine and coal fly ash." *Energy & Fuels*, 30(6), 5042-5051.
- Shi, C., and Spence, R. (2004). "Designing of cement-based formula for solidification/stabilization of hazardous, radioactive, and mixed wastes." *Critical Reviews in Environmental Science and Technology*, 34(4), 391-417.

USEPA (U.S. Environmental Protection Agency) (2015). Effluent Limitations Guidelines and Standards for the Steam Electric Power Generating Point Source Category; Final Rule 40 CFR Part 423 *US E P Agency Federal Register*.

Vieille, L., Rousselot, I., Leroux, F., Besse, J. P., and Taviot-Guého, C. (2003).

“Hydrocalumite and its polymer derivatives. 1. Reversible thermal behavior of Friedel's salt: a direct observation by means of high-temperature in situ powder X-ray diffraction.” *Chemistry of Materials*, 15(23), 4361-4368.

Zhang, M., and Reardon, E. J. (2003). “Removal of B, Cr, Mo, and Se from wastewater by incorporation into hydrocalumite and ettringite.” *Environmental science & technology*, 37(13), 2947-2952.

Zhang, D., Jia, Y., Ma, J., and Li, Z. (2011). “Removal of arsenic from water by Friedel's salt (FS: $3\text{CaO} \cdot \text{Al}_2\text{O}_3 \cdot \text{CaCl}_2 \cdot 10\text{H}_2\text{O}$).” *Journal of hazardous materials*, 195, 398-404.

CHAPTER 3: ASSESSMENT OF HIGH CONCENTRATION CHLORIDE REMOVAL PERFORMANCE BY PRECIPITATION OF FRIEDEL'S SALT

Abhisek Manikonda, Vincent O. Ogunro, Sunyoung Bae

Abstract

Hypersaline brines like FGD wastewater concentrate are difficult to treat because of high chloride (Cl^-) concentration and currently, there are a lack of cost-effective and energy-efficient technologies for removal of chlorides. This research explored the feasibility of removing chloride from high-salinity brines through the precipitation of Friedel's salt. Factors affecting the reduction of concentration of chloride like the initial molar concentration of chloride and the calcium to aluminum (Ca:Al) ratio and the interactions between them were evaluated. The stability of the Friedel's salt products at various prevailing solutions and environmental conditions was investigated and an optimal calcium to aluminum ratio for the effective removal of chloride was established. Experimental results confirmed that the initial chloride concentration, rather than the Ca:Al ratio, highly influenced the mass of chloride sequestered in the Friedel's salt samples. It was also observed that Friedel's salt samples undergo congruent dissolution when mixed in water or solution at pH 13, while dissolution rate of all the samples in pH 2 solution was high with little residues remaining. Based on the fourier-transform infrared spectroscopy (FTIR) results and thermogravimetric analysis (TGA), it could be hypothesized that the synthesis of Friedel's salt using a calcium to aluminum ratio of 3:1 will be optimal for effective removal of chloride from hypersaline solutions. In addition, the results suggest that this process is a simple and effective method to treat high-salinity brines.

3.1. Introduction

Management and disposal of high-salinity brines is a major environmental concern (Boelter et al. 1992; Pramanik et al. 2017). Discharge of wastewater with high total dissolved solids (TDS) concentration can lead to negative environmental consequences including, formation of carcinogenic disinfection byproducts, increased metal leaching from sediments, and promotion of pitting corrosion (Boelter et al. 1992). The heavy metals and halides can bioaccumulate in fishes, impairing fish reproduction which can lead to negative impacts on human health due to the consumption of fish contaminated with high TDS wastewaters. Some examples of hypersaline brines include zero-liquid discharge concentrate from treatment of flue gas desulfurization (FGD) wastewater (Gingerich et al. 2018), cooling towers and ash transport water, and concentrate from desalination (Pramanik et al. 2017). Hypersaline brines like FGD wastewater concentrate contain high concentrations of anions such as chloride (5000 mg/L (0.1 M) – 300,000 mg/L (8.5 M)). Discharge of such high concentration chloride (Cl^-) into water bodies can have a detrimental impact on aquatic life (Gardner and Royer 2010) and can also promote pitting corrosion. Therefore, hypersaline brines need to be adequately treated to remove the high concentration of chloride before disposal.

Currently, chlorides from wastewater are removed by membrane technologies (reverse osmosis), evaporation-based thermal treatments like crystallization, chemical precipitation, and electrodialysis (Gingerich et al. 2018; Tong and Elimelech 2016). However, these approaches are energy intensive and are not suitable for treatment of wastewater with high chloride concentration like hypersaline brines. Therefore, there is a

need to develop a cost-effective and energy-efficient method for removal of chlorides from hypersaline brines.

Chemical precipitation by formation of layered double hydroxides (LDHs) can be an alternative approach for the removal of chloride because it is membrane-less and not energy-intensive like evaporation crystallization. Layered double hydroxides are a class of two-dimensional lamellar compounds based on the structure of brucite, $\text{Mg}(\text{OH})_2$. They consist of positively charged octahedral layers with a negatively charged interlayer consisting of water and anion molecules (Goh et al. 2008). Layered double hydroxides can be good adsorbents and ion-exchangers of contaminant ions due to the presence of a significant number of exchangeable anions in the interlayer and the availability of large interlayer spaces (Yang et al. 2005). Friedel's salt $[\text{Ca}_2\text{Al}(\text{OH})_6\text{Cl}\cdot 2\text{H}_2\text{O}]$ is an anion-exchange mineral belonging to the LDHs family (Birnin-Yauri and Glasser 1998). It is composed of hydroxide layers with Ca^{+2} and Al^{+3} octahedral units and an interlayer of Cl^- ions. Friedel's salt (FS) has been widely employed for environmental remediation of heavy metals from wastewater because of its high adsorption efficiency (Dai et al. 2009; Ma et al. 2015; Zhang and Reardon 2003). However, only a few studies have characterized the effect of process variables like solution pH and reaction temperature, among others, on the structure of FS and the removal of chloride. Studies like Fang et al. (2018), Ma et al. (2015), and Manikonda et al. (2019) have investigated the effects of initial CaCl_2 concentration, calcium to aluminum (Ca:Al) molar ratio, reaction time, and reaction temperature on the structure of Friedel's salt. Ma et al. (2015) and Manikonda et al. (2019) state that the final structure of FS was consistent for any synthesis reaction temperatures below 100 °C. However, Fang et al. (2018) noted that the removal efficiency of chloride from solution

decreased as the reaction temperature increased from 25 °C to 60 °C because of the change in phase of FS above 35 °C. Ma et al. (2015) observed that the initial concentration of CaCl_2 did not influence the structure of FS but changed the morphology of FS particles. Ma et al. (2015) and Fang et al. (2018) reported that the optimum range of Ca:Al molar ratio is 2-3:1.

However, none of the studies investigated the interactions between initial chloride concentration and the Ca:Al molar ratio and its effect on the reduction of chloride concentration. This study aims to evaluate the performance of high concentration chloride removal by the precipitation of Friedel's salt. The influence of interactions between initial chloride concentration and the Ca:Al molar ratio on chloride removal performance was investigated. A series of experiments were carried out to assess the stability of the FS products at various prevailing solutions and environmental conditions to simulate field scenarios. An optimal calcium to aluminum ratio for the effective removal of chloride was also established.

3.2. Materials and Methods

Hypersaline brines like FGD wastewater concentrate are characterized with an extremely complex composition matrix. It would be challenging to understand the factors that influence the formation of FS if synthesized using FGD wastewater concentrate. Therefore, FS was synthesized using laboratory grade reagents to determine the optimum operating variables. The starting materials CaCl_2 , $\text{Al}(\text{OH})_3$, NaOH , NaAlO_2 , AlCl_3 , $\text{Ca}(\text{OH})_2$, and NaCl for the preparation of FS were of analytical grade and were used

without further purification. Ultrapure deionized water (18 M Ω) was used for solution preparation and washing.

3.2.1. Synthesis and Characterization of Friedel's Salt

Friedel's salt was prepared using three different protocols in order to determine an optimum protocol in terms of mass of chloride sequestered and the relative propinquity of the structure of the synthesized sample compared to a well-ordered sample. The synthesis protocols have been outlined in Manikonda et al. (2019) and summarized below. Each protocol was carried out at 25 °C because Manikonda et al. (2019) reported that reaction temperature did not have a significant influence on the structure of Friedel's salt. All the experiments were performed in a laboratory setting under ambient atmospheric conditions.

- Protocol 1 (P1) (Ma et al. 2015): Al(OH)₃ was dissolved in NaOH to form NaAl(OH)₄, and the reaction solution was heated to the desired temperature under continuous stirring. When the solution reached the desired temperature, CaCl₂ was added dropwise at a rate of 5 mL/min.

- Protocol 2 (P2) (Zhang et al. 2011): Reagent grade NaAlO₂ was dissolved directly in ultrapure water to form NaAl(OH)₄. The reaction solution was heated to the desired temperature, and CaCl₂ was then added dropwise at a rate of 5 mL/min under continuous stirring.

- Protocol 3 (P3) (Vieille et al. 2003): A mixed solution of CaCl₂ and AlCl₃ was added dropwise at a rate of 5 mL/min to the reactor containing NaOH solution under

continuous stirring. The sodium hydroxide solution was heated to the desired reaction temperature prior to the addition.

In the case of each synthesis protocol, stirring was continued for an additional one hour after the completion of the addition of the reagents. The precipitate was collected at the end of the stirring period by vacuum filtration using 0.45 μm PTFE filters. The precipitate was then washed with ultrapure water and finally dried in an oven at 60 $^{\circ}\text{C}$ for 24 hours.

The microstructure of the synthesized FS samples was characterized using thermogravimetric analysis and differential scanning calorimetry (TGA-DSC), Fourier transform infrared (FTIR) spectroscopy, and X-ray powder diffraction (XRD). The TGA-DSC analysis was performed using a SDT Q600 (TA Instruments, Delaware) by heating the specimen from room temperature to 1000 $^{\circ}\text{C}$ in a nitrogen atmosphere at a rate of 20 $^{\circ}\text{C}/\text{min}$. The FTIR spectra was collected using a Spectrum One FTIR spectrometer (PerkinElmer, Massachusetts) in the range of 450-4000 cm^{-1} with a resolution of 1 cm^{-1} under transmission mode using KBr pellet method. X-ray powder diffraction patterns were recorded using a PANalytical (Netherlands) X'Pert PRO diffractometer ($2\theta = 5\text{-}50^{\circ}$, stepsize 0.02 $^{\circ}$ with 0.5 s/step). The supernatant obtained from the filtration of the precipitate was analyzed for concentrations of Cl^{-} , using an ICS-3000 ion chromatography system (Dionex, California), and for Al^{+3} , Ca^{+2} , and Na^{+} , using a 5100 ICP-OES instrument (Agilent, California). The solution used to wash the precipitate was also analyzed for concentrations of chloride and other ions. The pH and conductivity of the supernatant was measured with a SevenExcellence S470-Kit pH/conductivity meter (Mettler Toledo, Ohio).

3.2.2. Variation of Protocol Variables

The optimum protocol determined in the previous section was varied to investigate the influence of variables like calcium-to-aluminum ratio, atmospheric conditions, and molar concentrations on the formation of Friedel's salt. Previous studies have conducted FS synthesis only in inert atmospheres; therefore, the effect of ambient atmospheric conditions and carbon dioxide rich atmosphere has not been examined. The optimum protocol was synthesized in inert (N_2) and CO_2 rich atmosphere and any alterations in the structure were observed.

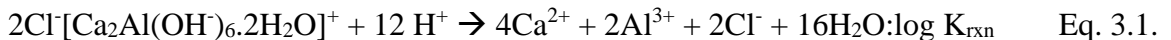
A two-factorial ANOVA design was implemented to understand the effect of variables like the molar concentration of Cl^- and Ca:Al ratio on the mass of chloride that was sequestered in the case of FS synthesis. The goal of the ANOVA design was to investigate the effects of the two variables and the interactions between them on the reduction of concentration of chloride. Table 3.1 summarizes the experimental conditions of the two variables, each at three levels, coded as -1, 0, and +1, for low, middle, and high values, respectively. The range of Ca:Al ratios were selected based on previous research by Fang et al. (2018), Ma et al. (2015), and Wang et al. (2018). The chloride concentration in FGD wastewater concentrate from different sources was found to be mainly between the range of 1 M to 2 M, therefore, the molar concentrations of chloride in the experimental design were selected accordingly. The additional calcium and chloride required to obtain the desired initial Ca:Al ratio and initial Cl^- concentration was supplemented using $Ca(OH)_2$ and NaCl, respectively.

Table 3.1. Levels of the factors tested in the two-factorial ANOVA design

Independent Factors	Coded and Absolute Levels		
	-1	0	1
Ca:Al Ratio	2:1	3:1	4:1
Initial Concentration of Cl ⁻	1 M	1.5 M	2 M

3.2.3. Solubility and Stability

In order to determine the stability and solubility product of FS in different environments, the synthesized samples were dispersed in three types of solutions (at 25 °C) at a liquid to solid ratio of 20 to 1: solution at pH natural (ultrapure water), solution at pH 2, and solution at pH 13. The dispersed samples were subjected to agitation for 18 hours. After agitation, the samples were extracted by vacuum filtration and were re-characterized. The supernatants were analyzed for concentrations of calcium, aluminum, and chloride. The measured molar concentrations were used as inputs to calculate the activities of the individual components using the geochemical speciation program PhreeqC (Parkhurst and Appelo 2013). Bothe and Brown (2004) used PhreeqC to calculate the solubility product (K_{sp}) of Friedel's salt. The dissociation equation (Equation 3.1) was presented by Bothe and Brown (2004) for the determination of the solubility product of Friedel's salt. Molar concentration of each component in Equation 3.1 was obtained experimentally and converted to their corresponding activities using PhreeqC. The equilibrium constant (log K_{rxn}) was specified as 73.5 (Bothe and Brown 2004) and other pertinent values were obtained from the wateq4f.dat database.



3.3. Results and Discussion

3.3.1. Selection of Optimum Protocol

In order to determine the optimum protocol, the three FS synthesis protocols (P1, P2, P3) were conducted with an initial chloride concentration of 1 M and at a Ca:Al ratio of 3:1. A FS sample synthesized using protocol P1 at a Ca:Al ratio of 3:1 (CA31) and an initial chloride concentration of 1M (CL1) is designated as P1CA31CL1.

Figure 3.1 reports the TGA and DSC curves of the FS samples synthesized using the three protocols. An ordered crystalline structure of FS has three weight loss steps: removal of interlayer water between the temperature range of 100 – 250 °C, dehydroxylation of hydroxide layers between 250 – 400 °C, and carbonate decomposition and recombination of hydroxyl groups between 400 – 1000 °C (Vieille et al. 2003). Carbonate phases could be formed during the sample preparation (Vieille et al. 2003; Yue et al. 2018). The total mass loss when ordered crystalline structure of FS sample is heated to 1000 °C is 32.9% (Vieille et al. 2003).

Evaluating the DSC (Figure 3.1(B)) and TGA (Figure 3.1(A)) curves, it can be observed that, for all the samples, a double endotherm centered at 170 °C and 320 °C was matched by two well-resolved mass loss steps. The total mass loss for P1, P2, and P3 protocols is 37.76%, 33.57%, and 34.22%, respectively (Table 3.2). Although, the total mass loss for the three protocols is comparable with the theoretical mass loss of an idealized FS structure (32.9%), the mass loss between the three individual temperature steps varies from the theoretical values for all the samples. Comparing the TGA and DSC curves and the values in Table 3.2, it is observed that there is a higher percentage of mass loss at the

100 – 250 °C step for all the three protocols compared to the 250 – 400 °C, contrary to the theoretical mass loss defined by Vieille et al. (2003). This suggests that a higher percentage of water molecules are present in the interlayer space instead of the main Ca-Al sheets (Yue et al. 2018). Also, all the samples had a higher percentage of mass loss in the 400 – 1000 °C range when the theoretical loss should have been less than one percent. Reactions between the raw chemicals like CaCl₂, NaAlO₂, AlCl₃, etc. could lead to formation of byproducts like NaCl and Al(OH)₃. These byproducts could be present in the samples which could be responsible for the higher percentage of mass loss between the temperature range of 100 – 250 °C. The increased mass loss after 400 °C can also be attributed to decomposition of the impurities and the carbonate phases in the samples. Among the three synthesis protocols, P1CA31CL1 had a higher mass loss (14.2%) in the 100 – 250 °C step compared to P2CA31CL1 (12.45 %) and P3CA31CL1 (11.29%), possibly due to presence of unreacted Al(OH)₃. It was observed that the P1CA31CL1 (12.79%) and P3CA31CL1 (11.32%) samples also lost a higher percentage of mass after 400 °C possibly due to the presence and decomposition of higher amounts of carbonate phase.

Table 3.2. Comparison of % mass lost recorded using TGA for samples synthesized using protocols P1, P2, and P3

Protocol	Loss of Sample Mass (%)			Total Mass Loss (%)
	100 °C <T < 250 °C	250 °C < T < 400 °C	T > 400°C	
Well-ordered FS	12.8	19.2	0.9	32.9
P1CA31CL1	14.22	9.21	12.79	37.76
P2CA31CL1	12.45	14.01	5.15	33.57
P3CA31CL1	11.29	10.33	11.32	34.22

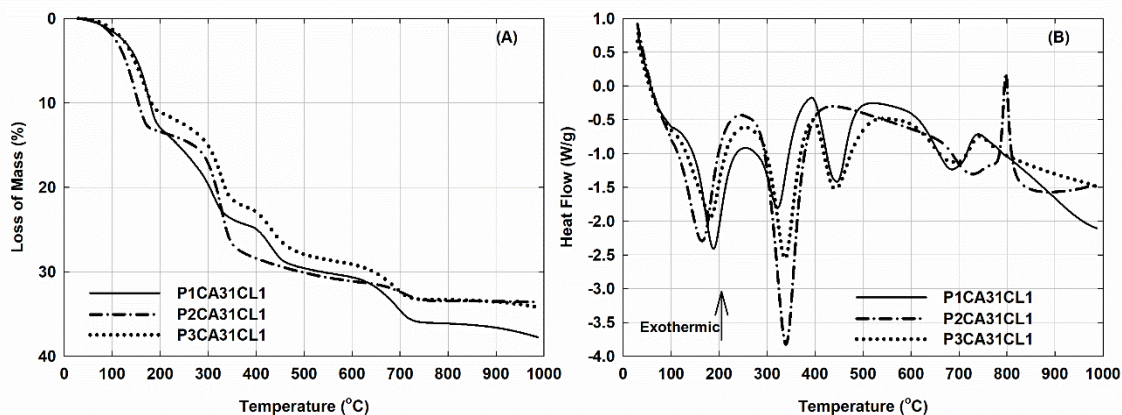


Figure 3.1. Comparison of (A) TGA and (B) DSC analysis for FS samples synthesized using protocols P1 (-), P2 (-.-.), and P3 (···)

Figure 3.2 depicts the IR spectra of the synthesized FS samples. The strong overlapping bands around 3630 cm^{-1} and 3475 cm^{-1} are ascribed to the stretching vibration of lattice water and metal-OH stretching mode of hydroxide layer, respectively. The peak around 1620 cm^{-1} is due to the H-O-H bending vibration of interlayer water molecule. The features around 788 cm^{-1} and $530/585\text{ cm}^{-1}$ are associated with bending and stretching vibration of Al-OH (Yue et al. 2018). The bands at 878 cm^{-1} and 1420 cm^{-1} are attributed to CO_3^{2-} groups in the carbonate phase of the sample. The areas under the peak at 1420 cm^{-1} for P1CA31CL1 (2821 \%T.cm^{-1}) and P3CA31CL1 (2455 \%T.cm^{-1}) samples are comparatively larger than that of the P2CA31CL1 (1272 \%T.cm^{-1}) sample implying incorporation of higher amounts of carbonate phase in P1CA31CL1 and P3CA31CL1. This is a further confirmation of the decomposition of higher amounts of carbonate phase observed in the TGA/DSC analysis.

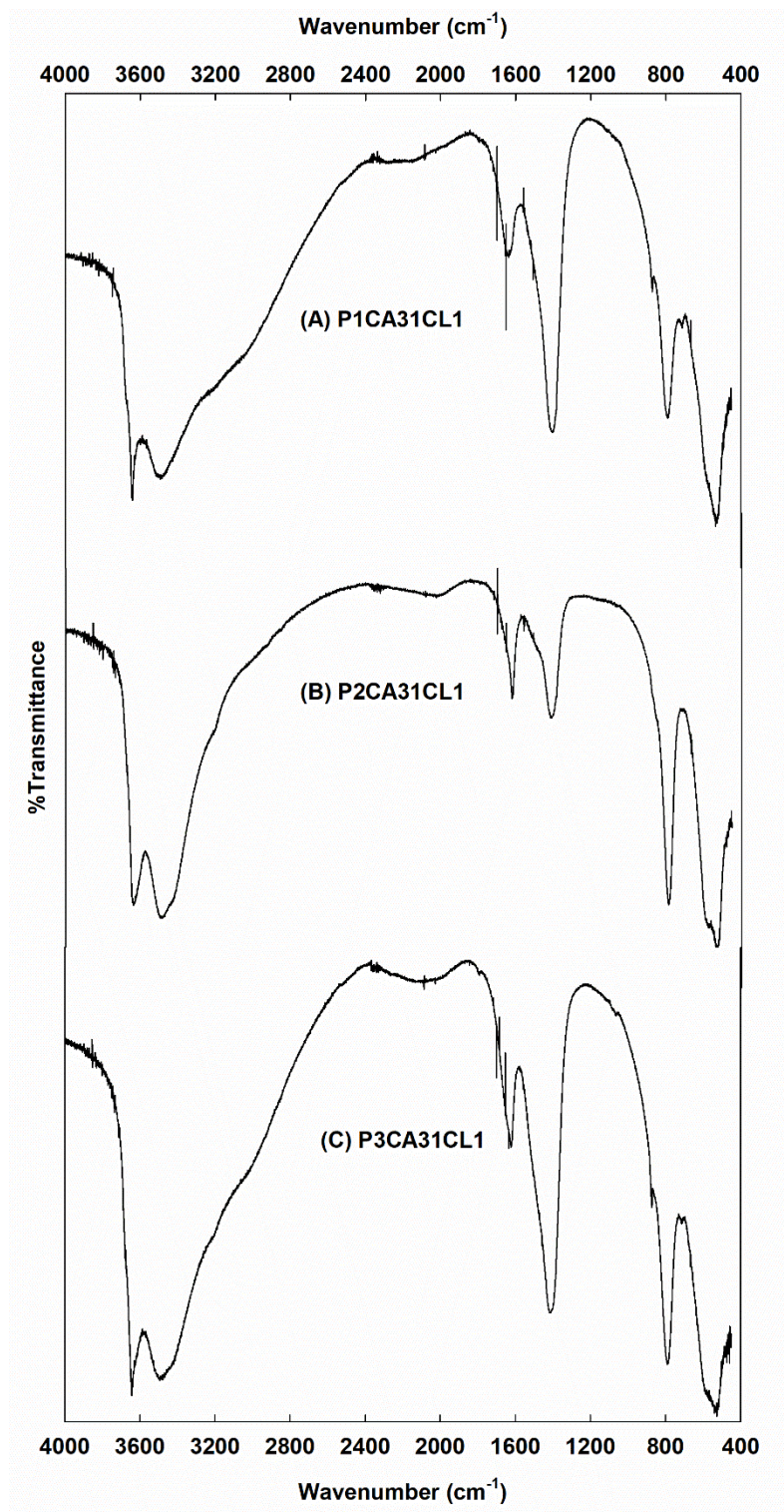


Figure 3.2. FTIR spectra of Friedel's salt samples synthesized using protocols (A) P1, (B) P2, and (C) P3

The fraction of chloride sequestered in the sample is similar for the three protocols (52.6%, 53.1%, and 52.8% for P1CA31CL1, P3CA31CL1, and P2CA31CL1 samples, respectively). Using the bulk chemical analysis of the supernatant and the water loss data from TGA, the mole fractions of the individual components were determined and the molecular formulas for the P1, P2, and P3 samples were adjusted accordingly. The new molecular formulas were calculated to be $\text{Ca}_{1.9}\text{Al}(\text{OH})_{5.6}\text{Cl}_{0.95}\cdot 1.9\text{H}_2\text{O}$, $\text{Ca}_2\text{Al}(\text{OH})_{6.3}\text{Cl}_{0.98}\cdot 2\text{H}_2\text{O}$, and $\text{Ca}_2\text{Al}(\text{OH})_{6.34}\text{Cl}_{0.83}\cdot 2\text{H}_2\text{O}$ for P1CA31CL1, P2CA31CL1, and P3CA31CL1 samples, respectively. Therefore, based on the TGA-DSC, FTIR results, and the calculated molecular formulas, it could be concluded that the sample synthesized using protocol 2 has a structure that is comparable to a well-ordered idealized FS sample with a molecular formula of $\text{Ca}_2\text{Al}(\text{OH})_6\text{Cl}\cdot 2\text{H}_2\text{O}$. This was further confirmed by the XRD pattern of P2CA31CL1 presented in Figure 3.3, which matches well with the standard PDF card No. 01-078-1219. As shown in Figure 3.3, the typical FS peaks ($2\theta = 11.17$ and 22.53) were identified with the d-spacing being 0.791 nm. Therefore, protocol 2 was then selected to be used in the following analysis to investigate the influence of variables like calcium-to-aluminum ratio, atmospheric conditions, and molar concentrations on the mass of chloride sequestered.

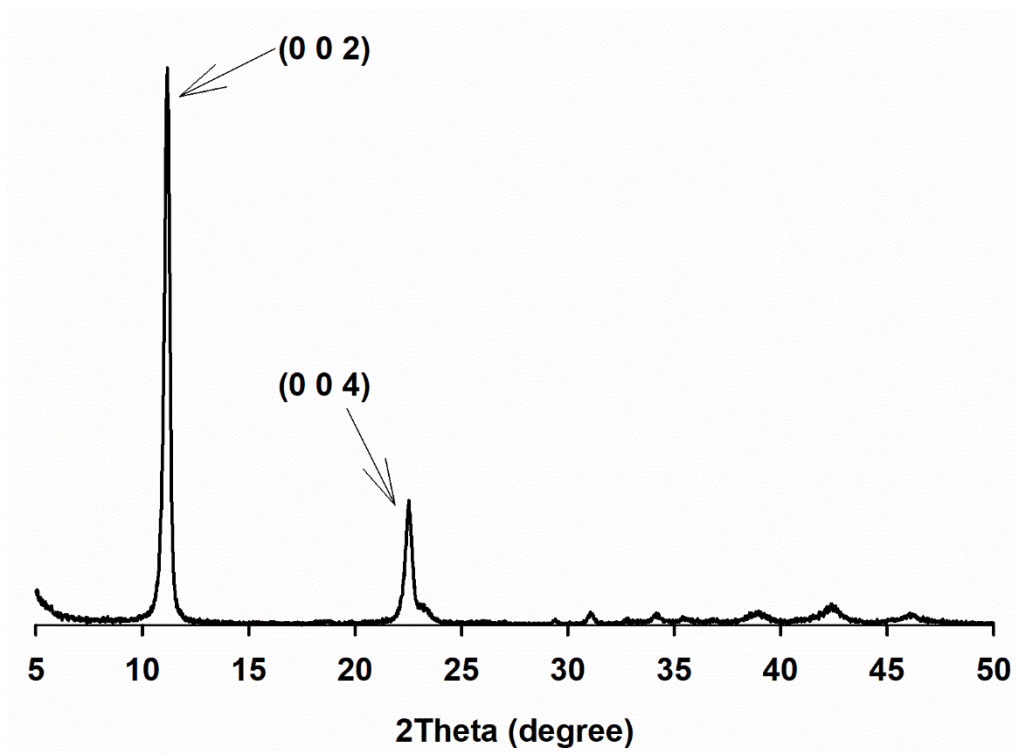


Figure 3.3. X-ray pattern of P2CA31CL1

3.3.2. Variation of Ca:Al ratio and Initial Cl⁻ Concentration

As mentioned previously, until now there was no comprehensive research conducted to understand the effect of molar concentration of Cl⁻ and Ca:Al ratio on the mass of chloride that was sequestered in synthesized Friedel's salt. Hence, in the current study, a two-factorial ANOVA design was implemented to understand the main effects of molar concentration of Cl⁻ and Ca:Al ratio on the reduction of chloride concentration and their interactions. Sample identification follows the same designation as presented in the previous section. P2CA31CL2 represents a synthesis protocol P2 at Ca:Al ratio of 3:1 and initial chloride concentration of 2M.

The TGA and DSC curves recorded for the samples synthesized using protocol 2 while the calcium to aluminum ratio and the initial chloride concentration were varied are shown in Figure 3.5 and Figure 3.4, respectively. In the case of samples with Ca:Al ratio of 3:1 and 4:1, a double endotherm centered at 170 °C and 320 °C (Figure 3.4) was matched by two well-resolved mass loss steps (Figure 3.5). The total mass loss for P2CA31 and P2CA41 samples are $33.34 \pm 0.28\%$ and $32.69 \pm 0.46\%$, respectively (Table 3.3). These results compare well with the theoretical total mass loss of an idealized FS formula. The behavior within the three temperature steps for P2CA31 and P2CA41 samples differs from the mass loss behavior of a well-ordered sample, especially in the 250 – 400 °C step. The percent of dehydroxylation from the main Ca-Al sheets (mass loss within 250 – 400 °C step) is less compared to a well-structured pure phase FS sample. It was also observed from Figure 3.5, Figure 3.4, and Table 3.3 that as the Ca:Al ratio was varied from 3:1 to 4:1, the percentage of mass loss between the temperature range of 400 °C – 1000 °C also increased. As the amount of calcium increased, incorporation of CO₂ into the sample during synthesis to form CaCO₃ could have increased. As a result, the decomposition of the carbonate phase after 400 °C increased because of the presence of higher amounts of CaCO₃ in the synthesized sample (Vieille et al. 2003).

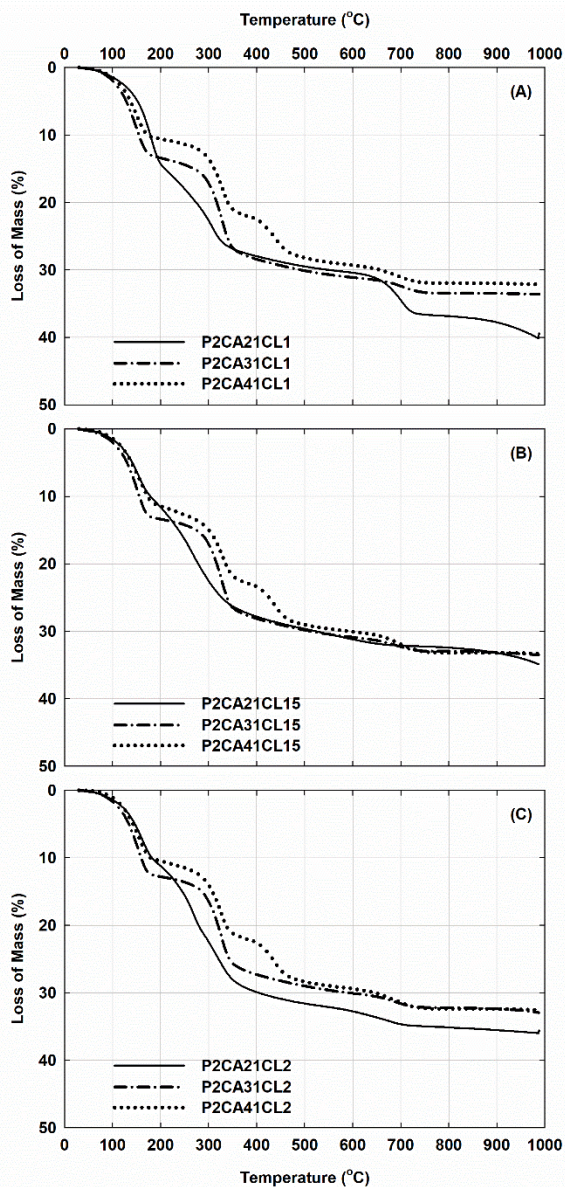


Figure 3.5. Comparison of weight loss data recorded by TGA for samples synthesized using protocol P2 with Ca:Al ratio and [Cl⁻] varied

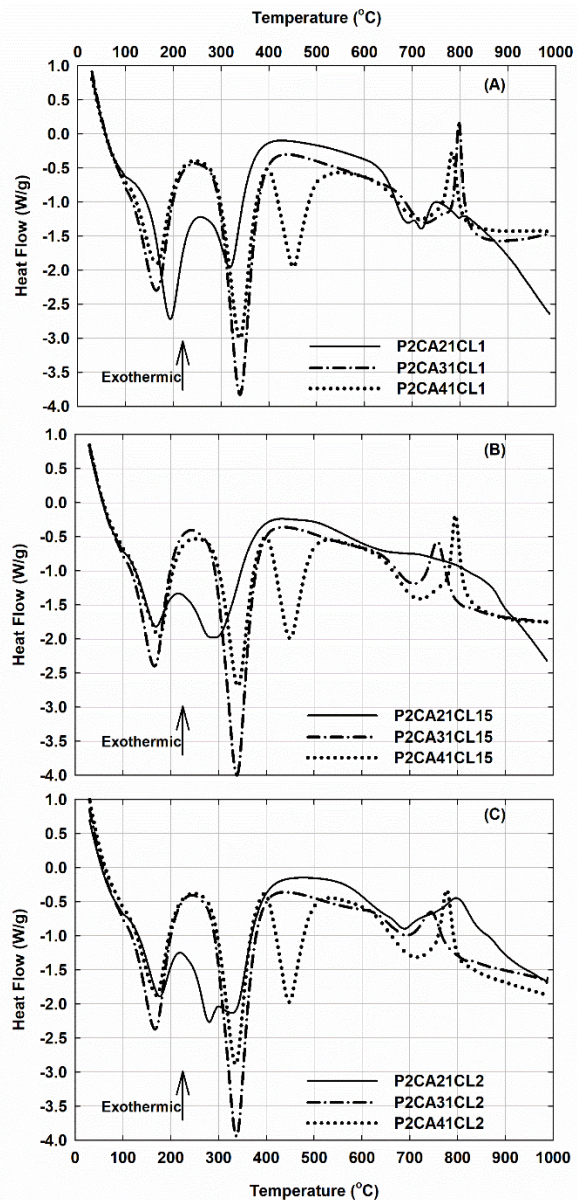


Figure 3.4. Comparison of DSC curves recorded for samples synthesized using protocol P2 with Ca:Al ratio and [Cl⁻] varied

Table 3.3. Comparison of % mass lost recorded using TGA for samples synthesized using protocol P2 while Ca:Al ratio and [Cl⁻] was varied

Protocol	Loss of Sample Mass (%)			Total Mass Loss (%)
	100 °C <T < 250 °C	250 °C < T < 400 °C	T > 400°C	
Well-ordered FS (Vieille et al. 2003)	12.8	19.2	0.9	32.9
P2CA21CL1	16.53	10.00	12.16	40.13
P2CA31CL1	12.45	14.01	5.15	33.57
P2CA41CL1	9.84	11.14	9.68	32.19
P2CA21CL15	14.80	11.45	7.08	34.88
P2CA31CL15	12.22	13.89	5.41	33.51
P2CA41CL15	11.28	10.64	9.95	33.30
P2CA21CL2	14.17	14.32	6.07	35.98
P2CA31CL2	11.94	13.69	5.63	32.94
P2CA41CL2	10.42	11.07	10.00	32.58

The incorporation of higher amounts of carbonate phase in the sample during sample preparation was further confirmed by the FTIR spectra of the synthesized FS samples (Figure 3.6). The area under the peaks at 1420 cm⁻¹ increased as the Ca:Al ratio increased from 3:1 to 4:1 (Yue et al. 2018).

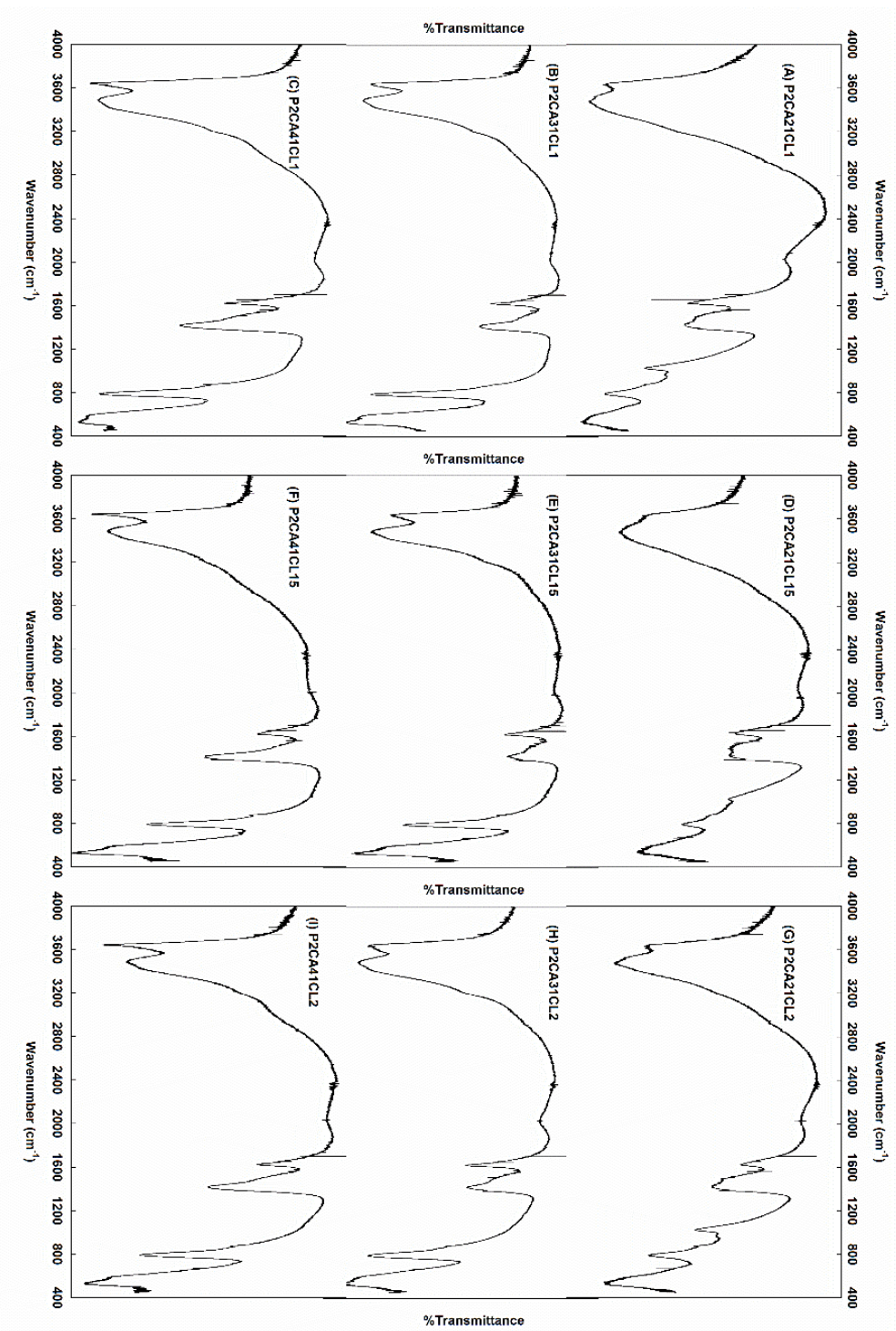


Figure 3.6. FTIR spectra of Friedel's salt samples synthesized using protocol P2 with Ca:Al ratio and [Cl⁻] varied

The samples synthesized at a calcium to aluminum of 2:1 did not yield a well-ordered structure of FS as evidenced by the TGS-DSC curves (Figure 3.5 and Figure 3.4) and the FTIR spectra (Figure 3.6 (A), (D), (G)). Although the total mass loss of P2CA21 samples ($37 \pm 2.56\%$) is comparable to the theoretical total mass loss of an idealized FS formula, the percentage of mass lost between the three temperature steps vary significantly from a well-ordered structure. The P2CA21 samples lost a higher percentage of mass in the 100 – 250 °C step compared to the 250 – 400 °C, contrary to the behavior of an idealized FS structure. The speculation is that the presence of impurities like unreacted NaAlO_2 could be the reason for difference in the behavior of P2CA21 samples. The presence of impurities was also evident on the FTIR spectra of the P2CA21 samples. A minor band was observed at 1024 cm^{-1} for all the three P2CA21 samples (Figure 3.6 (A), (D), (G)), possibly indicating the presence of impurities like NaAlO_2 on the FS samples (Yue et al. 2018).

A two-factorial ANOVA design was employed to investigate the effects of molar concentration of Cl^- and Ca:Al ratio, shown in Table 3.1, on the mass of chloride that was sequestered in the case of FS synthesis. Table 3.4 and Figure 3.7 report the statistical results of the ANOVA analysis. It is evident from Figure 3.7 that the influence of initial chloride concentration is dominant in the mass of chloride sequestered in the FS sample, compared to the calcium to aluminum ratio. The influence of interaction between initial chloride concentration and the calcium to aluminum ratio ($[\text{Cl}^-] * \text{Ca:Al}$) on the mass of chloride sequestered was also not significant. In addition, the p-value probability for $[\text{Cl}^-]$ is less than <0.05 , shown in Table 3.4, reflects the evidence that the initial concentration of chloride is predominant for the mass of chloride that is sequestered in FS during synthesis

for Ca:Al ratios used in this study. Furthermore, the p-value probabilities for Ca:Al ratio and the interaction between initial chloride concentration and calcium to aluminum ratio ($[Cl^-] * Ca:Al$) indicate that their influence on the sequestration of chloride is not significant.

Table 3.4. Analysis of variance (ANOVA) results

Response	Degree of freedom	Sum of squares	Mean square	F-statistic	P-value
Model	8	33.1	4.1	21.03	<.0001
[Cl ⁻]	2	32.1	16.0	81.50	<.0001
Ca:Al	2	0.58	0.29	1.46	0.28
[Cl ⁻] * Ca:Al	4	0.46	0.12	0.59	0.68
Error	9	1.77	0.20		
Total	17	34.87			

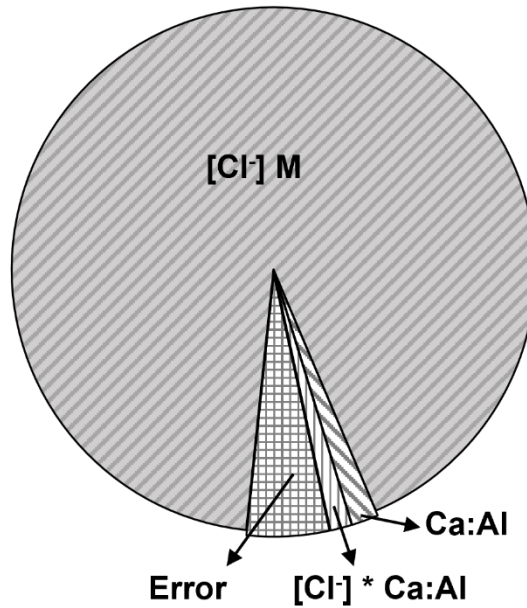


Figure 3.7. Influence of chloride concentration (1 M – 2 M) and Ca:Al ratio (2:1 – 4:1) variables on the mass of chloride sequestered

Given that the influence of the calcium to aluminum ratio was not significant on the mass of chloride sequestered, any ratio of calcium to aluminum within the range of 2:1 to 4:1 could be used for FS synthesis. However, as evidenced by the TGS-DSC curves (Figure 3.5 and Figure 3.4) and the FTIR spectra (Figure 3.6), the samples synthesized at a calcium to aluminum of 2:1 did not yield a well-ordered structure of Friedel's salt. Therefore, based on the FTIR (Figure 3.6), TGA-DSC (Figure 3.5 and Figure 3.4), and the ANOVA results (Figure 3.7), it could be concluded that the synthesis of FS using a calcium to aluminum ratio of 3:1 will be optimal for effective removal of chloride from the solution. A ratio of 3:1 was chosen over 4:1 to limit the incorporation of carbonate phase in the sample. This Ca:Al ratio of 3:1 was then used to understand the structure of FS in various atmospheric conditions.

3.3.3. Variation of Atmospheric Conditions

In order to understand the influence of atmospheric conditions on the structure of Friedel's salt, the optimum protocol determined above was synthesized in inert (N_2) and CO_2 rich atmosphere and the change in the structure was observed. Figure 3.8 depicts the IR spectra of P2CA31CL1 sample synthesized under ambient atmosphere (designated as P2CA31CL1-AA), inert atmosphere (designated as P2CA31CL1-IA), and carbon dioxide rich atmosphere (designated as P2CA31CL1-CO). Comparing the three IR spectra, it can be observed that the atmospheric conditions during synthesis does not have a considerable effect on the structure of Friedel's salt, except for the amount of CO_2 incorporated into the sample. The area under the peak at 1420 cm^{-1} , associated with the stretching vibration of CO_3^{2-} groups in the carbonate phase, is equivalent in the samples synthesized under the ambient atmosphere (1272 \%T.cm^{-1}) (Figure 3.8 (A)) and in the CO_2 rich atmosphere (1335

$\%T \cdot \text{cm}^{-1}$) (Figure 3.8 (C)), indicating that an increased concentration of carbon dioxide in the atmosphere will not significantly change the structure of the Friedel's salt. In the case of the sample synthesized under inert (N_2) atmosphere (Figure 3.8 (B)), a small peak at 1420 cm^{-1} can be still observed. However, the area under the peak is much less compared to samples at ambient or CO_2 rich atmospheres. Nevertheless, the lack of substantial effect by the atmospheric conditions during synthesis on the structure of FS is an advantage because the atmospheric conditions can be variable in a field environment.

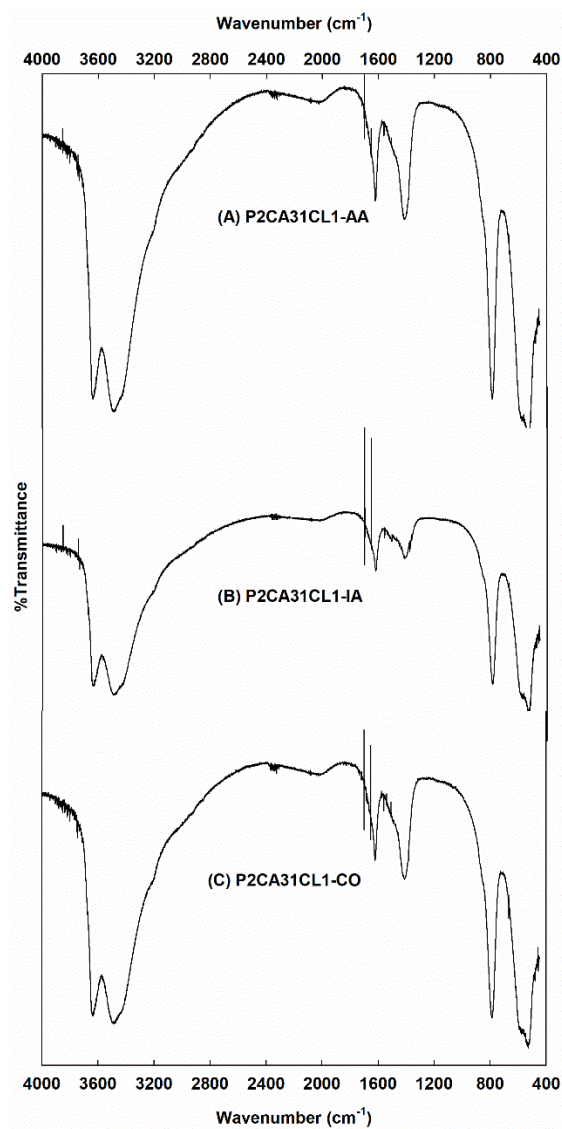


Figure 3.8. FTIR spectra for FS samples synthesized at (A) ambient atmosphere (B) inert atmosphere, and (C) carbon dioxide rich atmosphere

3.3.4. Variation of Environmental Conditions

The synthesized FS samples were dispersed and subjected to agitation in three types of solutions while solution pH was varied at pH 2, pH natural (ultrapure water), and pH 13, to investigate their stability. After the completion of agitation, the samples were extracted by vacuum filtration and were re-characterized using TGA-DSC. Figure 3.9 reports the

TGA and DSC curves recorded for FS samples characterized after dispersion in pH natural solution (designated as P2CA31CL2 – pH natural) and pH 13 solution (designated as P2CA31CL2 – pH 13). Comparing the TGA and DSC thermogram of P2CA31CL2 – pH natural and P2CA31CL2 – pH 13 samples with the thermogram of the initial (before dispersion) P2CA31CL2 sample (Figure 3.9), the behavior of the thermograms were quite similar and no discernable changes were observed. Similar to P2CA31CL2, the structures of all the FS samples (CA 21, 31, 41 and CL 1, 15, 2) did not differ when dispersed in pH natural or pH 13 solutions. However, when the synthesized FS samples were dispersed in pH 2 solutions, high dissolution rate of all the samples occurred with little residues for re-characterization using TGA-DSC or FTIR.

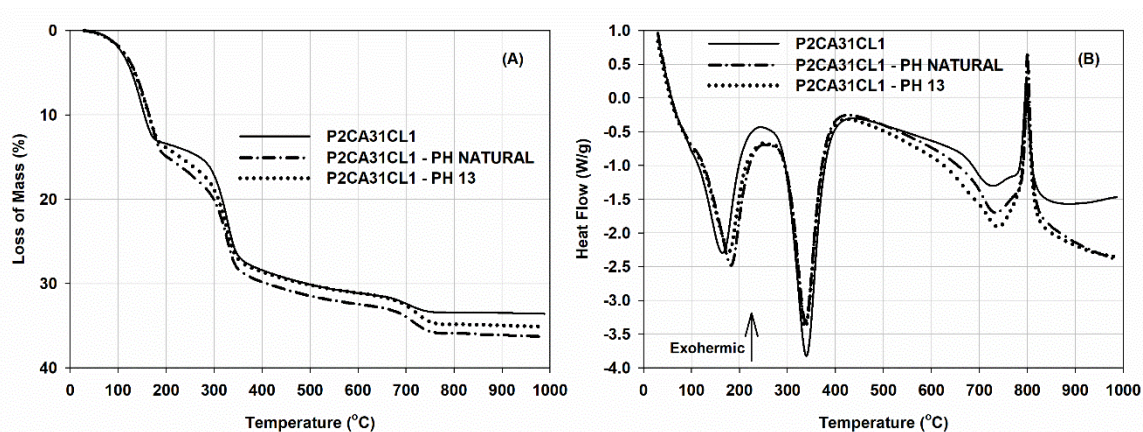


Figure 3.9. Comparison of (A) TGA and (B) DSC analysis for P2CA31CL1 samples dispersed in pH natural (-.-.) and pH 13 (...) with initial P2CA31CL1 sample (-)

3.3.5. Solubility of Friedel's Salt

The supernatant after filtration of the samples dispersed in solutions (at 25 °C) at various pH was analyzed for concentrations of calcium, aluminum, and chloride. The measured molar concentrations were used as inputs to calculate the activities of the individual components using PhreeqC. The activities were then used as inputs in Equation 3.1 to calculate the corresponding log K_{sp} value. Birnin-Yauri and Glasser (1998) measured the solubility product of FS in water at 20 °C as -27.10. Balonis et al. (2010) measured the value of log K_{sp} between -27.78 and -27.87 at 25 °C, while Bothe and Brown (2004) calculated the solubility product of FS to be within the range -28.8 and -27.6. Table 3.5 lists the solubility product constants of the various synthesized FS samples dispersed and agitated in solutions at natural pH, pH 2, and pH 13. The solubility of the FS samples dispersed in ultrapure water is slightly higher when compared with values reported in the literature, possibly due to the differences in the structures of the synthesized samples compared to a well-ordered FS sample. The log K_{sp} values of the samples in pH 2 is several orders of magnitude higher than the literature values and as reported previously, the dissolution of the sample was very high, and it was not possible to extract any FS sample for re-characterization. However, when the samples were agitated in solution at pH 13, the log K_{sp} values and the solubility decreased.

Table 3.5. Solubility of Friedel's salt samples

Sample	pH	log K_{sp}
P2CA21CL1	Natural	-24.82
P2CA31CL1		-26.55
P2CA41CL1		-26.61
P2CA21CL15		-22.68
P2CA31CL15		-24.79
P2CA41CL15		-25.77
P2CA21CL2		-25.94
P2CA31CL2		-24.68
P2CA41CL2		-25.55
P2CA21CL1	pH 13	-29.69
P2CA31CL1		-29.33
P2CA41CL1		-28.15
P2CA21CL15		-29.11
P2CA31CL15		-27.90
P2CA41CL15		-29.51
P2CA21CL2		-29.90
P2CA31CL2		-28.14
P2CA41CL2		-28.67
P2CA21CL1	pH 2	-16.66
P2CA31CL1		-11.84
P2CA41CL1		-11.56
P2CA21CL15		-16.04
P2CA31CL15		-11.90
P2CA41CL15		-11.52
P2CA21CL2		-14.12
P2CA31CL2		-11.96
P2CA41CL2		-11.59

3.4. Conclusions

Treatment of high TDS wastewater using chemical precipitation by formation of FS is a feasible approach for the removal of chloride because it is membrane-less and not energy-intensive like evaporation crystallization. In this study, the influence of initial chloride concentration and the Ca:Al molar ratio and their interactions on chloride removal performance was determined.

Friedel's salt was first synthesized using three different protocols and the samples were characterized using TGA-DSC and FTIR. Based on the TGA-DSC, FTIR results, and the calculated molecular formulas, it was concluded that the protocol outlined by Zhang et al. (2011) yielded a structure that is comparable to a well-ordered idealized FS sample. Therefore, this protocol was chosen to investigate the effect of molar concentration of Cl⁻ and Ca:Al ratio on the mass of chloride that was sequestered in the case of FS synthesis. The two-factorial ANOVA analysis confirmed that the initial chloride concentration highly influenced the mass of chloride sequestered in the FS samples. Also, atmospheric conditions (ambient or CO₂ rich atmospheres) did not significantly modify the structure of the FS sample. Similarly, it was observed that FS samples undergo congruent dissolution when mixed in ultrapure water or solution at pH 13, while dissolution rate of all the samples in pH 2 solution was high with little residues remaining. In conclusion, based on the FTIR and TGA-DSC analysis, the solubility constant values, and the ANOVA results, it could be established that the synthesis of FS using a calcium to aluminum ratio of 3:1 will be optimal for effective removal of chloride from hypersaline solutions. This optimized condition is recommended to synthesize FS and remove chloride from high TDS wastewater to establish the realistic removal potential in field relevant scenarios. In

addition, the results also suggest that synthesizing FS to remove chloride is a simple and effective method to treat high-salinity brines like FGD wastewater concentrate.

References

Balonis, M., Lothenbach, B., Le Saout, G., and Glasser, F. P. (2010). "Impact of chloride on the mineralogy of hydrated Portland cement systems." *Cement and Concrete Research*, Pergamon, 40(7), 1009–1022.

Birnin-Yauri, U. ., and Glasser, F. . (1998). "Friedel's salt, $\text{Ca}_2\text{Al}(\text{OH})_6(\text{Cl},\text{OH})\cdot 2\text{H}_2\text{O}$: its solid solutions and their role in chloride binding." *Cement and Concrete Research*, 28(12), 1713–1723.

Boelter, A. M., Lamming, F. N., Farag, A. M., and Bergman, H. L. (1992). "Environmental effects of saline oil-field discharges on surface waters." *Environmental Toxicology and Chemistry*, Wiley-Blackwell, 11(8), 1187–1195.

Bothe, J. V., and Brown, P. W. (2004). "PhreeqC modeling of Friedel's salt equilibria at 23 ± 1 °C." *Cement and Concrete Research*, Pergamon, 34(6), 1057–1063.

Dai, Y., Qian, G., Cao, Y., Chi, Y., Xu, Y., Zhou, J., Liu, Q., Xu, Z. P., and Qiao, S. Z. (2009). "Effective removal and fixation of Cr(VI) from aqueous solution with Friedel's salt." *Journal of Hazardous Materials*, Elsevier, 170(2–3), 1086–1092.

Fang, P., Tang, Z., Chen, X., Huang, J., Tang, Z., and Cen, C. (2018). "Chloride Ion Removal from the Wet Flue Gas Desulfurization and Denitrification Wastewater Using Friedel's Salt Precipitation Method." *Journal of Chemistry*, 2018, 1–9.

Gardner, K. M., and Royer, T. V. (2010). "Effect of Road Salt Application on Seasonal Chloride Concentrations and Toxicity in South-Central Indiana Streams." *Journal of Environmental Quality*, 39(3), 1036–1042.

Gingerich, D. B., Grol, E., and Mauter, M. S. (2018). "Fundamental challenges and engineering opportunities in flue gas desulfurization wastewater treatment at coal fired

- power plants.” *Environmental Science: Water Research and Technology*, Royal Society of Chemistry, 4(7), 909–925.
- Goh, K.-H., Lim, T.-T., and Dong, Z. (2008). “Application of layered double hydroxides for removal of oxyanions: A review.” *Water Research*, Pergamon, 42(6–7), 1343–1368.
- Ma, J., Li, Z., Jiang, Y., and Yang, X. (2015). “Synthesis, characterization and formation mechanism of Friedel’s salt (FS: $3\text{CaO}\cdot\text{Al}_2\text{O}_3\cdot\text{CaCl}_2\cdot 10\text{H}_2\text{O}$) by the reaction of calcium chloride with sodium aluminate.” *Journal Wuhan University of Technology, Materials Science Edition*, 30(1), 76–83.
- Manikonda, A., Ogunro, V. O., Ellison, K. M., and Moo-Young, K. (2019). “Synthesis of Friedel’s Salt for Application in Halide Sequestration Using Paste Encapsulation Technology.” *Geo-Congress 2019*, Proceedings, 167–176.
- Parkhurst, D. L., and Appelo, C. A. J. (2013). “PHREEQC (Version 3)-A Computer Program for Speciation, Batch-Reaction, One-Dimensional Transport, and Inverse Geochemical Calculations.” *Modeling Techniques*, book 6, 497.
- Pramanik, B. K., Shu, L., and Jegatheesan, V. (2017). “A review of the management and treatment of brine solutions.” *Environmental Science: Water Research and Technology*, Royal Society of Chemistry, 3(4), 625–658.
- Tong, T., and Elimelech, M. (2016). “The Global Rise of Zero Liquid Discharge for Wastewater Management: Drivers, Technologies, and Future Directions.” *Environmental Science & Technology*, 50(13), 6846–6855.
- Vieille, L., Rousselot, I., Leroux, F., Besse, J. P., and Taviot-Guého, C. (2003). “Hydrocalumite and Its Polymer Derivatives. 1. Reversible Thermal Behavior of Friedel’s Salt: A Direct Observation by Means of High-Temperature in Situ Powder X-ray Diffraction.” *Chemistry of Materials*, American Chemical Society, 15(23), 4361–4368.

Wang, L. P., Lee, W. H., Tseng, S. M., and Cheng, T. W. (2018). "Removal of chloride ions from an aqueous solution containing a high chloride concentration through the chemical precipitation of Friedel's salt." *Materials Transactions*, 59(2), 297–302.

Yang, L., Shahrivari, Z., Liu, P. K. T., Sahimi, M., and Tsotsis, T. T. (2005). "Removal of trace levels of arsenic and selenium from aqueous solutions by calcined and uncalcined layered double hydroxides (LDH)." *Industrial and Engineering Chemistry Research*, 44(17), 6804–6815.

Yue, Y., Wang, J. J., Basheer, P. A. M., and Bai, Y. (2018). "Raman spectroscopic investigation of Friedel's salt." *Cement and Concrete Composites*, Elsevier Ltd, 86, 306–314.

Zhang, D., Jia, Y., Ma, J., and Li, Z. (2011). "Removal of arsenic from water by Friedel's salt (FS: $3\text{CaO} \cdot \text{Al}_2\text{O}_3 \cdot \text{CaCl}_2 \cdot 10\text{H}_2\text{O}$)." *Journal of Hazardous Materials*, 195, 398–404.

Zhang, M., and Reardon, E. J. (2003). "Removal of B, Cr, Mo, and Se from wastewater by incorporation into hydrocalumite and ettringite." *Environmental Science and Technology*, American Chemical Society, 37(13), 2947–2952.

CHAPTER 4: BROMIDE ION REMOVAL FROM HYPERSALINE BRINES BY CAL-LAYERED DOUBLE HYDROXIDES

Abhisek Manikonda, Rui He, Vincent O. Ogunro

Abstract

Elevated concentrations of bromide in source waters can promote the formation of significantly more toxic brominated disinfection byproducts over chlorinated disinfection byproducts. Hypersaline brines like FGD wastewater concentrate often contain high concentrations of bromide and are difficult to treat because of the high solubility of bromide ion. Therefore, conventional water treatment processes are not suitable for removal of bromide. This research explored the feasibility of removing bromide from high-salinity brines through the precipitation of layered double hydroxides with the bromide ion in the interlayer. Parameters affecting the reduction of concentration of bromide like the initial molar concentration of bromide, the calcium to aluminum ratio, and the interactions between them were evaluated. The stability of the bromide substituted layered double hydroxide products at various prevailing solutions was investigated and an optimal calcium to aluminum ratio for the effective removal of bromide was established. Experimental results confirmed that the dominant factor influencing bromide sequestration in the layered double hydroxide samples is the initial bromide concentration for the Ca:Al ratio range of 2:1 – 4:1 investigated in this study. It was also observed that layered double hydroxide samples undergo congruent dissolution when mixed in water or a solution at pH 13, while the dissolution rate of all the samples in pH 2 solution was high with little residues remaining. Based on the fourier-transform infrared spectroscopy results and thermogravimetric analysis, it could be hypothesized that the synthesis of layered double

hydroxides using a calcium to aluminum ratio of 2:1 will be optimal for effective removal of bromide from hypersaline solutions. In addition, the results suggest that this process is a simple and effective method to treat high-salinity brines with high bromide concentration.

4.1. Introduction

The presence of elevated concentrations of bromide in source waters can accelerate the rate and extent of disinfection byproduct (DBP) formation at drinking water treatment plants (Mctigue et al. 2014). Furthermore, the presence of bromide also promotes the formation of brominated DBPs over chlorinated DBPs, which are more toxic and can pose health risk to humans and can also have a detrimental impact on aquatic life (Good and Vanbriesen 2017; Sawade et al. 2016). Some point source discharges of bromide into surface water include discharges from coal mines (Cravotta and Brady 2015), effluent from plastics and textile manufacturing (Mctigue et al. 2014), wastewater during oil and gas extraction (Landis et al. 2016), and coal combustion residue wastewater (Ruhl et al. 2012). Hypersaline brines from processes like zero-liquid discharge concentrate from treatment of flue gas desulfurization wastewater (FGDWW) and concentrate from desalination often also contain high concentrations of bromide (Gingerich et al. 2018; Pramanik et al. 2017). Bromine is naturally available in coal in trace amounts and bromide is also added to coal to control mercury emissions from power plants. Therefore, bromide is found to be present in elevated concentrations in FGDWW at some power plants.

Historically, there have been no regulations for bromide in the form of water quality standards or discharge limits. However, because of the increasingly elevated concentrations of bromide in surface water and groundwater near some coal fired power

plants and its influence on formation of DBPs, the U.S. Environmental Protection Agency (EPA) recently included bromide in the Safe Drinking Water Act (SDWA) fourth Unregulated Contaminant Monitoring Rule (UCMR 4) (USEPA 2016). The U.S. EPA also discussed the potential for bromide discharges from FGD wastewater affecting the surface water quality in the Steam Electric Power Effluent Limitation Guidelines (ELG) which regulate FGD wastewater and other processed water (USEPA 2015) (USEPA 2015). Therefore, hypersaline brines and other wastewater discharges need to be adequately treated to remove the high concentration of bromide before disposal.

Bromide is an extremely soluble, monovalent anion that is difficult to remove from water, therefore, conventional water treatment processes are not suitable for removal of bromide (Francis et al. 2010). Removal of bromide from wastewater can be achieved through membrane technologies (reverse osmosis, nanofiltration), capacitive deionization, or evaporation-based thermal treatments like distillation, crystallization, and electro dialysis (Gingerich et al. 2018; Tong and Elimelech 2016). However, these technologies can be prohibitively energy intensive, have high operating costs, and are not suitable for treatment of wastewater like hypersaline brines. Therefore, there is a need to develop a cost-effective and energy-efficient method for removal of bromide from hypersaline brines. Chemical precipitation methods, such as layered double hydroxides (LDHs) precipitation, can be an alternative approach for the removal of bromide since it is not energy-intensive compared to evaporation crystallization and is not constrained by operational problems associated with membrane technology.

Layered double hydroxides are a class of two-dimensional lamellar compounds. They consist of positively charged octahedral layers with a negatively charged interlayer

consisting of water and anion molecules (Goh et al. 2008). Layered double hydroxides are often considered as efficient ion-exchangers of contaminant ions due to their high anion exchange capacity (Ma et al. 2018) and the availability of large interlayer spaces (Yang et al. 2005). Friedel's salt is an anion-exchange mineral belonging to the LDHs family (Birnin-Yauri and Glasser 1998). It is composed of hydroxide layers with Ca^{+2} and Al^{+3} octahedral units and an interlayer of negatively charged ions. Friedel's salt (FS) $[\text{Ca}_2\text{Al}(\text{OH})_6\text{X}\cdot 2\text{H}_2\text{O}$; X = halides, oxyanions] has been widely employed for environmental remediation of chloride and heavy metals from wastewater because of its high adsorption efficiency (Fang et al. 2018; Yang et al. 2005; Zhang et al. 2021; Zhang and Reardon 2003). A few studies have characterized the effect of process parameters like solution pH and reaction temperature, among others, on the structure of Friedel's salt and the removal of chloride. Studies like Fang et al. (2018), Ma et al. (2015), Manikonda et al. (2019), and Manikonda et al. (2020) have investigated the effects of initial CaCl_2 concentration, calcium to aluminum (Ca:Al) molar ratio, reaction time, and reaction temperature on the structure of Friedel's salt. Ma et al. (2015) and Manikonda et al. (2019) state that the final structure of FS was consistent for any synthesis reaction temperatures below 100 °C, however, Fang et al. (2018) noted that the removal efficiency of chloride from solution decreased as the reaction temperature increased from 25 °C to 60 °C. Manikonda et al. (2020) observed that the initial chloride concentration highly influenced the mass of chloride sequestered in the Friedel's salt sample. Ma et al. (2015), Manikonda et al. (2020), and Fang et al. (2018) reported that the optimum range of calcium to aluminum ratio is 3:1.

However, there is a gap in knowledge on the ability of LDHs to successfully sequester bromide. Rapin et al. (1999) and Renaudin et al. (2004) characterized bromide substituted LDHs to understand the influence of intercalated anion on the structural phase of Friedel's salt. Lv et al. (2008) and Ji et al. (2017) investigated the uptake of bromide and bromate (BrO_3^-) using Mg-Al layered double hydroxides, respectively. There is little additional information available about the solubility product constants of bromide substituted layered double hydroxides (Br-LDHs), and therefore the stability of bromide dominated system has not been studied. This study aims to evaluate the performance of high concentration bromide removal through the precipitation of LDHs, with the structure of the LDH similar to the structure of Friedel's salt consisting of bromide in the interlayer instead of chloride ions. The influence of initial bromide concentration and its interactions with the Ca:Al molar ratio on bromide removal performance was investigated. A series of experiments were carried out to assess the stability of the Br-LDH products at various prevailing solution pH conditions. An optimal calcium to aluminum ratio for the effective removal of bromide was also established.

4.2. Materials and Methods

Hypersaline brines like FGD wastewater concentrate are characterized with an extremely complex composition matrix. It would be challenging to understand the factors that will influence the formation of layered double hydroxides, similar to the structure of Friedel's salt, if synthesized using FGD wastewater concentrate. Therefore, Br-LDH phases was synthesized using laboratory grade reagents to determine the optimum operating parameters. The starting materials CaBr_2 , NaAlO_2 , and $\text{Ca}(\text{OH})_2$ for the preparation of bromide substituted LDHs were of analytical grade and were used without

further purification. Ultrapure deionized water (18 M Ω) was used for solution preparation and washing.

4.2.1. Synthesis of Bromide Substituted LDHs

Manikonda et al. (2020) compared three different Friedel's salt synthesis protocols in order to determine the optimum protocol in terms of mass of chloride sequestered and the relative propinquity of the structure of the synthesized sample compared to a well-ordered sample. They concluded that the Friedel's salt synthesized using the protocol outlined by Zhang et al. (2011) has a structure that is comparable to a well-ordered idealized sample. Therefore, the synthesis protocol by Zhang et al. (2011) was used to investigate the performance of bromide removal by LDH phases.

Reagent grade NaAlO₂ was dissolved directly in ultrapure water to form NaAl(OH)₄. The reaction solution was heated to 25 °C, and CaBr₂ was then added dropwise at a rate of 5 mL/min under continuous stirring. Stirring was continued for an additional one hour after the completion of the addition procedure. The precipitate was collected at the end of the stirring period by vacuum filtration using 0.45 μ m PTFE filters. The precipitate was then washed with ultrapure water to remove any remaining ions, and finally dried in an oven at 60 °C for 24 hours. The synthesis was carried out at 25 °C because Manikonda et al. (2019) reported that reaction temperature did not have a significant influence on the structure of Friedel's salt. All the experiments were performed in ambient atmospheric conditions.

4.2.2. Characterization of Bromide Substituted LDHs

The microstructure of the synthesized samples was characterized using thermogravimetric analysis and differential scanning calorimetry (TGA-DSC), Fourier transform infrared (FTIR) spectroscopy, and X-ray powder diffraction (XRD). The TGA-DSC analysis was performed using a SDT Q600 (TA Instruments, Delaware) by heating the specimen from room temperature to 1000 °C in a nitrogen atmosphere at a rate of 20 °C/min. The FTIR spectra was collected using a Spectrum One FTIR spectrometer (PerkinElmer, Massachusetts) in the range of 450-4000 cm^{-1} with a resolution of 1 cm^{-1} under transmission mode using KBr pellet method. X-ray powder diffraction patterns were recorded using a PANalytical (Netherlands) X'Pert PRO diffractometer ($2\theta = 5-50^\circ$, stepsize 0.02° with 0.5 s/step). The supernatant obtained from the filtration of the precipitate was analyzed for concentrations of Br^- , using an ICS-3000 ion chromatography system (Dionex, California), and for Al^{+3} and Ca^{+2} , using a 5100 ICP-OES instrument (Agilent, California). The pH and conductivity of the supernatant was measured with a SevenExcellence S470-Kit pH/conductivity meter (Mettler Toledo, Ohio).

4.2.3. Variation of Protocol Parameters

A two-factorial design was implemented to understand the effect of parameters like the molar concentration of Br^- and the calcium to aluminum (Ca:Al) ratio on the mass of bromide that was sequestered during the synthesis. The goal of this two-factorial design was to investigate the effects of the two parameters and the interactions between them on the reduction of concentration of bromide. Table 4.1 provides the experimental conditions of the two parameters, each at three levels, along with the identifiers for each sample. A

bromide substituted LDH sample synthesized using a Ca:Al ratio of 3:1 (CA31) and an initial bromide concentration of 0.25 M (BR25) is identified as FSCA31BR25. The range of Ca:Al ratios were selected based on previous research by Manikonda et al. (2020), Fang et al. (2018), Ma et al. (2015), and Wang et al. (2018). The molar concentrations of bromide were selected based on the range of concentrations found in concentrated brine of FGD wastewater in the industry.

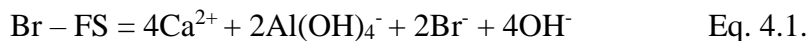
Table 4.1. Levels of parameters tested in the two-factorial ANOVA design along with the identifiers for each sample

		Ca:Al Ratio		
		2:1	3:1	4:1
Molar Concentration of Br ⁻	0.25 M	FSCA21BR25	FSCA31BR25	FSCA41BR25
	0.50 M	FSCA21BR50	FSCA31BR50	FSCA41BR50
	0.75 M	FSCA21BR75	FSCA31BR75	FSCA41BR75

4.2.4. Stability and Solubility of Bromide Substituted LDHs

In order to determine the stability and solubility product of bromide substituted LDHs in different environments, the synthesized samples were dispersed in three types of solutions (at 25 °C) at a liquid to solid ratio of 20 to 1: solution at pH natural (ultrapure water), solution at pH 2, and solution at pH 13. The dispersed samples were subjected to agitation for 18 hours. After agitation, the samples were extracted by vacuum filtration and were re-characterized. The supernatants were analyzed for concentrations of calcium, aluminum, and bromide. The geochemical speciation program PhreeqC (Parkhurst and Appelo 2013) was used to convert the measured molar concentrations of each component to their corresponding activities. The dissociation equation presented by Bothe & Brown

(2004) for Friedel's salt was modified (Equation 4.1) to determine the solubility product of bromide substituted layered double hydroxides.



4.3. Results and Discussion

4.3.1. Characterization of Synthesized Bromide Substituted LDHs

Figure 4.2 and Figure 4.1 report the TGA and DSC curves recorded for the bromide substituted LDH samples synthesized while the calcium to aluminum ratio and the initial bromide concentration were varied, respectively. The theoretical total mass loss for a well-ordered crystalline Br-LDH sample when heated to 1000 °C was calculated to be 27.69%. An ordered structure of Br-LDH will have two well-resolved weight loss steps between 100 – 400 °C (Grishchenko et al. 2013; Ma et al. 2009; Vieille et al. 2003). The loss in the first step (11.07%) between the temperature range of 100 – 250 °C is associated with removal of the interlayer water giving rise to a product with reduced crystallinity with a composition of $3\text{Ca}(\text{OH})_2 \cdot 2\text{Al}(\text{OH})_3 \cdot \text{CaBr}_2$. The second effect (16.62%) between 250 – 400 °C is ascribed to the dehydroxylation in the Ca-Al layers yielding mainly $3\text{CaO} \cdot \text{Al}_2\text{O}_3 \cdot \text{CaBr}_2$ (Birnin-Yauri and Glasser 1998). The mass loss after 400 °C could be associated with carbonate decomposition and recombination of hydroxyl groups. The exothermic peaks visible at around 830 °C in Figure 4.1 could be due to the recrystallization of the amorphous anhydrous product (Grishchenko et al. 2013). Lv et al. (2008) reported an endothermic peak at 900 °C in the differential thermal analysis profile of their bromide-Mg/Al LDHs, which they assigned to the removal of bromide ions from

the interlayers. However, no endothermic peaks at 900 °C were observed in the DSC profiles (Figure 4.1) of the synthesized Br-LDH samples.

Evaluating the TGA (Figure 4.2) and DSC (Figure 4.1) curves, a double endotherm centered around 175 °C and 350 °C matched by two well-resolved mass loss steps was observed for all the samples. The total mass loss for FSCA21, FSCA31, and FSCA41 samples are $32.31 \pm 1.43\%$, $32.74 \pm 0.61\%$, and $31.63 \pm 0.36\%$, respectively (Table 4.2), higher than the theoretical total mass loss for a well-ordered Br-LDH sample. However, the mass loss configurations for all the samples between 100 – 400 °C, corresponding to the removal of water molecules in the interlayers and the Ca-Al layers, is less than the theoretical mass loss for a well-ordered sample (27.69%). It was also observed that as the Ca:Al ratio increased from 2:1 to 4:1, the percent loss in mass between 100 – 400 °C decreased. It could be inferred based on the decrease in the percent mass loss that the molar fraction of water molecules in Br-LDH samples decreased as the Ca:Al ratio increased. The percent mass loss in the 100 – 250 °C range for all the samples is comparable to the theoretical percent mass loss in an idealized Br-LDH sample, with the exception of FSCA21BR25 (14.21%). However, the percent mass loss between the 250 – 400 °C step for all the synthesized samples (between 7.10% and 12.11%) is lower compared to the percent mass loss in a well-ordered Br-LDH sample (16.62%), indicating the presence of a lower amount of hydroxide ions in the Ca-Al layers.

All the samples also had a higher percentage of mass loss in the 400 – 1000 °C range (Table 4.2) when the theoretical mass loss should have been less than one percent. The mass loss after 400 °C can be attributed to a number of factors, including the dehydroxylation of unreacted Ca(OH)_2 , decomposition of any impurities and also the

carbonate phases in the sample. The dehydroxylation of Ca(OH)_2 takes places at around 460 °C (Scrivener et al. 2018) and the endotherm centered around 450 °C observed in the DSC curves (Figure 4.1) for FSA31 and FSCA41 samples confirms the presence of unreacted Ca(OH)_2 in the sample. It can also be observed that as the Ca:Al ratio increased from 2:1 to 4:1, the percentage of mass loss between the temperature range of 400 °C – 1000 °C also increased. As the amount of calcium increased, incorporation of CO_2 into the sample during synthesis to form CaCO_3 could have increased (Vieille et al. 2003; Yue et al. 2018). As a result, the decomposition of the carbonate phase after 400 °C might have increased because of the presence of higher amounts of CaCO_3 in the synthesized sample.

Table 4.2. Comparison of % mass lost recorded using TGA for Br-LDH samples synthesized while Ca:Al ratio and $[\text{Br}^-]$ were varied

Protocol	Loss of Sample Mass (%)			Total Mass Loss (%)
	100 °C < T < 250 °C	250 °C < T < 400 °C	T > 400°C	
Well-ordered Br-LDH	11.07	16.62	< 1%	27.69
FSCA21BR25	14.21	10.40	7.40	34.32
FSCA31BR25	11.88	8.52	11.50	33.58
FSCA41BR25	9.90	7.10	13.50	32.08
FSCA21BR50	11.61	12.11	5.30	31.12
FSCA31BR50	11.34	9.57	9.50	32.49
FSCA41BR50	9.40	7.81	12.08	31.20
FSCA21BR75	11.35	12.11	6.11	31.50
FSCA31BR75	11.48	10.50	8.09	32.15
FSCA41BR75	10.14	8.51	11.35	31.61

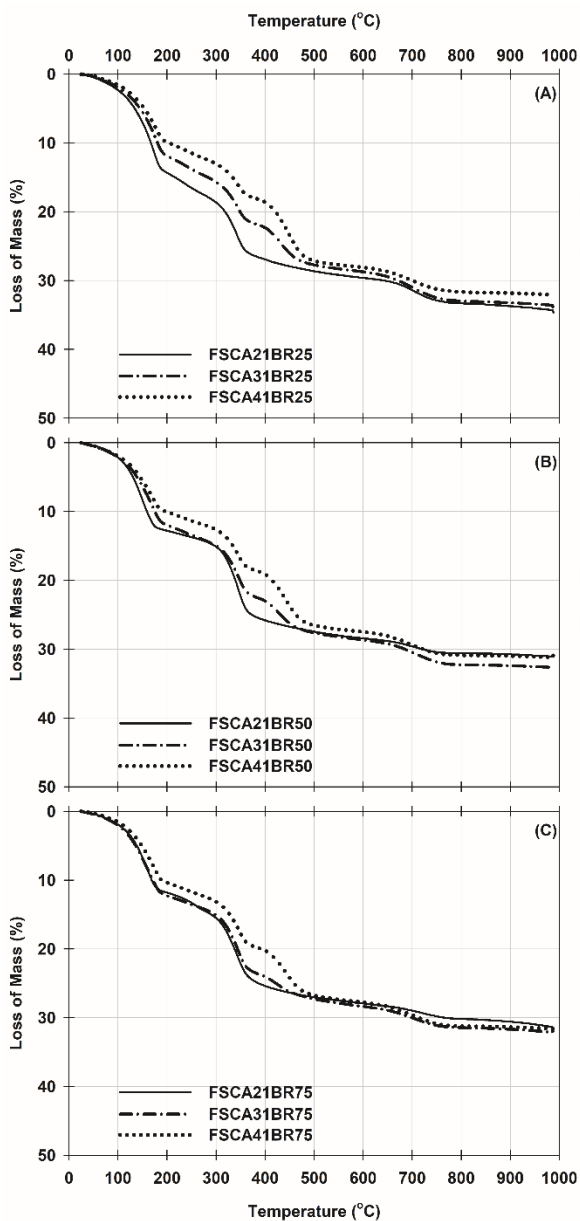


Figure 4.2. Comparison of weight loss data recorded by TGA for Br-LDH samples synthesized with Ca:Al ratio and $[Br^-]$ varied

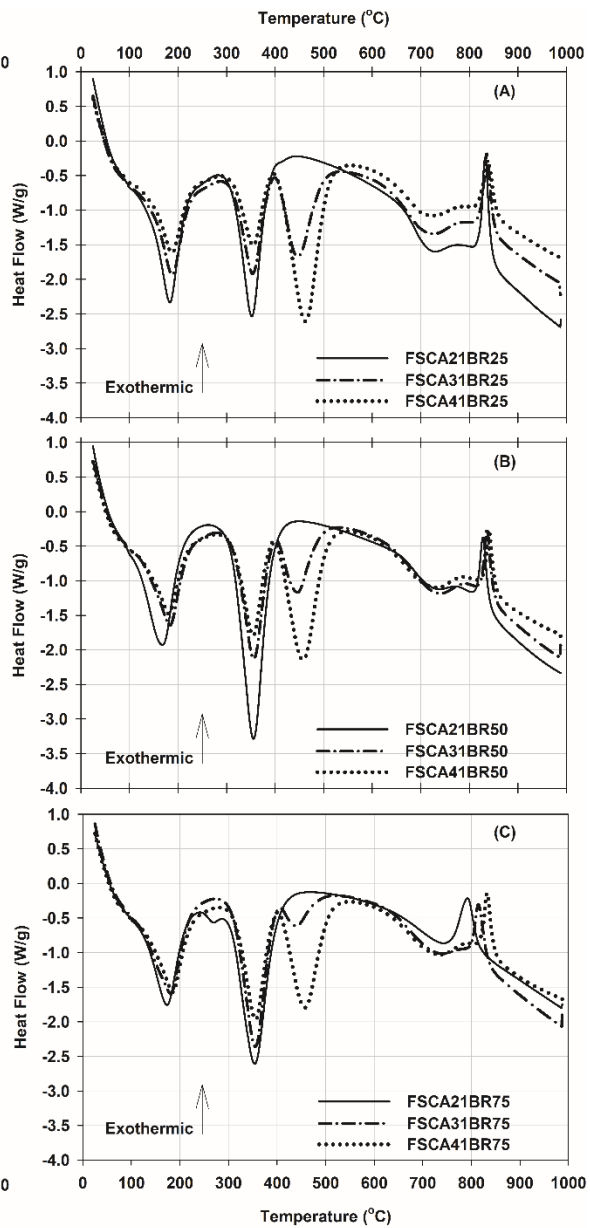


Figure 4.1. Comparison of DSC curves recorded for Br-LDH samples synthesized with Ca:Al ratio and $[Br^-]$ varied

The FT-IR spectra of the Br-LDH samples are shown in Figure 4.3. The bands around 788 cm^{-1} and 530 cm^{-1} could be due to the bending and stretching vibrations of Al-OH. The features observed at 1620 cm^{-1} are characteristic of H-O-H bending vibration of interlayer water molecule. The strong overlapping bands around 3630 cm^{-1} and 3475 cm^{-1} are ascribed to the stretching vibration of lattice water and metal-OH stretching mode of hydroxide layer, respectively (Yue et al. 2018). The bands observed at 1420 cm^{-1} for all the samples could be attributed to the adsorption of CO_3^{2-} on to the sample (Yue et al. 2018), further confirming the decomposition of carbonate phase observed in the TGA/DSC analysis. Furthermore, the area under the peak at 1420 cm^{-1} increased as the Ca:Al ratio increased from 2:1 to 4:1.

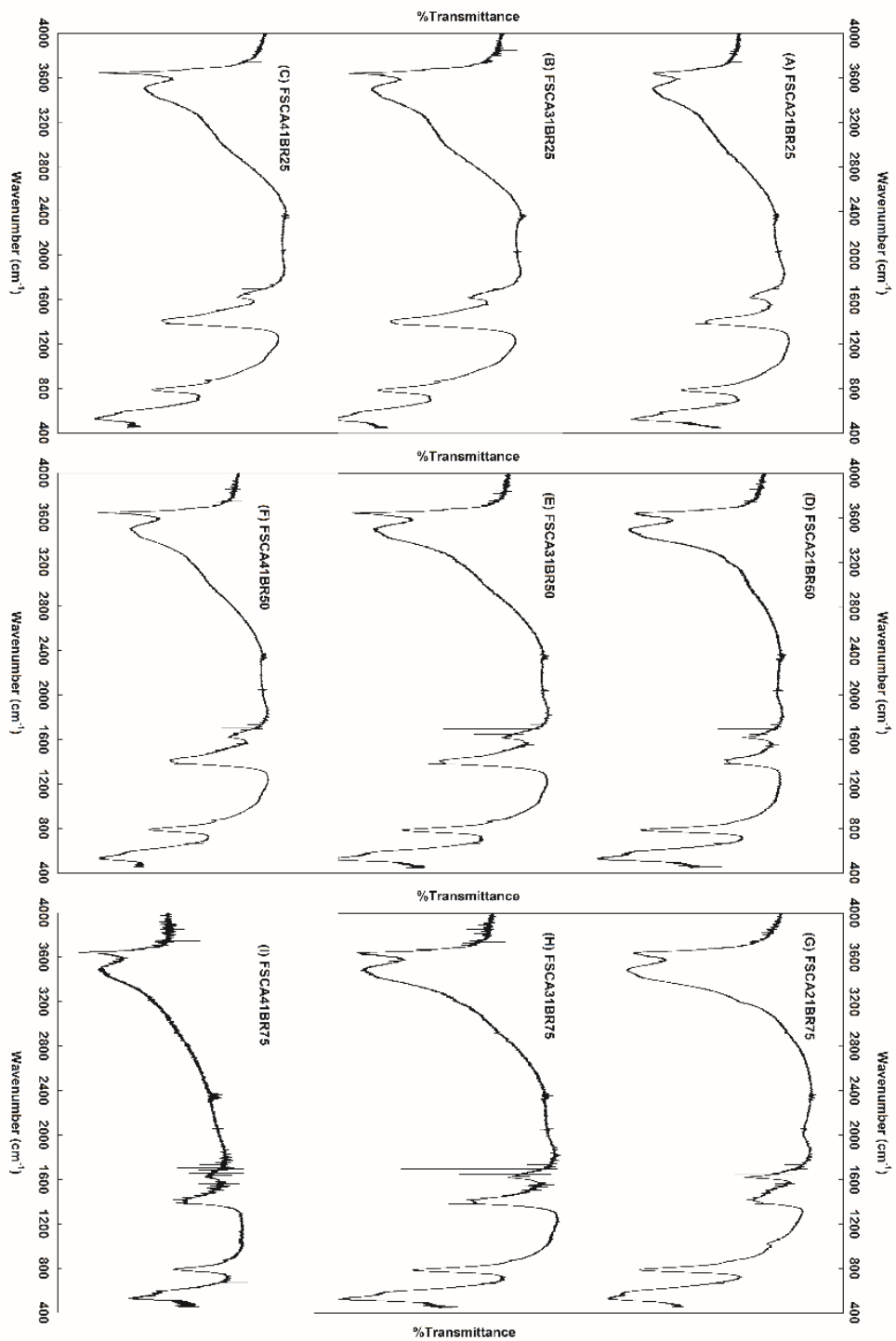


Figure 4.3. FTIR spectra for Br-LDH samples synthesized with Ca:Al ratio and [Br⁻] varied

The XRD patterns of the Br-LDH samples (Figure 4.4) show sharp and symmetric peaks characteristic of layered double hydroxide compounds. The reflections at 2θ around 10.80° , 21.75° , and 22.90° corresponding to (006), (0012), and (018) planes, respectively, are typical Miller-Bravais indices of bromide substituted layered double hydroxides. The basal spacing of the (006) reflection ($2\theta = 10.80^\circ$) is 0.82 nm is in agreement with the d-spacing reported by Rapin et al. (1999) for a bromide substituted layered double hydroxides. The interspacing distance between the $[\text{Ca}_2\text{Al}(\text{OH})_6]^+$ layers of 0.82 nm in Br-LDH is higher than the distance measured in a Friedel's salt sample with chloride ions (Cl-FS) in the interlayer (0.79 nm), which corresponds well with the increase in ionic radii from a chloride ion (0.181 nm) to a bromide ion (0.196 nm). The XRD patterns for all the samples also feature a rhombohedral structure as opposed to a monoclinic structure expected in the case of a Cl-FS, which is similar to the observations made by Rapin et al. (1999) and Renaudin et al. (2004). This indicates the presence of the bromide (Br^-) ion in the interspacing, and therefore, it can be inferred that the uptake of bromide by LDHs mainly occurs through intercalation in the interlayers of Ca-Al layers.

Some secondary phases corresponding to $\text{Ca}(\text{OH})_2$ and NaBr were also identified in the XRD patterns of the synthesized sample (Figure 4.4). The peak around 18.08° corresponds to $\text{Ca}(\text{OH})_2$ (Scrivener et al. 2018) which confirms the presence of unreacted calcium hydroxide in the sample observed in the TGA/DSC analysis. The peak around 29.64° corresponds to presence of sodium bromide (Scrivener et al. 2018) in the synthesized sample, which could have resulted from the associated reactions between the starting chemicals, like CaBr_2 and NaAlO_2 , used during the synthesis processes.

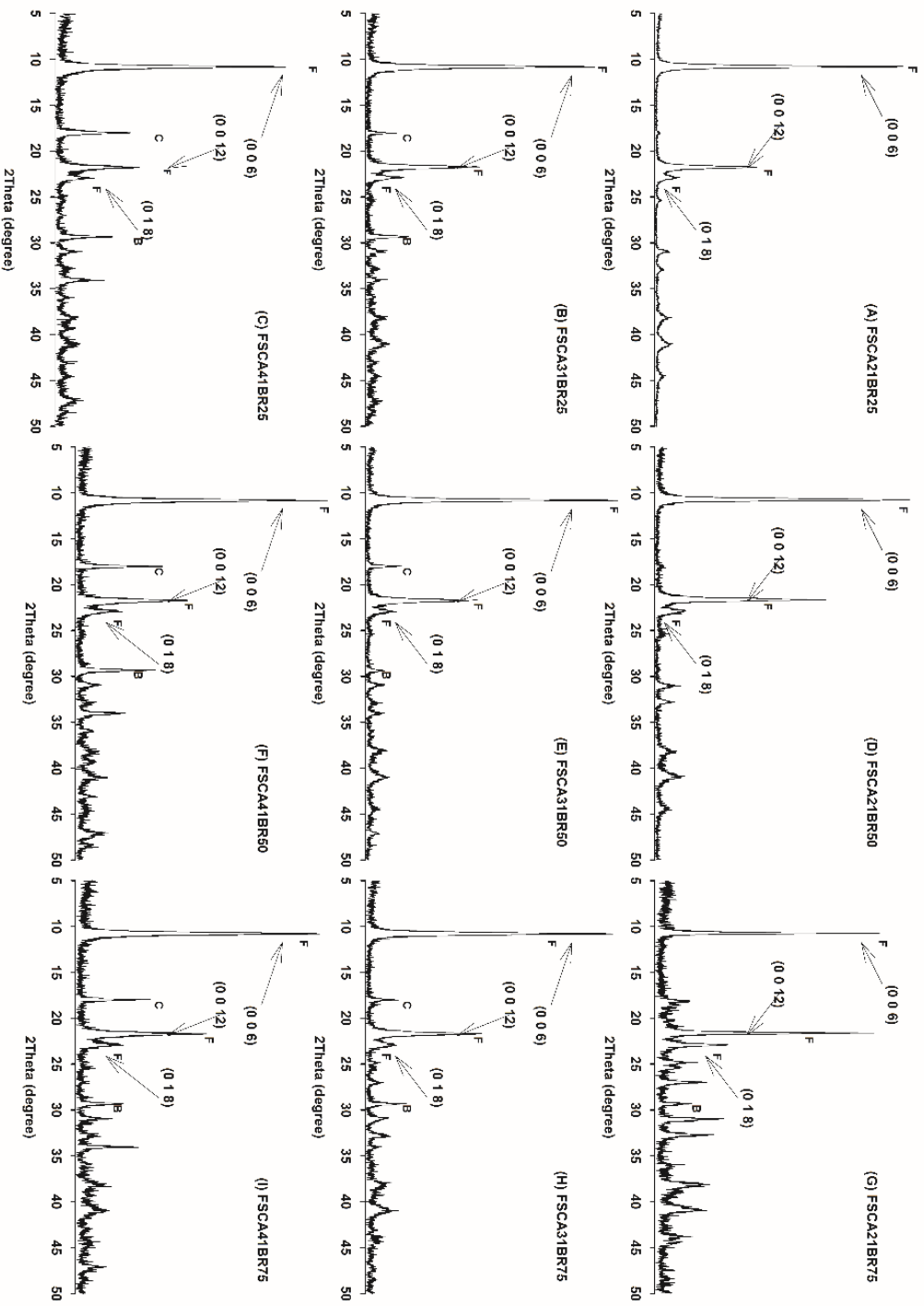


Figure 4.4. Powder XRD patterns for Br-LDH samples synthesized with Ca:Al ratio and [Br⁻] varied, where F: Br-LDH, C: Ca(OH)₂, and B: NaBr

Based on the results above, it can be concluded that well-ordered structures of LDH samples were synthesized and they can be used to sequester bromide. The uptake of bromide mainly occurs through intercalation of bromide ion in the interlayers of Ca-Al layered double hydroxides. However, the increase of the calcium to aluminum ratio increases the incorporation of carbonate in the sample, while secondary reactions between starting chemicals could lead to the presence of impurities in the sample.

4.3.2. Effect of Variation of Protocol Parameters on Bromide Removal

A two-factorial design was employed to investigate the effects of initial molar concentration of Br⁻ and Ca:Al ratio, as shown in Table 4.1, on the mass of bromide that was sequestered during the synthesis. Additionally, the calcium to aluminum ratio is controlled by the ratio of added calcium bromide and calcium hydroxide, thus an additional variable of CaBr₂/Ca(OH)₂ ratio was also investigated. The sequestration of bromide is evaluated by the removal of bromide from the solution and the bromide sequestered by unit mass of calcium. The bromide ion removal rate can be expressed using Equation 4.2, while the mass of bromide sequestered by a unit mass of calcium is expressed using Equation 4.3.

$$\Gamma_{\text{Br}} = \frac{M_i - M_f}{M_i} \quad \text{Eq. 4.2.}$$

$$\Gamma_{\text{Br/Ca}} = \frac{M_i - M_f}{M_{\text{Ca},i} - M_{\text{Ca},f}} \quad \text{Eq. 4.3.}$$

Where Γ_{Br} is the Br⁻ removal efficiency and $\Gamma_{\text{Br/Ca}}$ is the Br⁻ sequestered per mass of calcium. M_i and M_f are the initial and final mass of bromide ions in the solution (mg),

respectively, and $M_{Ca,i}$ and $M_{Ca,f}$ are the initial and final mass of calcium in the solution (mg), respectively.

Table 4.3 summarizes the results of the statistical testing of the ANOVA model and it is evident that the only class that shows a statistical significance is the bromide removal at different initial bromide concentrations using a confidence level of 0.05. The influence of calcium to aluminum ratio on the mass of bromide sequestered was not significant.

Table 4.3. Influence of bromide concentration and Ca:Al ratio parameters on the mass of bromide sequestered

Pr>F	Br ⁻ removal	Br ⁻ sequestered per mass of calcium
Initial bromide concentration	<.0001	0.0736
Calcium to aluminum ratio	0.9863	0.2765

The fraction of bromide removed and sequestered in Br-LDH decreased from 87% and 79.7% for initial Br⁻ concentrations of 0.25 M and 0.50 M, respectively, to 71.8% for an initial Br⁻ concentration of 0.75 M. The result indicates that the percentage removal of bromide decreases as the initial bromide concentration increases. However, it was observed that the absolute mass of bromide sequestered in Br-LDH still increased as the initial bromide concentration increased. The investigation into the bromide sequestered per calcium shows a linear dependency on the natural log of CaBr₂/Ca(OH)₂ ratio, calcium to aluminum ratio, and an interaction term of CaBr₂/Ca(OH)₂ ratio*initial bromide concentration. The statistical testing of the ANOVA model is shown in Table S4.1 while the regression statistic is shown in Table S4.2. It can be inferred from Table S4.1 that the fraction of bromide sequestered per calcium is strongly dependent on the natural log of

CaBr₂/Ca(OH)₂ ratio. Although, the calcium to aluminum ratio and the interaction term (CaBr₂/Ca(OH)₂ ratio*[Br⁻]) are significant, the influence of CaBr₂/Ca(OH)₂ ratio on the fraction of bromide sequestered per calcium is dominant compared to the Ca:Al ratio and the interaction term.

Bulk chemical analysis was used to determine the mole fractions of the individual components for each sample. Table 4.4 shows the synthesized molar compositions of the materials formed after reaction, with the molecular formula adjusted according to the determined mole fractions. Based on the ANOVA and regression statistics, and the characterization results, it could be inferred that calcium to aluminum ratio does not influence the sequestration of bromide in Br-LDH and therefore, it could be concluded that the synthesis of Br-LDHs using a calcium to aluminum ratio of 2:1 will be optimal for effective removal of bromide from the solution. A ratio of 2:1 was chosen over 3:1 or 4:1 to limit the incorporation of carbonate phase in the sample.

Table 4.4. Molar compositions of synthesized Br-LDH samples

Identifier	Ca:Al Ratio	Synthesized Molar Compositions
FSCA21BR25	2:1	$\text{Ca}_{1.8}\text{Al}(\text{OH})_{4.9}\text{Br}_{1.8}\cdot 1.8\text{H}_2\text{O}$
FSCA31BR25	3:1	$\text{Ca}_3\text{Al}(\text{OH})_{7.2}\text{Br}_{1.7}\cdot 1.5\text{H}_2\text{O}$
FSCA41BR25	4:1	$\text{Ca}_4\text{Al}(\text{OH})_{9.2}\text{Br}_{1.7}\cdot 1.2\text{H}_2\text{O}$
FSCA21BR50	2:1	$\text{Ca}_{1.9}\text{Al}(\text{OH})_{3.6}\text{Br}_{3.2}\cdot 1.7\text{H}_2\text{O}$
FSCA31BR50	3:1	$\text{Ca}_{2.8}\text{Al}(\text{OH})_{5.4}\text{Br}_{3.2}\cdot 1.5\text{H}_2\text{O}$
FSCA41BR50	4:1	$\text{Ca}_{3.8}\text{Al}(\text{OH})_{7.4}\text{Br}_{3.1}\cdot 1.2\text{H}_2\text{O}$
FSCA21BR75	2:1	$\text{Ca}_{1.6}\text{Al}(\text{OH})_{1.6}\text{Br}_{4.6}\cdot 1.7\text{H}_2\text{O}$
FSCA31BR50	3:1	$\text{Ca}_{2.4}\text{Al}(\text{OH})_{3.5}\text{Br}_{4.4}\cdot 1.6\text{H}_2\text{O}$
FSCA41BR50	4:1	$\text{Ca}_{1.6}\text{Al}(\text{OH})_{5.5}\text{Br}_{4.3}\cdot 1.3\text{H}_2\text{O}$

4.3.3. Stability of Br-LDHs in Varying Environmental Conditions

The synthesized Br-LDH samples were dissolved in solutions at various pH conditions in order to investigate their stability. The samples were extracted post-dissolution and were re-characterized using TGA-DSC and FTIR. Figure 4.5 and Figure 4.6 report the TGA-DSC curves and FTIR spectra recorded for one Br-LDH sample (FSCA21BR25), respectively. Comparing the TGA and DSC thermogram of FSCA21BR25 – pH natural and FSCA21BR25 – pH 13 samples with the thermogram of the initial (before dispersion) FSCA21BR25 sample (Figure 4.5), the behavior of the thermograms were quite similar and no discernable alterations to the structure were observed. Furthermore, the FTIR spectra (Figure 4.6) for the FSCA21BR25 – pH natural and FSCA21BR25 – pH 13 samples were also consistent with the initial FSCA21BR25 sample. Therefore, it is important to note that dissolution in either pH 13 or in a solution at natural pH was essentially congruent, and in turn, post-dissolution analysis of the solids did not show any deterioration of the structure or the formation of any secondary phases. Similar to FSCA21BR25, the structures of all the Br-LDH samples (CA 21, 31, 41 and BR

25, 50, 75) did not differ after dispersion in pH natural or pH 13 solutions. However, when the synthesized Br-LDH samples were dispersed in pH 2 solutions, high dissolution rate of all the samples occurred with little residues remaining for post-dissolution analysis using TGA-DSC or FTIR.

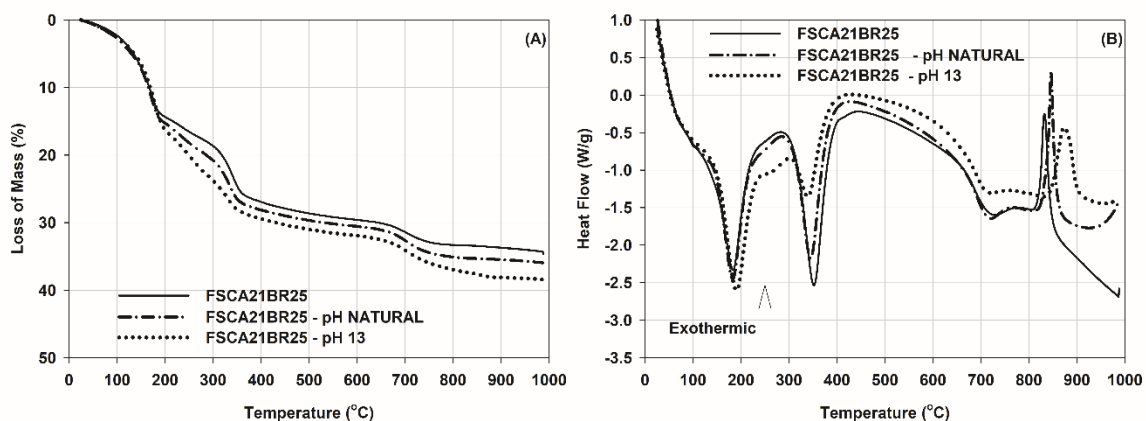


Figure 4.5. Comparison of (A) TGA and (B) DSC analysis for FSCA21BR25 samples dispersed in pH natural (---) and pH 13 (···) compared to initial FSCA21BR25 sample (-)

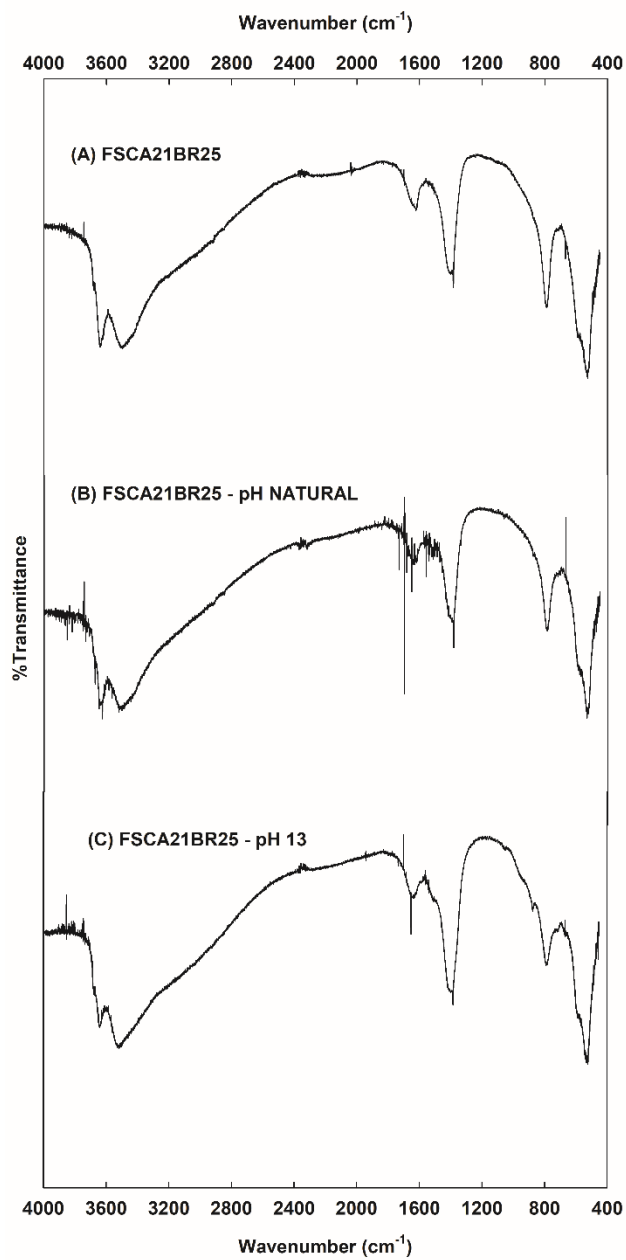


Figure 4.6. Comparison of FTIR spectrum for FSCA21BR25 samples dispersed in (B) pH natural and (C) pH 13 compared to (A) initial FSCA21BR25 sample

4.3.4. Solubility of Bromide Substituted LDHs

The molar concentrations of calcium, aluminum, and bromide, measured post-dissolution in solutions at various pH, were used to calculate the activities using PhreeqC, which were then used as inputs in Equation 4.1 to calculate the solubility product (log K_{sp}) values. The solubility of bromide substituted LDHs has not been studied in the literature, therefore, they have been compared with the solubility product values of chloride substituted Friedel's salt (Cl-FS). Balonis et al. (2010) and Bothe and Brown (2004) measured the solubility product of Cl-FS in water at 25 °C around -27.7, while Manikonda et al. (2020) reported that the log K_{sp} of Cl-FS was -28.9 at pH 13 and -12.6 at pH 2. Table 4.5 lists the log K_{sp} values of the synthesized Br-LDH samples dissolved in solutions at natural pH, pH 2, and pH 13. The solubility of the Br-LDH samples dispersed in ultrapure water is slightly higher compared to Cl-FS (Balonis et al. 2010; Birnin-Yauri and Glasser 1998; Bothe and Brown 2004), but less than the values reported by Manikonda et al. (2020) at equivalent conditions. The log K_{sp} values of the Br-LDH samples dissolved at pH 2 is several orders of magnitude higher than the log K_{sp} recorded at natural pH and as reported previously, the dissolution of the sample was very high, and it was not possible to extract any Br-LDH sample for post-dissolution characterization. However, when the samples were agitated in solution at pH 13, the K_{sp} values and the solubility decreased, similar to observations made for Cl-FS by Manikonda et al. (2020).

Table 4.5. Solubility product constants of synthesized Br-LDH samples at various pH conditions

Sample	pH	Average log K_{sp}
FSBR25 (CA 21, 31, 41)	Natural	-26.4
FSBR50 (CA 21, 31, 41)		-26.4
FSBR75 (CA 21, 31, 41)		-26.3
FSBR25	pH 13	-30.1
FSBR50		-28.5
FSBR75		-28.7
FSBR25	pH 2	-12.1
FSBR50		-12.1
FSBR75		-12.3

4.4. Conclusions

Hypersaline brines from processes like zero-liquid discharge concentrate from treatment of FGDWW and concentrate from desalination often contain high concentrations of bromide. Treatment of such brines using chemical precipitation by the formation of layered double hydroxides is a feasible approach for the removal of bromide because it is not energy-intensive like evaporation crystallization. In this study, the influence of initial bromide concentration and its interactions with the Ca:Al molar ratio on bromide removal performance was investigated.

Bromide substituted LDHs were synthesized using the optimum protocol selected by Manikonda et al. (2020) and the synthesized samples were characterized using TGA-DSC, FTIR, and XRD. The XRD patterns indicates the presence of the bromide (Br^-) ion in the interspacing, and therefore, it could be inferred that the uptake of bromide by LDHs occurs through intercalation in the interlayers of main Ca-Al layers. Based on the TGA-DSC, FTIR, XRD analysis, and the calculated molecular formulas, it was determined that

a calcium to aluminum ratio of 2:1 will be optimal for effective removal of bromide from the solution. The two-factorial ANOVA analysis and the regression analysis confirmed that the initial bromide concentration highly influenced the mass of bromide sequestered in the LDH samples compared to the calcium to aluminum ratio. Similarly, it was observed that Br-LDH samples undergo congruent dissolution when dissolved in ultrapure water or in a solution at pH 13, while dissolution rate at pH 2 was high with little residues remaining. In conclusion, it was established that the synthesis of Br-LDH using a calcium to aluminum ratio of 2:1 will be optimal for effective removal of bromide from hypersaline solutions. This optimized condition will be employed to synthesize Br-LDH and remove bromide from hypersaline brines to establish the realistic removal potential in field relevant scenarios. In addition, the results also suggest that synthesizing Br-LDH to remove bromide is a simple and effective method to treat high-salinity brines like FGD wastewater concentrate.

References

- Balonis, M., Lothenbach, B., Le Saout, G., and Glasser, F. P. (2010). "Impact of chloride on the mineralogy of hydrated Portland cement systems." *Cement and Concrete Research*, Pergamon, 40(7), 1009–1022.
- Birnin-Yauri, U., and Glasser, F.. (1998). "Friedel's salt, $\text{Ca}_2\text{Al}(\text{OH})_6(\text{Cl},\text{OH})\cdot 2\text{H}_2\text{O}$: its solid solutions and their role in chloride binding." *Cement and Concrete Research*, 28(12), 1713–1723.
- Bothe, J. V., and Brown, P. W. (2004). "PhreeqC modeling of Friedel's salt equilibria at 23 ± 1 °C." *Cement and Concrete Research*, Pergamon, 34(6), 1057–1063.

- Cravotta, C. A., and Brady, K. B. C. (2015). “Priority pollutants and associated constituents in untreated and treated discharges from coal mining or processing facilities in Pennsylvania, USA.” *Applied Geochemistry*, Elsevier Ltd, 62, 108–130.
- Fang, P., Tang, Z., Chen, X., Huang, J., Tang, Z., and Cen, C. (2018). “Chloride Ion Removal from the Wet Flue Gas Desulfurization and Denitrification Wastewater Using Friedel’s Salt Precipitation Method.” *Journal of Chemistry*, 2018, 1–9.
- Francis, R. A., Vanbriesen, J. M., and Small, M. J. (2010). “Bayesian statistical modeling of disinfection byproduct (DBP) bromine incorporation in the ICR database.” *Environmental Science and Technology*, American Chemical Society, 44(4), 1232–1239.
- Gingerich, D. B., Grol, E., and Mauter, M. S. (2018). “Fundamental challenges and engineering opportunities in flue gas desulfurization wastewater treatment at coal fired power plants.” *Environmental Science: Water Research and Technology*, Royal Society of Chemistry, 4(7), 909–925.
- Goh, K.-H., Lim, T.-T., and Dong, Z. (2008). “Application of layered double hydroxides for removal of oxyanions: A review.” *Water Research*, Pergamon, 42(6–7), 1343–1368.
- Good, K. D., and Vanbriesen, J. M. (2017). “Power Plant Bromide Discharges and Downstream Drinking Water Systems in Pennsylvania.” *Environmental Science and Technology*, 51(20), 11829–11838.
- Grishchenko, R. O., Emelina, A. L., and Makarov, P. Y. (2013). “Thermodynamic properties and thermal behavior of Friedel’s salt.” *Thermochimica Acta*, 570, 74–79.
- Ji, H., Wu, W., Li, F., Yu, X., Fu, J., and Jia, L. (2017). “Enhanced adsorption of bromate from aqueous solutions on ordered mesoporous Mg-Al layered double hydroxides (LDHs).” *Journal of Hazardous Materials*, Elsevier B.V., 334, 212–222.
- Karen Scrivener, Ruben Snellings, B. L. (2018). *A Practical Guide to Microstructural Analysis of Cementitious Materials. A Practical Guide to Microstructural Analysis of Cementitious Materials.*

- Landis, M. S., Kamal, A. S., Kovalcik, K. D., Croghan, C., Norris, G. A., and Bergdale, A. (2016). “The impact of commercially treated oil and gas produced water discharges on bromide concentrations and modeled brominated trihalomethane disinfection byproducts at two downstream municipal drinking water plants in the upper Allegheny River, Pennsylvania, .” *Science of the Total Environment*, Elsevier, 542, 505–520.
- Lv, L., Wang, Y., Wei, M., and Cheng, J. (2008). “Bromide ion removal from contaminated water by calcined and uncalcined MgAl-CO₃ layered double hydroxides.” *Journal of Hazardous Materials*, Elsevier, 152(3), 1130–1137.
- Ma, B., Fernandez-Martinez, A., Grangeon, S., Tournassat, C., Findling, N., Carrero, S., Tisserand, D., Bureau, S., Elkaim, E., Marini, C., Aquilanti, G., Koishi, A., Marty, N. C. M., and Charlet, L. (2018). “Selenite Uptake by Ca-Al LDH: A Description of Intercalated Anion Coordination Geometries.” *Environmental Science and Technology*, American Chemical Society, 52(3), 1624–1632.
- Ma, J., Li, Z., Jiang, Y., and Yang, X. (2015). “Synthesis, characterization and formation mechanism of Friedel’s salt (FS: 3CaO·Al₂O₃·CaCl₂·10H₂O) by the reaction of calcium chloride with sodium aluminate.” *Journal Wuhan University of Technology, Materials Science Edition*, 30(1), 76–83.
- Ma, J., Li, Z., Zhang, Y., and Demopoulos, G. P. (2009). “Desilication of sodium aluminate solution by Friedel’s salt (FS: 3CaO·Al₂O₃·CaCl₂·10H₂O).” *Hydrometallurgy*, Elsevier B.V., 99(3–4), 225–230.
- Manikonda, A., Bae, S., and Ogunro, V. O. (2020). Assessment of High Concentration Chloride Removal Performance by Precipitation of Friedel’s Salt. *Environmental Engineering Science*. Manuscript submitted for publication.
- Manikonda, A., Ogunro, V. O., Ellison, K. M., and Moo-Young, K. (2019). “Synthesis of Friedel’s Salt for Application in Halide Sequestration Using Paste Encapsulation Technology.” *Geo-Congress 2019*, Proceedings, 167–176.

- Mctigue, N. E., Cornwell, D. A., Graf, K., and Brown, R. (2014). "Occurrence and consequences of increased bromide in drinking water sources." *Journal - American Water Works Association*, American Water Works Association, 106(11), E492–E508.
- Parkhurst, D. L., and Appelo, C. A. J. (2013). "PHREEQC (Version 3)-A Computer Program for Speciation, Batch-Reaction, One-Dimensional Transport, and Inverse Geochemical Calculations." *Modeling Techniques, book 6*, 497.
- Pramanik, B. K., Shu, L., and Jegatheesan, V. (2017). "A review of the management and treatment of brine solutions." *Environmental Science: Water Research and Technology*, Royal Society of Chemistry, 3(4), 625–658.
- Rapin, J.-P., Noor, N. M., and François, M. (1999). "The double layered hydroxide $3\text{CaO} \cdot \text{Al}_2\text{O}_3 \cdot \text{CaBr}_2 \cdot 10\text{H}_2\text{O}$." *Acta Crystallographica Section C Crystal Structure Communications*, International Union of Crystallography (IUCr), 55(8), IUC9900092.
- Renaudin, G., Rapin, J.-P., Elkaim, E., and François, M. (2004). "Polytypes and polymorphs in the related Friedel's salt $[\text{Ca}_2\text{Al}(\text{OH})_6][\text{X} \cdot 2\text{H}_2\text{O}]^-$ halide series." *Cement and Concrete Research*, 34(10), 1845–1852.
- Ruhl, L., Vengosh, A., Dwyer, G. S., Hsu-Kim, H., Schwartz, G., Romanski, A., and Smith, S. D. (2012). "The Impact of Coal Combustion Residue Effluent on Water Resources: A North Carolina Example." *Environmental Science & Technology*, American Chemical Society, 46(21), 12226–12233.
- Sawade, E., Fabris, R., Humpage, A., and Drikas, M. (2016). "Effect of increasing bromide concentration on toxicity in treated drinking water." *Journal of Water and Health*, IWA Publishing, 14(2), 183–191.
- Tong, T., and Elimelech, M. (2016). "The Global Rise of Zero Liquid Discharge for Wastewater Management: Drivers, Technologies, and Future Directions." *Environmental Science & Technology*, 50(13), 6846–6855.

USEPA. (2015). “Steam Electric Power Generating Effluent Guidelines - 2015 Final Rule.” <<https://www.epa.gov/eg/steam-electric-power-generating-effluent-guidelines-2015-final-rule>> (Oct. 16, 2020).

USEPA. (2016). “Fourth Unregulated Contaminant Monitoring Rule | Monitoring the Occurrence of Unregulated Drinking Water Contaminants | US EPA.” *Web Page*, <<https://www.epa.gov/dwucmr/fourth-unregulated-contaminant-monitoring-rule>> (Sep. 20, 2020).

Vieille, L., Rousselot, I., Leroux, F., Besse, J. P., and Taviot-Guého, C. (2003). “Hydrocalumite and Its Polymer Derivatives. 1. Reversible Thermal Behavior of Friedel’s Salt: A Direct Observation by Means of High-Temperature in Situ Powder X-ray Diffraction.” *Chemistry of Materials*, American Chemical Society, 15(23), 4361–4368.

Wang, L. P., Lee, W. H., Tseng, S. M., and Cheng, T. W. (2018). “Removal of chloride ions from an aqueous solution containing a high chloride concentration through the chemical precipitation of Friedel’s salt.” *Materials Transactions*, 59(2), 2–7.

Yang, L., Shahrivari, Z., Liu, P. K. T., Sahimi, M., and Tsotsis, T. T. (2005). “Removal of trace levels of arsenic and selenium from aqueous solutions by calcined and uncalcined layered double hydroxides (LDH).” *Industrial and Engineering Chemistry Research*, 44(17), 6804–6815.

Yue, Y., Wang, J. J., Basheer, P. A. M., and Bai, Y. (2018). “Raman spectroscopic investigation of Friedel’s salt.” *Cement and Concrete Composites*, Elsevier Ltd, 86, 306–314.

Zhang, D., Jia, Y., Ma, J., and Li, Z. (2011). “Removal of arsenic from water by Friedel’s salt (FS: $3\text{CaO}\cdot\text{Al}_2\text{O}_3\cdot\text{CaCl}_2\cdot 10\text{H}_2\text{O}$).” *Journal of Hazardous Materials*, 195, 398–404.

Zhang, L., Lv, P., He, Y., Li, S., Peng, J., Zhang, L., Chen, K., and Yin, S. (2021). “Ultrasound-assisted cleaning chloride from wastewater using Friedel’s salt precipitation.” *Journal of Hazardous Materials*, Elsevier B.V., 403, 123545.

Zhang, M., and Reardon, E. J. (2003). "Removal of B, Cr, Mo, and Se from wastewater by incorporation into hydrocalumite and ettringite." *Environmental Science and Technology*, American Chemical Society, 37(13), 2947–2952.

Supplementary Information

Table S4.1. Analysis of variance (ANOVA) results when Br/Ca is the dependent variable

<i>Response</i>	<i>Degree of freedom</i>	<i>Sum of squares</i>	<i>Mean square</i>	<i>F-statistic</i>	<i>P-value</i>
Model	3	4.470	1.490	2047.37	<.0001
Ln(CaBr ₂ /Ca(OH) ₂)	1	4.345	4.345	5970.26	<.0001
Calcium to Aluminum ratio	1	0.008	0.008	10.99	0.0211
Ln(CaBr ₂ /Ca(OH) ₂)*initial Bromide concentration	1	0.117	0.117	160.87	<.0001
Error	5	0.004	0.001		
Total	8	4.474			

Table S4.2. Regression statistic results when Br/Ca is the dependent variable

Parameter	Estimate	Standard Error	t Value	Pr > t
Intercept	1.6221	0.0438	37.08	<.0001
Ln(CaBr ₂ /Ca(OH) ₂)	-0.5367	0.0223	-24.05	<.0001
Calcium to Aluminum ratio	0.0463	0.0150	3.08	0.0273
Ln(CaBr ₂ /Ca(OH) ₂)*initial Bromide concentration	-0.0070	0.0006	-12.68	<.0001

CHAPTER 5: LAYERED DOUBLE HYDROXIDE PRECIPITATION FOR MANAGING SULFATE AND CHLORIDE RICH BRINES: FEASIBILITY AND PARAMETER ASSESSMENT

Abhisek Manikonda, Vincent O. Ogunro

Abstract

Hypersaline brines like FGD wastewater concentrate are difficult to treat because of lack of cost-effective and energy-efficient technologies. Such brines are especially challenging when composed of elevated concentrations of both sulfate and chloride ions. This research explored the feasibility of removing sulfate and chloride from high-salinity brines through the precipitation of calcium-aluminum based layered double hydroxides like Kuzel's salt and Friedel's salt. Parameters affecting the reduction of concentration of sulfate and chloride like the initial molar concentration of chloride, initial molar concentration of sulfate, the calcium to aluminum ratio, and the interactions between the three parameters were evaluated. The stability of the Ca-Al layered double hydroxides at various prevailing solutions was investigated and an optimal calcium to aluminum ratio for the effective removal of chloride and sulfate was established. Experimental results confirmed that the initial sulfate concentration highly influenced the mass of chloride and sulfate sequestered in the Ca-Al layered double hydroxides. It was also observed that Ca-Al layered double hydroxides undergo congruent dissolution when dispersed in water or solution at pH 13, while dissolution at pH 2 was incongruent in nature. Based on the Raman spectroscopy results, thermogravimetric analysis, and X-ray diffraction analysis, it could be hypothesized that the synthesis of Ca-Al layered double hydroxides using a calcium to aluminum ratio of 2:1 will be optimal for effective removal of chloride and sulfate from

hypersaline solutions. In addition, the results suggest that this process is a simple and effective method to treat high-salinity brines which are rich in sulfate and chloride.

5.1. Introduction

Management of high-salinity brines is a major environmental concern for industries around the world (Boelter et al. 1992; Pramanik et al. 2017). Some examples of hypersaline brines include zero-liquid discharge concentrate from treatment of flue gas desulfurization (FGD) wastewater (Gingerich et al. 2018), cooling towers and ash transport water, concentrate from desalination (Pramanik et al. 2017), discharges from coal mines (Cravotta and Brady 2015), effluent from plastics and textile manufacturing (Mctigue et al. 2014), and wastewater during oil and gas extraction (Landis et al. 2016). Hypersaline brines like FGD wastewater concentrate often contain high concentrations of anions such as chloride and sulfate. In addition to negative environmental impacts of the discharge of wastewater with high concentrations of chloride (Cl^-) into water bodies (Boelter et al. 1992), high concentrations of sulfate (SO_4^{2-}) can lead to the formation of hydrogen sulfide in water bodies, Hydrogen sulfide is a poisonous gas, can corrode concrete and metal structures, and can also be responsible for odor issues (Dou et al. 2017; Tait et al. 2009). The presence of high concentration is sulfate can also promote mineralization of water and cause scaling of equipment (Dou et al. 2017). Therefore, hypersaline brines need to be adequately treated to remove the high concentrations of sulfate and chloride before disposal.

Currently, hypersaline brines are treated to remove chloride and sulfate using membrane technologies (reverse osmosis), evaporation-based thermal treatments like crystallization, and electrodialysis (Gingerich et al. 2018; Tong and Elimelech 2016).

However, these approaches are energy intensive and are not suitable for treatment of wastewater like hypersaline brines. Chemical precipitation methods, such as layered double hydroxides (LDHs) precipitation, can be an alternative approach for the removal of chloride and sulfate because it is membrane-less and not energy-intensive like evaporation crystallization. Layered double hydroxides are a class of two-dimensional lamellar compounds consisting of positively charged octahedral layers and a negatively charged interlayer containing water and anion molecules (Goh et al. 2008). Layered double hydroxides (LDH) are often considered as efficient ion-exchangers of contaminant ions due to their high anion exchange capacity (Ma et al. 2018) and the availability of large interlayer spaces (Yang et al. 2005). Studies like Maziarz et al. (2019) and Tian (et al. 2020) investigated the removal of sulfate from wastewater like acid mine drainage water by precipitation using LDHs of the Mg/Al type. Multiple studies have also examined the treatment of brines containing high concentrations of sulfate through the precipitation of ettringite, which is a hydroxy calcium alumino-sulfate mineral belonging to the LDH family and is represented by $[\text{Ca}_6\text{Al}_2(\text{SO}_4)_3(\text{OH})_{12}\cdot 26\text{H}_2\text{O}]$ (Almasri et al. 2015; Dou et al. 2017; Fang et al. 2018b; Jin et al. 2020; Tait et al. 2009).

However, Balonis et al. (2010) state that the presence of chloride in wastewater can inhibit the formation of ettringite. Their attempts to synthesize chloride-ettringite was not successful and instead resulted in the formation of other LDH compounds. They postulate that chloride-ettringite occurs in a thermodynamically stable form at temperatures below 0 °C. Alternatively, removal of sulfate and chloride from wastewater can be achieved through precipitation of Ca-Al LDHs like Kuzel's salt and Friedel's salt. Kuzel's salt (KS) is a chloride and sulfate ordered compound and has a composition of

$3\text{CaO}\cdot\text{Al}_2\text{O}_3\cdot\frac{1}{2}\text{CaCl}_2\cdot\frac{1}{2}\text{CaSO}_4\cdot\sim 11\text{H}_2\text{O}$ (Balonis et al. 2010). The main layer of KS consists of aluminum-oxygen-calcium (Al-O-Ca) bonds. Kuzel's salt has a staging structure, with succession of interlayers populated with $[\text{Cl}\cdot 2\text{H}_2\text{O}]^-$ followed by interlayer filled with $[(\text{SO}_4)_{0.5}\cdot 3\text{H}_2\text{O}]^-$ (Mesbah et al. 2011). Friedel's salt $[\text{Ca}_2\text{Al}(\text{OH})_6\text{Cl}\cdot 2\text{H}_2\text{O}]$ is an anion-exchange mineral, also belonging to the LDHs family (Birnin-Yauri and Glasser 1998). It is composed of hydroxide layers with Ca^{+2} and Al^{+3} octahedral units and an interlayer of Cl^- ions. Balonis et al. (2010), Brown and Bothe (2004), and Glasser et al. (1999) modelled the thermodynamic stability of a Ca-Al LDH system to determine the binding affinity for chloride and sulfate. They state that treatment of hypersaline brines through precipitation of KS is possible if the sulfate concentration ($[\text{SO}_4]$) in the wastewater is greater than three times the chloride concentration ($[\text{Cl}]$). However, as the chloride concentration increases and the $[\text{SO}_4]/[\text{Cl}]$ ratio decreases below three, the formation of FS is promoted, and the sulfate ions precipitate out as ettringite (Balonis et al. 2010).

Friedel's salt has been widely employed for environmental remediation of chloride and heavy metals from wastewater because of its high adsorption efficiency (Fang et al. 2018a; Yang et al. 2005; Zhang et al. 2021; Zhang and Reardon 2003). A few studies have characterized the effect of process parameters like solution pH and reaction temperature, among others, on the structure of Friedel's salt and the removal of chloride. Studies like Fang et al. (2018a), Ma et al. (2015), Manikonda et al. (2019), and Manikonda et al. (2020) have investigated the effects of initial CaCl_2 concentration, calcium to aluminum (Ca:Al) molar ratio, reaction time, and reaction temperature on the structure of Friedel's salt. Ma et al. (2015) and Manikonda et al. (2019) state that the final structure of FS was consistent

for any synthesis reaction temperatures below 100 °C. Manikonda et al. (2020) observed that the initial chloride concentration highly influenced the mass of chloride sequestered in the Friedel's salt sample. Ma et al. (2015), Manikonda et al. (2020), and Fang et al. (2018a) reported that the optimum range of calcium to aluminum ratio is 3:1. However, there is a gap in knowledge about the ability of KS to successfully sequester sulfate and chloride from brines. There is little information available about the effect of parameters including, initial chloride concentration, initial sulfate concentration, calcium to aluminum (Ca:Al) ratio on the removal of sulfate and chloride from wastewater. This study aims to evaluate the performance of high concentration sulfate and chloride removal by the precipitation of LDHs like Kuzel's salt and Friedel's salt. The conditions under which either of KS and FS and/or both LDHs are formed will be investigated. Influence of key parameters such as initial sulfate and chloride concentration and their interaction with the Ca:Al molar ratio on removal performance was investigated. A series of experiments were carried out to assess the stability of the LDH products at various prevailing solution pH conditions. An optimal calcium to aluminum ratio for the effective removal of sulfate and chloride was established.

5.2. Materials and Methods

Hypersaline brines like FGD wastewater concentrate are characterized with an extremely complex composition matrix. It would be challenging to understand the factors that will influence the formation of LDHs if synthesized using FGD wastewater concentrate. Therefore, the removal of sulfate and chloride through precipitation of Ca-Al LDHs was studied using synthetic FGD wastewater concentrate to determine the optimum operating parameters. The starting materials CaCl_2 , NaAlO_2 , Na_2SO_4 , and $\text{Ca}(\text{OH})_2$ for the

preparation of Ca-Al LDHs were of analytical grade and were used without further purification. Ultrapure deionized water (18 M Ω) was used for solution preparation and washing.

5.2.1. Synthesis of Ca-Al LDH Synthesis

Manikonda et al. (2020) compared three different protocols for the synthesis of Ca-Al LDHs in order to determine the optimum protocol in terms of mass of chloride sequestered and the relative propinquity of the structure of the synthesized sample compared to a well-ordered sample. They concluded that the protocol outlined by Zhang et al. (2011) has a structure that is comparable to a well-ordered idealized sample. Therefore, the synthesis protocol by Zhang et al. (2011) was used to investigate the performance of sulfate and chloride removal by Ca-Al LDH compounds.

Reagent grade NaAlO₂ was dissolved directly in ultrapure water to form NaAl(OH)₄. The reaction solution was heated to 25 °C, and a mixture of CaCl₂ and Na₂SO₄ was then added dropwise at a rate of 5 mL/min under continuous stirring. Stirring was continued for an additional one hour after the completion of the addition of the reagents. The precipitate was collected at the end of the stirring period by vacuum filtration using 0.45 μ m PTFE filters, washed with ultrapure water, and finally dried in an oven at 60 °C for 24 hours. The synthesis was carried out at 25 °C because Manikonda et al. (2019) reported that reaction temperature did not have a significant influence on the structure of Ca-Al LDH compounds. All the experiments were performed in ambient atmospheric conditions.

5.2.2. Characterization of Ca-Al LDH Samples

The microstructure of the synthesized samples was characterized using thermogravimetric analysis and differential scanning calorimetry (TGA-DSC), Raman spectroscopy, and X-ray powder diffraction (XRD). The TGA-DSC analysis was performed using a SDT Q600 (TA Instruments, Delaware) by heating the specimen from 25 °C to 1300 °C in a nitrogen atmosphere at a rate of 10 °C/min. Micro-Raman spectra was recorded at room temperature in the back-scattering geometry using a Horiba (Japan) LabRam HR800 confocal Raman microscope with a 1200g/mm grating. A 532 nm laser beam was focused on a 1 μm^2 area on the sample surface using a long working distance 50x microscope lens with NA = 0.5. Laser power at the sample level was kept low (< 10 mW) in order to avoid any damage to the material. The Raman detector was a charge coupled device (CCD) detector. Spectral resolution of the experiment setup was better than 1 cm^{-1} . X-ray powder diffraction patterns were recorded using a PANalytical (Netherlands) X'Pert PRO diffractometer ($2\theta = 5\text{-}50^\circ$, stepsize 0.02° with 0.5 s/step). The supernatant obtained from the filtration of the precipitate was analyzed for concentrations of Cl^- and SO_4^{2-} , using an ICS-3000 ion chromatography system (Dionex, California), and for Al^{+3} and Ca^{+2} , using a 5100 ICP-OES instrument (Agilent, California). The pH and conductivity of the supernatant was measured with a SevenExcellence S470-Kit pH/conductivity meter (Mettler Toledo, Ohio).

5.2.3. Variation of Protocol Parameters

A Latin square design with repeated measures was implemented to understand the effect of parameters like the molar concentration of Cl^- and SO_4^{2-} and the calcium to

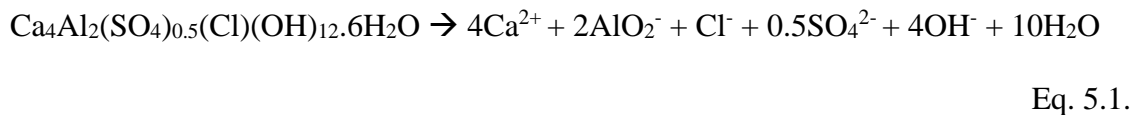
aluminum (Ca:Al) ratio on the mass of chloride and sulfate that was sequestered during Ca-Al LDH synthesis. The goal of the Latin square design was to understand the individual effects of initial chloride concentration, initial sulfate concentration, Ca:Al ratio, and the interactions between the three factors on chloride and sulfate removal efficiency. A Latin square design with repeated measures was chosen to maximize the interactions while minimizing the number of runs. Table 5.1 provides the experimental conditions of the three parameters in the Latin square design, each at three levels. A Ca-Al LDH sample synthesized using a Ca:Al ratio of 3:1 (CA31) with an initial chloride concentration of 0.1 M (CL01) and an initial sulfate concentration of 1 M (SO10) is identified as KSCA31CL01SO10. The range of Ca:Al ratios were selected based on previous research by Manikonda et al. (2020), Fang et al. (2018a), Ma et al. (2015), and Wang et al. (2018). The range of molar concentrations of sulfate and chloride were selected to reflect FGD wastewater concentrates with sulfate concentrations ($[SO_4]$) greater than three times the chloride concentrations ($[Cl]$). The additional calcium required to obtain the desired initial Ca:Al ratio was supplemented using $Ca(OH)_2$.

Table 5.1. Levels of parameters tested in the Latin square design, where $C_{Sulfate}$ is the molar concentration of SO_4^{2-}

		Ca:Al Ratio		
		2:1	3:1	4:1
Molar Concentration of Cl^-	0.1 M	$C_{Sulfate} = 0.75 \text{ M}$	$C_{Sulfate} = 1 \text{ M}$	$C_{Sulfate} = 0.5 \text{ M}$
	0.2 M	$C_{Sulfate} = 1 \text{ M}$	$C_{Sulfate} = 0.5 \text{ M}$	$C_{Sulfate} = 0.75 \text{ M}$
	0.3 M	$C_{Sulfate} = 0.5 \text{ M}$	$C_{Sulfate} = 0.75 \text{ M}$	$C_{Sulfate} = 1 \text{ M}$

5.2.4. Stability and Solubility of Ca-Al LDH Samples

In order to determine the stability and solubility product of Ca-Al LDH samples in different environments, the synthesized samples were dispersed in three types of solutions (at 25 °C) at a liquid to solid ratio of 20 to 1: solution at pH natural (ultrapure water), solution at pH 2, and solution at pH 13. The dispersed samples were subjected to agitation for 18 hours. After agitation, the samples were extracted by vacuum filtration and were re-characterized. The supernatants were analyzed for concentrations of calcium, aluminum, sulfate, and chloride. The geochemical speciation program PhreeqC (Parkhurst and Appelo 2013) was used to convert the measured molar concentrations of each component to their corresponding activities. The solubility product of KS was measured using the dissolution reaction presented by Glasser et al. (1999) and is defined in Equation 5.1. The dissociation equation presented by Bothe and Brown (2004) for FS was used (Equation 5.2) to determine the solubility product of FS samples.



5.3. Results and Discussion

5.3.1. Effect of Variation of Protocol Parameters on Structure of Ca-Al LDHs

Figure 5.2 and Figure 5.1 report the TGA and DSC curves recorded for the Ca-Al LDH samples synthesized while the calcium to aluminum ratio, the initial chloride

concentration, and the initial sulfate concentration were varied, respectively. When the $[\text{SO}_4]/[\text{Cl}]$ ratio is between 10 and 3, the formation of KS is expected to be promoted over FS (Balonis et al. 2010), therefore, the TGA and DSC data of the synthesized Ca-Al LDH samples were compared to the thermogravimetric profiles of Kuzel's salt. Similar to FS, a well-ordered KS also has three main weight losses over the temperature ranges 25 – 300 °C (dehydration of water molecules), 450 – 900 °C (release of chloride), and 1000 – 1200 °C (decomposition of sulfate). The mass loss at 25 – 300 °C should be 34.08%, in the second step (450 – 900 °C) should be 7.53%, and in the last step (1000 - 1300 °C) is 6.94% (Mesbah et al. 2011).

Evaluating the TGA (Figure 5.2) and DSC (Figure 5.1) curves, an endotherm centered around 140 °C matched by a well-resolved mass loss step was observed for all the samples. The total mass losses for KSCA21, KSCA31, and KSCA41 samples are $46.0 \pm 1.4\%$, $49.1 \pm 1.9\%$, and $54.4 \pm 2.2\%$, respectively (Table 5.2). The total mass loss for KSCA21 and KSCA31 samples is comparable to a theoretical total mass loss for a well-ordered KS sample (48.6%), while the total mass loss for KSCA41 samples is higher than a well-ordered KS sample. The mass loss configurations for Ca-Al LDH samples with Ca:Al ratio of 2-3:1 and chloride concentrations of 0.1 M and 0.2 M between 25 – 300 °C, corresponding to the dehydration of water molecules, is similar when compared to the mass loss of a well-ordered KS sample. However, the Ca-Al LDH samples synthesized using Ca:Al ratio of 4:1 had a higher percent mass loss between 25 – 300 °C and lower mass loss in the temperature ranges of 450 – 900 °C and 1000 - 1300 °C, which correspond to the release of chloride and decomposition of sulfate, respectively. The behavior of the Ca-Al LDH samples synthesized with an initial chloride concentration of 0.3 M was also different

when compared to the mass loss behavior of a well-ordered KS sample. All the samples also displayed minor underestimation of chloride content, which could be explained by carbonate contamination of the samples.

Table 5.2. Comparison of % mass lost recorded using TGA for Ca-Al LDH samples synthesized with Ca:Al ratio, [Cl⁻], and [SO₄²⁻] varied

Protocol	Loss of Sample Mass (%)			Total Mass Loss (%)
	25 °C < T < 300 °C	450 °C < T < 900 °C	1000 °C < T < 1300 °C	
Well-ordered KS	34.1	7.5	6.9	48.6
KSCA21CL01SO75	35.6	6.5	5.9	48.0
KSCA31CL01SO10	30.7	10.2	6.8	47.7
KSCA41CL01SO05	48.0	3.7	5.4	57.2
KSCA21CL02SO10	35.1	5.0	5.0	45.1
KSCA31CL02SO05	35.5	6.0	6.2	47.8
KSCA41CL02SO75	43.3	5.5	5.3	54.1
KSCA21CL03SO05	32.6	6.4	5.9	45.0
KSCA31CL03SO75	41.4	4.5	5.9	51.9
KSCA41CL03SO10	42.0	5.8	4.0	51.8

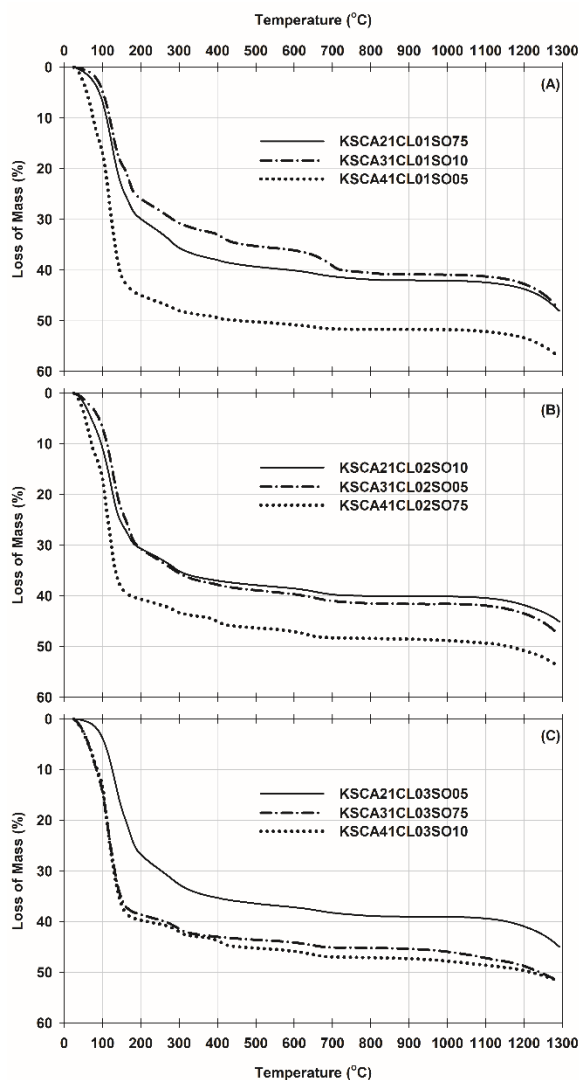


Figure 5.2. Comparison of weight loss data recorded by TGA for Ca-Al LDH samples synthesized with Ca:Al ratio, $[\text{Cl}^-]$, and $[\text{SO}_4^{2-}]$ varied

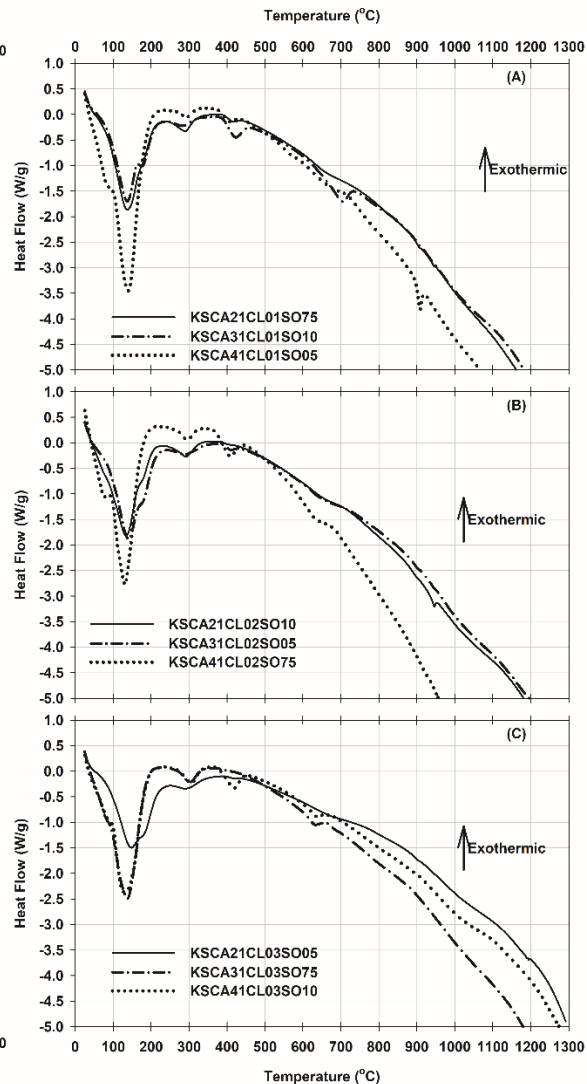


Figure 5.1. Comparison of DSC curves recorded for Ca-Al LDH samples synthesized with Ca:Al ratio, $[\text{Cl}^-]$, and $[\text{SO}_4^{2-}]$ varied

The carbonate contamination of the samples was confirmed by the Raman spectra recorded for the Ca-Al LDH samples, shown in Figure 5.3. The vibration around 1086 cm^{-1} , visible for all the samples, is ascribed to the presence of a carbonate ion in the interlayer (Mesbah et al. 2011). In Figure 5.3, the most intense band for all the samples is observed at 984 cm^{-1} , representing the vibration mode of S-O bonds in the sulfate

molecules. The minor bands around 453 cm^{-1} are also assigned to the vibration of the S-O bonds. The hump around 531 cm^{-1} , visible for samples synthesized with a Ca:Al ratio of 2:1 and 3:1 (Figure 5.3 (A) (B) (D) (E) (G) (H)), are unique in Ca-Al LDHs and is attributed to the stretching vibration mode of the Al-OH bonds (Mesbah et al. 2011; Yue et al. 2018). However, no similar hump around 531 cm^{-1} was observed in the samples that synthesized with a Ca:Al ratio of 4:1 (Figure 5.3 (C) (F) (I)), possibly indicating that the final structure of these synthesized samples does not represent a layered double hydroxide. Furthermore, all the three KSCA41 samples have a sharp band around 710 cm^{-1} , which can be assigned to modes from calcium hydroxide (Schmida and Dariz 2014).

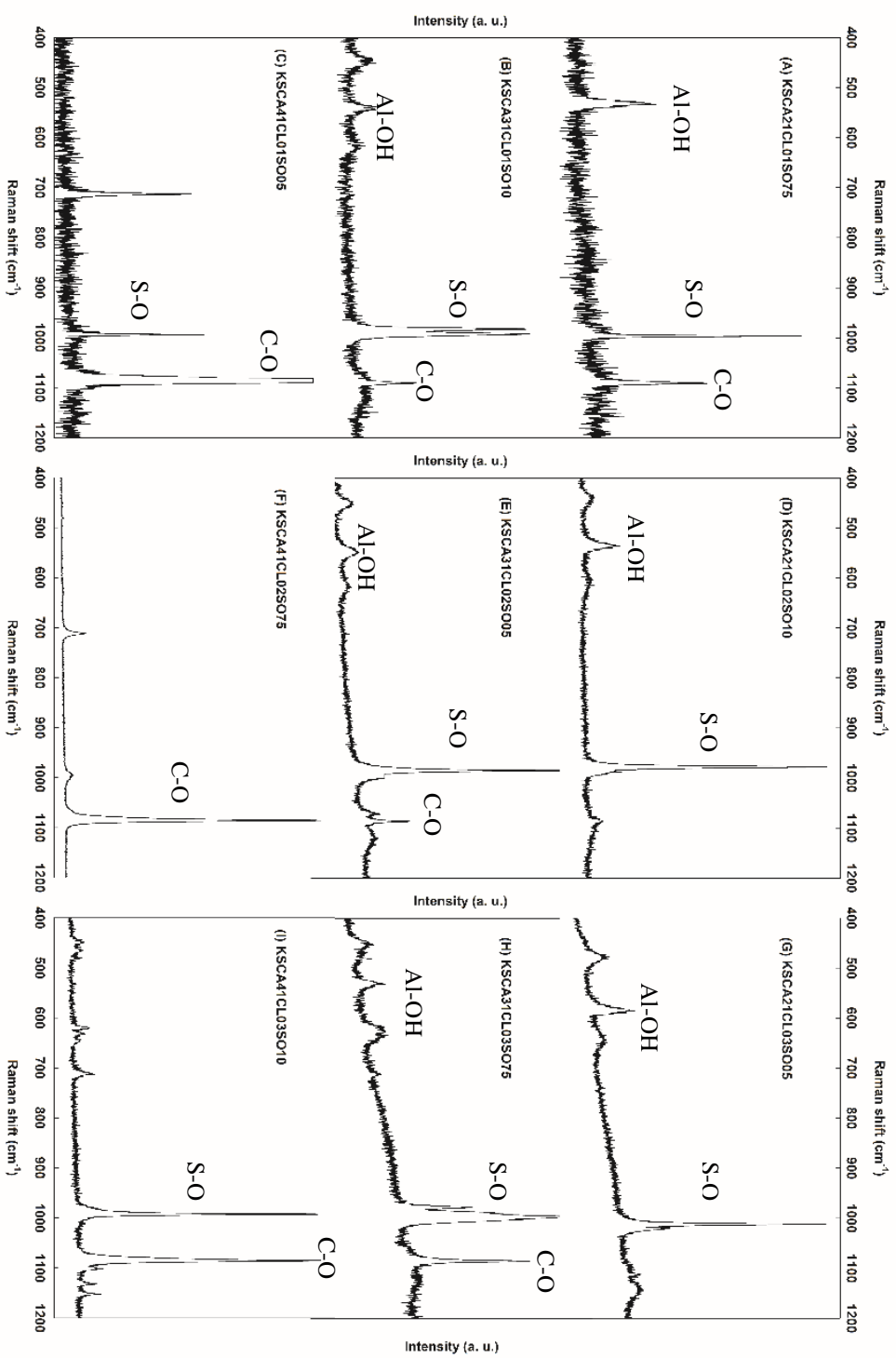


Figure 5.3. Raman spectra in the range 400–1200 cm^{-1} for Ca-Al LDH samples synthesized with Ca:Al ratio, $[\text{Cl}^-]$, and $[\text{SO}_4^{2-}]$ varied

The XRD patterns of the synthesized Ca-Al LDH samples are shown in Figure 5.4. The reflections observed at 2θ around 10.54° and 22.80° for KSCA21 and KSCA31 samples correspond to typical Miller-Bravais indices of Kuzel's salt. The basal spacing of the $2\theta = 10.80^\circ$ reflection is 0.84 nm is in agreement with the d-spacing reported by Balonis et al. (2010) for Kuzel's salt. Furthermore, as the initial chloride concentration increased to 0.3 M ($[\text{SO}_4]/[\text{Cl}] = 1.7 - 2.5$), the peak that emerged around 11.15° in XRD patterns of KSCL03 samples (Figure 5.4 (G) (H)) indicates the presence of Friedel's salt along with Kuzel's salt. However, in the case of KSCA41 samples, there were no peaks that were observed at 2θ around 10.54° . Similar to the observations made in the Raman spectra, the final structure of these synthesized samples does not represent a layered double hydroxide. Therefore, it can be concluded that a calcium to aluminum ratio of 4:1 does not result in the formation of Ca-Al LDHs in brines that have high concentrations of sulfate and chloride. Multiple secondary phases were also observed in the XRD patterns of the synthesized sample (Figure 5.4), possibly indicating that the final synthesized samples are not well-ordered Ca-Al LDH structures. This variability in the structures was also evident in the thermogravimetric behavior of the synthesized samples (Figure 5.1 and Figure 5.2). However, these synthesized Ca-Al LDH phases have still sequestered a significant mass of sulfate and chloride from the solution into their interlayers. The fraction of sulfate removed and sequestered is 65% for initial Cl^- concentration of 0.1 M and 0.2 M, while the fraction of chloride removed is around 42%. However, when the initial chloride concentration is 0.3 M, the fraction of sulfate decreased to 55% while the fraction of chloride removed from the solution and sequestered in the Ca-Al LDH sample increased to 48%.

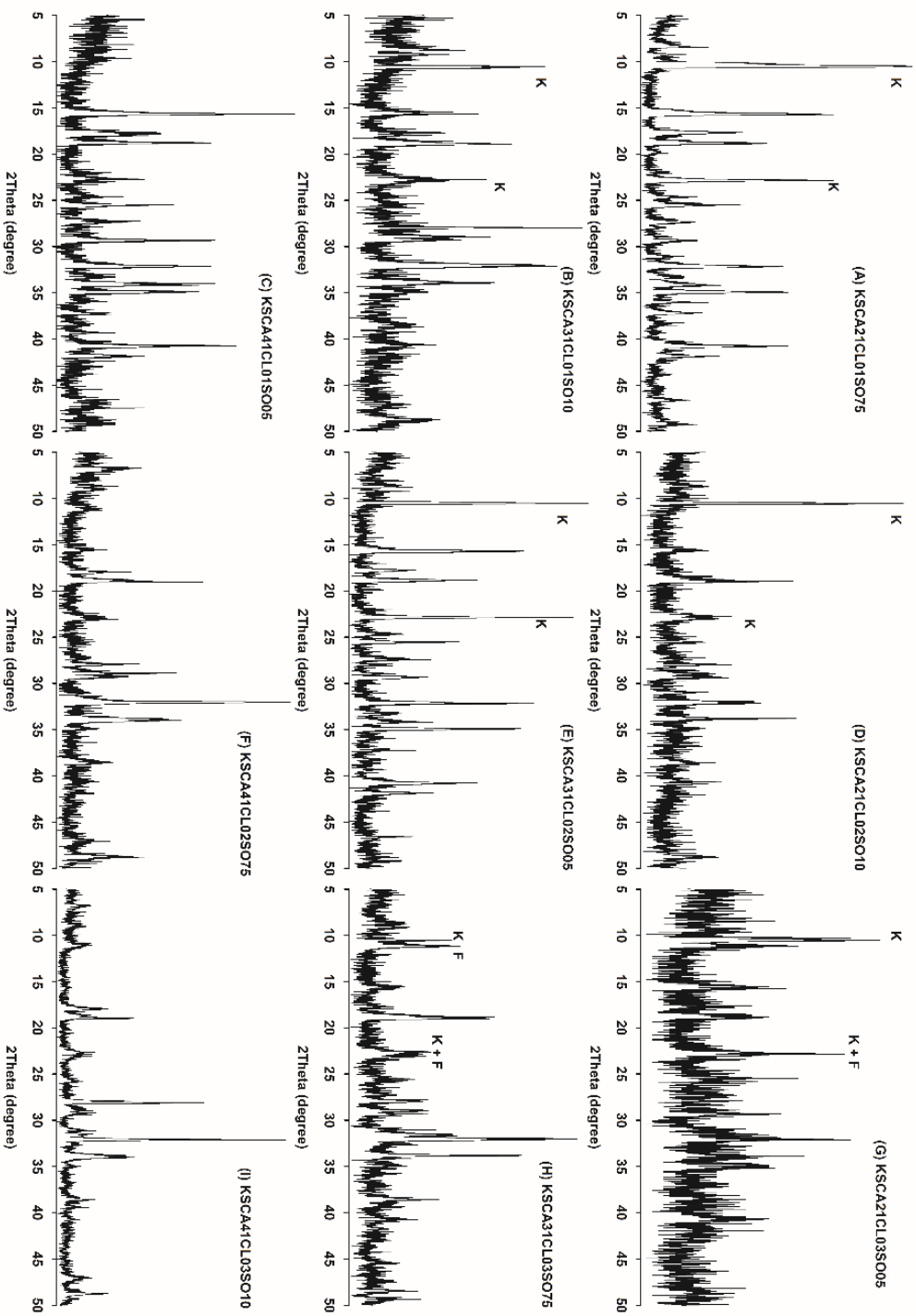


Figure 5.4. Powder XRD patterns for Ca-Al LDH samples synthesized with Ca:Al ratio, $[Cl^-]$, and $[SO_4^{2-}]$ varied where K: Kuzel's salt and F: Friedel's salt

In order to understand the effect of parameters like the molar concentration of Cl^- and SO_4^{2-} and the calcium to aluminum (Ca:Al) ratio on the mass of chloride and sulfate that was sequestered, a Latin square design was implemented, as shown in Table 5.1, and an ANOVA analysis was performed on the experimental design. The statistical analysis showed that only parameter that was significant on the mass of sulfate sequestered was the initial concentration of sulfate. The influence of the molar concentrations of Cl^- and SO_4^{2-} was not significant on the mass of chloride sequestered in the Ca-Al LDH samples. The influence of interactions between initial chloride concentration, initial sulfate concentration and the calcium to aluminum ratio on the mass of chloride and sulfate sequestered was also not significant. In addition, the p-value probability for $[\text{SO}_4^{2-}]$ is less than <0.05 , which reflects the evidence that the initial concentration of sulfate is predominant for the mass of sulfate that is sequestered in Ca-Al LDH during synthesis for Ca:Al ratios used in this study. Furthermore, the p-value probabilities for Ca:Al ratio and the interactions between initial chloride and sulfate concentration and calcium to aluminum ratio indicate that their influence on the sequestration of sulfate and chloride is not significant.

Based on the ANOVA statistics, it could be inferred that calcium to aluminum ratio does not influence the sequestration of sulfate and chloride in the Ca-Al LDH samples. However, as evidenced by the TGS-DSC curves (Figure 5.1 and Figure 5.2) and the XRD spectra (Figure 5.4), the samples synthesized at a calcium to aluminum of 4:1 did not yield a layered double hydroxide. Therefore, it could be concluded that the synthesis of Ca-Al LDH using a calcium to aluminum ratio of 2:1 or 3:1 will be optimal for effective removal of sulfate and chloride from the solution. A ratio of 2:1 was chosen over 3:1 to limit the incorporation of carbonate phase in the sample.

5.3.2. Stability and Solubility of Ca-Al LDH Samples

The synthesized Ca-Al LDH samples were dissolved in solutions at various pH conditions in order to investigate their stability. The samples were extracted post-dissolution and were re-characterized using TGA-DSC. Figure 5.5 report the TGA curves recorded for one Ca-Al LDH sample (KSCA21CL01SO75). Comparing the structures of the samples dissolved in ultrapure water or solution at pH 13 (Figure 5.5 (A)) to the initial (before dispersion) structure, no discernable alterations to the structures were observed. Therefore, it is important to note that dissolution in either pH 13 or in a solution at natural pH was essentially congruent, and in turn, post-dissolution analysis of the solids did not show any deterioration of the structure or the formation of any secondary phases. Similar to KSCA21CL01SO75, the structures of all the Ca-Al LDH samples (CA 21, 31 and CL 01, 02, 03) did not differ after dispersion in pH natural or pH 13 solutions. However, when the synthesized Ca-Al LDH samples were dispersed in pH 2 solutions, the dissolution rate of all the samples was high. The residues remaining post-dissolution were characterized using TGA-DSC and were determined to be hydrated calcium sulfate compounds.

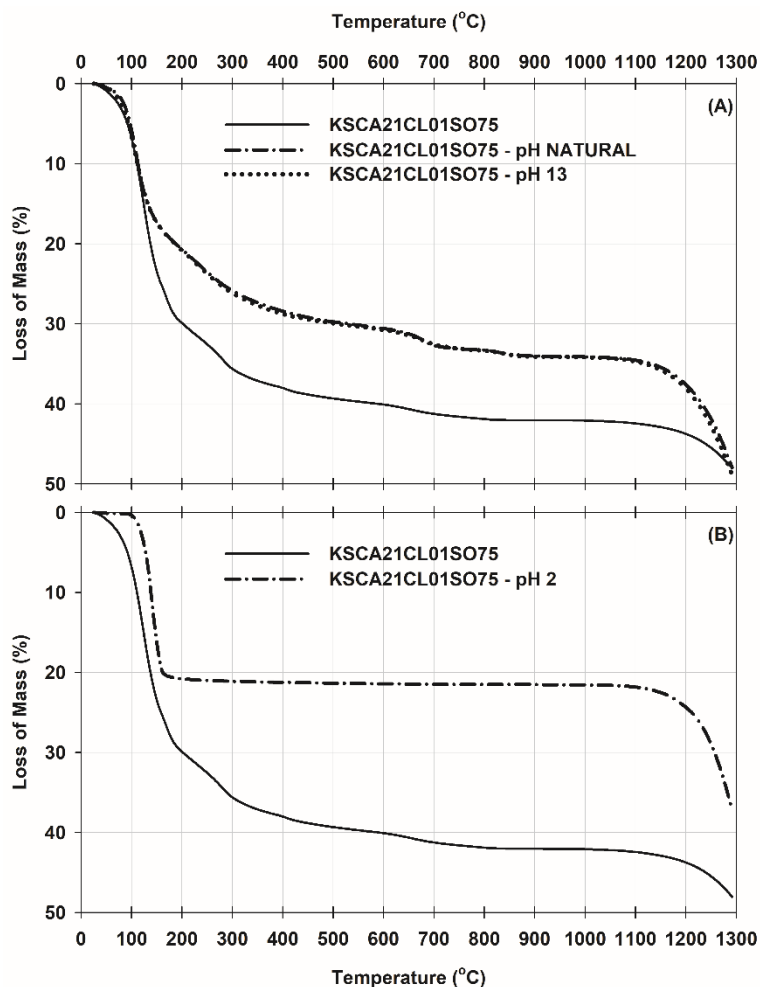


Figure 5.5. Comparison of TGA for KSCA21CL01SO75 samples dispersed in (A) pH natural and pH 13 (B) pH 2 compared to initial KSCA21CL01SO75 sample

The molar concentrations of calcium, aluminum, sulfate, and chloride, measured post-dissolution in solutions at various pH, were used to calculate the activities using PhreeqC, which were then used as inputs in Equation 5.1 and Equation 5.2 to calculate the solubility product ($\log K_{sp}$) values of the synthesized Ca-Al LDH samples. Balonis et al. (2010) measured the solubility product ($\log K_{sp}$) at 25 °C of KS to be in the range -28.25 to -28.53, while Glasser et al. (1999) estimated the solubility product of KS to be -28.54. Balonis et al. (2010) and Bothe and Brown (2004) measured the solubility product of FS

in water at 25 °C around -27.7, while Manikonda et al. (2020) reported that the log K_{sp} of FS was -28.9 at pH 13 and -12.6 at pH 2. Table 5.3 lists the log K_{sp} values of the synthesized Ca-Al LDH samples dissolved in solutions at natural pH, pH 2, and pH 13. The solubility of the Ca-Al LDH samples dispersed in ultrapure water is lower when compared with values reported in the literature, possibly due to the differences in the structures of the synthesized samples compared to a well-ordered FS sample. The log K_{sp} values of the samples in pH 2 is several orders of magnitude higher than the literature values and as reported previously, the dissolution of the sample was very high. However, when the samples were agitated in solution at pH 13, the log K_{sp} values and the solubility decreased compared to the log K_{sp} in ultrapure water, however, it still lower than the literature values. The variability in the structures of the synthesized Ca-Al LDH samples could be responsible for the variation in the solubility product constants.

Table 5.3. Solubility product constants of for Ca-Al LDH samples at various pH conditions

Sample	pH	Average log K_{sp}
KS (CA 21, 31) (CL 01, 02, 03) (SO 50, 75, 10)	Natural	-32.1
KS	pH 13	-29.7
KS	pH 2	-15.7

5.4. Conclusions

Hypersaline brines from processes like zero-liquid discharge concentrate from treatment of FGD wastewater often contain high concentrations of chloride and sulfate. Treatment of such brines using chemical precipitation by the formation of calcium-aluminum layered double hydroxides is a feasible approach for the removal of sulfate and

chloride because it is not energy-intensive like evaporation crystallization. In this study, the influence of initial concentrations of chloride and sulfate and their interactions with the Ca:Al molar ratio on sulfate and chloride removal performance was investigated.

Calcium-aluminum LDHs were synthesized using the optimum protocol selected by Manikonda et al. (2020) and the synthesized samples were characterized using TGA-DSC, Raman spectroscopy, and XRD. Based on the TGA-DSC and XRD analysis, and the calculated molecular formulas, it was determined that a calcium to aluminum ratio of 2:1 will be optimal for effective removal of sulfate and chloride from the solution and minimize carbonate formation, while a Ca:Al ratio of 4:1 did not yield a layered double hydroxide. The ANOVA analysis confirmed that the initial sulfate concentration highly influenced the mass of sulfate sequestered in the Ca-Al LDH samples compared to the other parameters like calcium to aluminum ratio and the initial chloride concentration. Similarly, it was observed that Ca-Al LDH samples undergo congruent dissolution when dissolved in ultrapure water or in a solution at pH 13. However, the dissolution rate at pH 2 was high and the dissolution was incongruent in nature, with the residues post-dissolution determined to be sulfate compounds. In conclusion, it could be established that the synthesis of Ca-Al LDHs using a calcium to aluminum ratio of 2:1 will be optimal for effective removal of sulfate and chloride from the solution. This optimized condition is recommended to remove sulfate and chloride from hypersaline brines to establish the realistic removal potential in field relevant scenarios.

References

- Almasri, D., Mahmoud, K. A., and Abdel-Wahab, A. (2015). "Two-stage sulfate removal from reject brine in inland desalination with zero-liquid discharge." *Desalination*, Elsevier, 362, 52–58.
- Balonis, M., Lothenbach, B., Le Saout, G., and Glasser, F. P. (2010). "Impact of chloride on the mineralogy of hydrated Portland cement systems." *Cement and Concrete Research*, Pergamon, 40(7), 1009–1022.
- Birnin-Yauri, U. ., and Glasser, F. . (1998). "Friedel's salt, $\text{Ca}_2\text{Al}(\text{OH})_6(\text{Cl},\text{OH})\cdot 2\text{H}_2\text{O}$: its solid solutions and their role in chloride binding." *Cement and Concrete Research*, 28(12), 1713–1723.
- Boelter, A. M., Lamming, F. N., Farag, A. M., and Bergman, H. L. (1992). "Environmental effects of saline oil-field discharges on surface waters." *Environmental Toxicology and Chemistry*, Wiley-Blackwell, 11(8), 1187–1195.
- Bothe, J. V., and Brown, P. W. (2004). "PhreeqC modeling of Friedel's salt equilibria at 23 ± 1 °C." *Cement and Concrete Research*, Pergamon, 34(6), 1057–1063.
- Brown, P., and Bothe, J. (2004). "The system $\text{CaO}-\text{Al}_2\text{O}_3-\text{CaCl}_2-\text{H}_2\text{O}$ at 23 ± 2 °C and the mechanisms of chloride binding in concrete." *Cement and Concrete Research*, Pergamon, 34(9), 1549–1553.
- Cravotta, C. A., and Brady, K. B. C. (2015). "Priority pollutants and associated constituents in untreated and treated discharges from coal mining or processing facilities in Pennsylvania, USA." *Applied Geochemistry*, Elsevier Ltd, 62, 108–130.
- Dou, W., Zhou, Z., Jiang, L. M., Jiang, A., Huang, R., Tian, X., Zhang, W., and Chen, D. (2017). "Sulfate removal from wastewater using ettringite precipitation: Magnesium ion inhibition and process optimization." *Journal of Environmental Management*, Academic Press, 196, 518–526.

Fang, P., Tang, Z., Chen, X., Huang, J., Tang, Z., and Cen, C. (2018a). "Chloride Ion Removal from the Wet Flue Gas Desulfurization and Denitrification Wastewater Using Friedel's Salt Precipitation Method." *Journal of Chemistry*, 2018, 1–9.

Fang, P., Tang, Z. J., Chen, X. B., Huang, J. H., Tang, Z. X., and Cen, C. P. (2018b). "Removal of High-Concentration Sulfate Ions from the Sodium Alkali FGD Wastewater Using Ettringite Precipitation Method: Factor Assessment, Feasibility, and Prospect." *Journal of Chemistry*, Hindawi Limited, 2018.

Gingerich, D. B., Grol, E., and Mauter, M. S. (2018). "Fundamental challenges and engineering opportunities in flue gas desulfurization wastewater treatment at coal fired power plants." *Environmental Science: Water Research and Technology*, Royal Society of Chemistry, 4(7), 909–925.

Glasser, F. P., Kindness, A., and Stronach, S. A. (1999). "Stability and solubility relationships in AFm phases. Part I. Chloride, sulfate and hydroxide." *Cement and Concrete Research*, Pergamon, 29(6), 861–866.

Goh, K.-H., Lim, T.-T., and Dong, Z. (2008). "Application of layered double hydroxides for removal of oxyanions: A review." *Water Research*, Pergamon, 42(6–7), 1343–1368.

Jin, Y., Lee, J., Gwak, G., Chung, C. M., Choi, J. W., Cho, K., and Hong, S. W. (2020). "Sequential combination of nanofiltration and ettringite precipitation for managing sulfate-rich brines." *Environmental Research*, Academic Press Inc., 187, 109693.

Landis, M. S., Kamal, A. S., Kovalcik, K. D., Croghan, C., Norris, G. A., and Bergdale, A. (2016). "The impact of commercially treated oil and gas produced water discharges on bromide concentrations and modeled brominated trihalomethane disinfection byproducts at two downstream municipal drinking water plants in the upper Allegheny River, Pennsylvania, ." *Science of the Total Environment*, Elsevier, 542, 505–520.

Ma, B., Fernandez-Martinez, A., Grangeon, S., Tournassat, C., Findling, N., Carrero, S., Tisserand, D., Bureau, S., Elkaïm, E., Marini, C., Aquilanti, G., Koishi, A., Marty, N. C. M., and Charlet, L. (2018). "Selenite Uptake by Ca-Al LDH: A Description of Intercalated

Anion Coordination Geometries.” *Environmental Science and Technology*, American Chemical Society, 52(3), 1624–1632.

Ma, J., Li, Z., Jiang, Y., and Yang, X. (2015). “Synthesis, characterization and formation mechanism of Friedel’s salt (FS: $3\text{CaO}\cdot\text{Al}_2\text{O}_3\cdot\text{CaCl}_2\cdot 10\text{H}_2\text{O}$) by the reaction of calcium chloride with sodium aluminate.” *Journal Wuhan University of Technology, Materials Science Edition*, 30(1), 76–83.

Manikonda, A., Bae, S., and Ogunro, V. O. (2020). Assessment of High Concentration Chloride Removal Performance by Precipitation of Friedel’s Salt. *Environmental Engineering Science*. Manuscript submitted for publication.

Manikonda, A., Ogunro, V. O., Ellison, K. M., and Moo-Young, K. (2019). “Synthesis of Friedel’s Salt for Application in Halide Sequestration Using Paste Encapsulation Technology.” *Geo-Congress 2019*, Proceedings, 167–176.

Maziarz, P., Matusik, J., and Leiviskä, T. (2019). “Mg/Al LDH Enhances Sulfate removal and Clarification of AMD Wastewater in Precipitation Processes.” *Materials*, MDPI AG, 12(14), 2334.

Mctigue, N. E., Cornwell, D. A., Graf, K., and Brown, R. (2014). “Occurrence and consequences of increased bromide in drinking water sources.” *Journal - American Water Works Association*, American Water Works Association, 106(11), E492–E508.

Mesbah, A., François, M., Cau-Dit-Coumes, C., Frizon, F., Filinchuk, Y., Leroux, F., Ravaux, J., and Renaudin, G. (2011). “Crystal structure of Kuzel’s salt $3\text{CaO}\cdot\text{Al}_2\text{O}_3\cdot\frac{1}{2}\text{CaSO}_4\cdot\frac{1}{2}\text{CaCl}_2\cdot 11\text{H}_2\text{O}$ determined by synchrotron powder diffraction.” *Cement and Concrete Research*, Pergamon, 41(5), 504–509.

Parkhurst, D. L., and Appelo, C. A. J. (2013). “PHREEQC (Version 3)-A Computer Program for Speciation, Batch-Reaction, One-Dimensional Transport, and Inverse Geochemical Calculations.” *Modeling Techniques*, book 6, 497.

Pramanik, B. K., Shu, L., and Jegatheesan, V. (2017). "A review of the management and treatment of brine solutions." *Environmental Science: Water Research and Technology*, Royal Society of Chemistry, 3(4), 625–658.

Schmida, T., and Dariz, P. (2014). "Shedding light onto the spectra of lime: Raman and luminescence bands of CaO, Ca(OH)₂ and CaCO₃." *Journal of Raman Spectroscopy*, John Wiley and Sons Ltd, 46(1), 141–146.

Tait, S., Clarke, W. P., Keller, J., and Batstone, D. J. (2009). "Removal of sulfate from high-strength wastewater by crystallisation." *Water Research*, Elsevier Ltd, 43(3), 762–772.

Tian, X., Zhou, Z., Wu, W., Xin, Y., Jiang, L. M., Zhao, X., An, Y., and Wang, Z. (2020). "Sulfate removal by Mg–Al layered double hydroxide precipitates: Mechanism, settleability, techno-economic analysis and recycling as demulsifier." *Journal of Cleaner Production*, Elsevier Ltd, 242, 118503.

Tong, T., and Elimelech, M. (2016). "The Global Rise of Zero Liquid Discharge for Wastewater Management: Drivers, Technologies, and Future Directions." *Environmental Science & Technology*, 50(13), 6846–6855.

Wang, L. P., Lee, W. H., Tseng, S. M., and Cheng, T. W. (2018). "Removal of chloride ions from an aqueous solution containing a high chloride concentration through the chemical precipitation of Friedel's salt." *Materials Transactions*, 59(2), 2–7.

Yang, L., Shahrivari, Z., Liu, P. K. T., Sahimi, M., and Tsotsis, T. T. (2005). "Removal of trace levels of arsenic and selenium from aqueous solutions by calcined and uncalcined layered double hydroxides (LDH)." *Industrial and Engineering Chemistry Research*, 44(17), 6804–6815.

Yue, Y., Wang, J. J., Basheer, P. A. M., and Bai, Y. (2018). "Raman spectroscopic investigation of Friedel's salt." *Cement and Concrete Composites*, Elsevier Ltd, 86, 306–314.

Zhang, D., Jia, Y., Ma, J., and Li, Z. (2011). “Removal of arsenic from water by Friedel’s salt (FS: $3\text{CaO}\cdot\text{Al}_2\text{O}_3\cdot\text{CaCl}_2\cdot 10\text{H}_2\text{O}$).” *Journal of Hazardous Materials*, 195, 398–404.

Zhang, L., Lv, P., He, Y., Li, S., Peng, J., Zhang, L., Chen, K., and Yin, S. (2021). “Ultrasound-assisted cleaning chloride from wastewater using Friedel’s salt precipitation.” *Journal of Hazardous Materials*, Elsevier B.V., 403, 123545.

Zhang, M., and Reardon, E. J. (2003). “Removal of B, Cr, Mo, and Se from wastewater by incorporation into hydrocalumite and ettringite.” *Environmental Science and Technology*, American Chemical Society , 37(13), 2947–2952.

CHAPTER 6: OVERALL CONCLUSIONS AND RESEARCH CONTRIBUTIONS

6.1. Overall Conclusions

Hypersaline brines from processes like zero-liquid discharge concentrate from treatment of FGDWW and concentrate from desalination often contain high concentrations of halides. Treatment of such brines using chemical precipitation by the formation of layered double hydroxides is a feasible approach for the removal of halides because it is not as energy-intensive like evaporation crystallization. This dissertation uses an integrated approach at understanding the various parameters that influence the formation of layered double hydroxides like Friedel's salt and Kuzel's salt to sequester halides from hypersaline brines. Chapters 2-5 explore the influence of parameters including reaction temperature, initial halide concentration, calcium to aluminum ratio, environmental conditions, stability and solubility in solutions at various pH, and initial sulfate concentration on the formation and stability of layered double hydroxides. Appendix A employs the optimal condition determined previously on simulated brines and examines the removal efficiency of halides and their sequestration into the interlayers of the layered double hydroxides.

In Chapter 2, the synthesis of Friedel's salt was investigated using three different protocols that were outlined in the literature and the synthesized samples were characterized using XRD and TGA-DSC. The synthesis was also performed at three different temperatures (25 °C, 50 °C, 75 °C) for all the three protocols. The influence of the reaction temperature was not significant for two synthesis protocols, but the third protocol at 25 °C had a different TGA-DSC profile compared to samples at 50 °C and 75 °C. The diffractograms recorded for the three reaction temperatures were similar. Therefore, it can

be concluded that the reaction temperature does not alter the structure of the final product. This is significant in field conditions since the synthesis would be carried out at ambient outdoor temperature.

In Chapter 3, an optimum protocol for the synthesis of Friedel's salt was determined in terms of mass of chloride sequestered and the relative propinquity of the structure of the synthesized sample compared to a well-ordered FS phase. Using the optimum protocol, the influence of initial chloride concentration and the Ca:Al molar ratio and their interactions on chloride removal performance was determined. The factorial analysis confirmed that the initial chloride concentration highly influenced the mass of chloride sequestered in the FS samples. Also, atmospheric conditions (ambient or CO₂ rich atmospheres) did not significantly modify the structure of the FS sample. In conclusion, it was established that the synthesis of FS using a calcium to aluminum ratio of 3:1 will be optimal for effective removal of chloride.

In Chapter 4, the influence of initial bromide concentration and its interactions with the Ca:Al molar ratio on bromide removal performance was investigated. It was established that a calcium to aluminum ratio of 2:1 will be optimal for effective removal of bromide from the solution. The ANOVA analysis and the regression analysis confirmed that the initial bromide concentration highly influenced the mass of bromide sequestered in the LDH samples compared to the calcium to aluminum ratio. It was observed that both FS and Br-LDH samples undergo congruent dissolution when dissolved in ultrapure water or in a solution at pH 13, while dissolution rate at pH 2 was high with little residues remaining.

In Chapter 5, the influence of initial concentrations of chloride and sulfate and their interactions with the Ca:Al molar ratio on sulfate and chloride removal was investigated. It was established that a calcium to aluminum ratio of 2:1 will be optimal for effective removal of sulfate and chloride from the solution, while a Ca:Al ratio of 4:1 did not yield a layered double hydroxide. The ANOVA analysis confirmed that the initial sulfate concentration highly influenced the mass of sulfate sequestered in the Ca-Al LDH samples compared to the other parameters like calcium to aluminum ratio and the initial chloride concentration. Similarly, it was observed that Ca-Al LDH samples undergo congruent dissolution when dissolved in ultrapure water or basic pH conditions. However, the dissolution rate at acidic conditions was high and the dissolution was incongruent in nature, with the residues post-dissolution determined to be sulfate compounds.

In Appendix A, the optimal condition of Ca:Al ratio of 3:1 was employed to remove halides from three different simulated FGD wastewater brines. X-ray diffraction and thermogravimetric analysis showed that the structure of the precipitate after treatment of the simulated brine is similar to a layered double hydroxide, especially Friedel's salt, with chloride ions mainly in the interlayers. The chloride removal efficiency was between 53-65% and the bromide removal efficiency was between 30-40%. However, the removal efficiency of halides decreased when sulfate is present in the solution, possibly indicating that sulfate inhibits the removal of halides. To minimize the inhibitory impact of sulfate on the removal efficiency of halides, a two-tier staged treatment of the brines was proposed, involving an initial treatment to mainly remove the sulfate ions from the brines prior to the second stage treatment to remove the halides.

6.2. Research Contributions

This dissertation research provides a laboratory based experimental approach to address the research questions and objectives on the formation layered double hydroxides to sequester halides from hypersaline brines. The relevant contributions of this dissertation research are discussed in the following paragraphs.

- This research demonstrated that the precipitation of layered double hydroxides is a highly effective technology to remove halides from high-salinity brines. The XRD and TGA analysis of the precipitate after the treatment of the simulated brines shows that precipitate is a layered double hydroxide of Friedel's salt. This method is inexpensive and has a high application value for the treatment of high concentration halide wastewater.
- The optimal conditions that were determined in this research will provide a framework to treat field samples like real FGD wastewater concentrates. These optimal conditions can also be employed to treat other sources of wastewater with high salinity and TDS, including RO reject water from desalination, produced water from oil and gas fracking, and rejects from industrial cooling towers.
- This research also demonstrated the stability of layered double hydroxides at various pH conditions. The layered double hydroxides undergo congruent dissolution at neutral and basic pH and do not form any secondary phases post-dissolution. However, these layered double hydroxides have a high dissolution rate in acidic conditions and little residues remain after dispersion in a solution at acidic pH.

- It was exhibited that the temperature during the formation of the layered double hydroxide does not influence the structure of the final product and the removal efficiency of the halides. This is significant in field conditions since the formation of LDHs would be carried out at ambient outdoor temperature. Similarly, it was also shown that atmospheric conditions (ambient or CO₂ rich atmospheres) did not significantly modify the structure of the LDH sample, and this is particularly important in areas closer to power plants where there would likely be a higher concentration of carbon dioxide in the air.
- In order to further improve the removal efficiency, a two-stage treatment of the wastewater should be employed to remove the halides. The two-tiered treatment would be especially beneficial in the case of sulfate containing brines. The first stage will mainly remove the sulfate ions from the brines which will lower the inhibitory effect of the sulfate ions. The second stage could then remove the halides at a higher efficiency.
- This research will lead to a better understanding of the formation of LDHs in cementitious systems while contributing to the evaluation of variables that influence the long-term sequestration of halides in the cementitious systems. This research demonstrates that variables like Ca/Al ratio, and molar concentrations can be optimized to allow for realistic formation potential when materials such as fly ash, wastewater brine, and chemical binders are used in field relevant conditions. Thus, improving the paste mix design providing for long term sequestration of halides in the paste cementitious systems. In summary, the research findings will lead to potential design considerations that could contribute to meeting both the

USEPA Coal Combustion Residuals Rule and the Effluent Limitation Guidelines which includes responsible management and disposal of CCRs and FGD wastewater and for the protection of surface water and groundwater resources.

APPENDIX A: PRACTICAL APPLICATION OF LAYERED DOUBLE HYDROXIDES PRECIPITATION METHOD FOR REMOVAL OF HIGH CONCENTRATION HALIDES FROM SIMULATED BRINE

A.1. Introduction

The results from the previous chapters indicate that using layered double hydroxides precipitation is an effective method to remove halides like chloride and bromide from hypersaline brines. The removal of halides primarily depends on the initial halide concentration. However, the formation of a well-ordered layered double hydroxide is dependent on the calcium to aluminum ratio. Figure A.1 summarizes the optimal Ca:Al ratios that were determined while the removal of individual halides was investigated. In the case of chloride, it was observed that samples synthesized at a optimal Ca:Al ratio of 2:1 did not yield a well-ordered structure of layered double hydroxides. Therefore, it was established that the synthesis of LDHs using a calcium to aluminum ratio of 3-4:1 would be more effective for the removal of chloride. The Ca:Al ratio for the range used in this study (2-4:1) did not impact the structure of the LDHs in the case of bromide ion and yielded a well-ordered structure of layered double hydroxides. However, when the formation of LDHs for the removal of sulfate and chloride was investigated, it was observed that, unlike Ca:Al ratios of 2:1 and 3:1, a Ca:Al ratio of 4:1 did not yield a LDH phase. Therefore, based on the outcomes discussed above, it can be established that a calcium to aluminum ratio of 3:1 would be effective for the formation of layered double hydroxides to sequesters anions like halides and sulfate from hypersaline brines. This optimal calcium to aluminum ratio of 3:1 was applied to three different types of simulated

brines containing halides and sulfate, in order to understand the effectiveness of the removal of the anions through precipitation of layered double hydroxides.

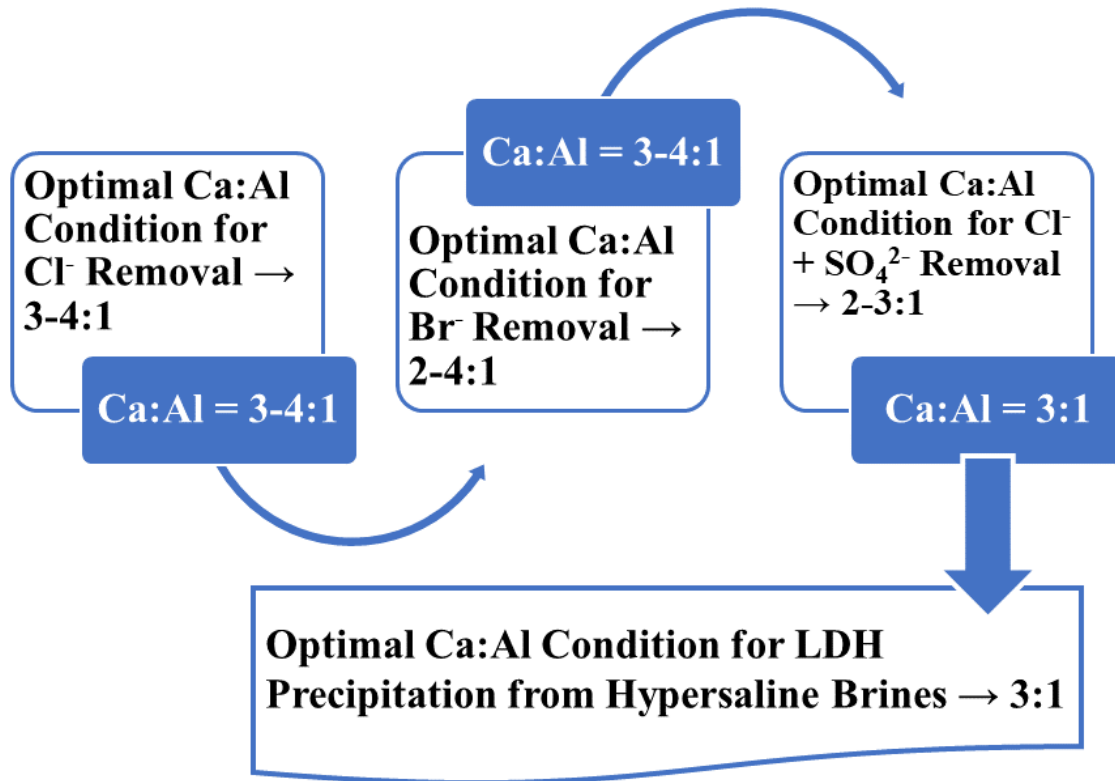


Figure A.1. Summary of the Optimal Conditions for LDH Precipitation

A.2. Experimental Setup

In order to investigate the effectiveness of the optimal removal condition, three simulated brines containing different concentrations of chloride, bromide, and sulfate were prepared and treated at a calcium to aluminum ratio of 3:1. The simulated concentrated FGD brines were formulated based on compositions from a coal-fired power plant in the southeastern United States and also based on the compositions used by Renew et al. (2016).

The concentrations of Cl^- , Br^- , and SO_4^{2-} utilized in the experiments are shown in Table A.1. The simulated brines were prepared by mixing reagent grade CaCl_2 , CaBr_2 , and Na_2SO_4 in ultrapure water. The reagents were allowed to dissolve completely under continuous stirring before the experiments to make sure that no solids were visible in the brines.

Table A.1. Composition of Simulated FGD Brines

Composition	Level 1 (SBL 1) (mg/L)	Level 2 (SBL 2) (mg/L)	Level 3 (SBL 3) (mg/L)
Cl^-	100000	50000	25000
Br^-	10000	5000	2500
SO_4^{2-}	0	0	10000

The simulated brine solution was heated to 25 °C, and a solution of NaAlO_2 was then added dropwise at a rate of 5 mL/min under continuous stirring. The concentration of NaAlO_2 was calculated based on the total Ca^{+2} concentration in the simulated brine. An example of the experimental test setup is shown in Figure A.2. Stirring was continued for an additional one hour after the completion of the addition of the reagents. The precipitate was collected at the end of the stirring period by vacuum filtration using 0.45 μm PTFE filters, washed with ultrapure water, and finally dried in an oven at 60 °C for 24 hours. All the experiments were performed in the laboratory at ambient atmospheric conditions. The microstructure of the synthesized samples was characterized using thermogravimetric analysis and differential scanning calorimetry (TGA-DSC) and X-ray powder diffraction (XRD). The TGA-DSC analysis was performed using a SDT Q600 (TA Instruments, Delaware) by heating the specimen from 25 °C to 1300 °C in a nitrogen atmosphere at a rate of 20 °C/min. X-ray powder diffraction patterns were recorded using a PANalytical

(Netherlands) X'Pert PRO diffractometer ($2\theta = 5-50^\circ$, stepsize 0.02° with 0.5 s/step). The supernatant obtained from the filtration of the precipitate was analyzed for concentrations of Cl^- , Br^- , and SO_4^{2-} , using an ICS-3000 ion chromatography system (Dionex, California), and for Al^{+3} and Ca^{+2} , using a 5100 ICP-OES instrument (Agilent, California). The pH and conductivity of the supernatant was measured with a SevenExcellence S470-Kit pH/conductivity meter (Mettler Toledo, Ohio).

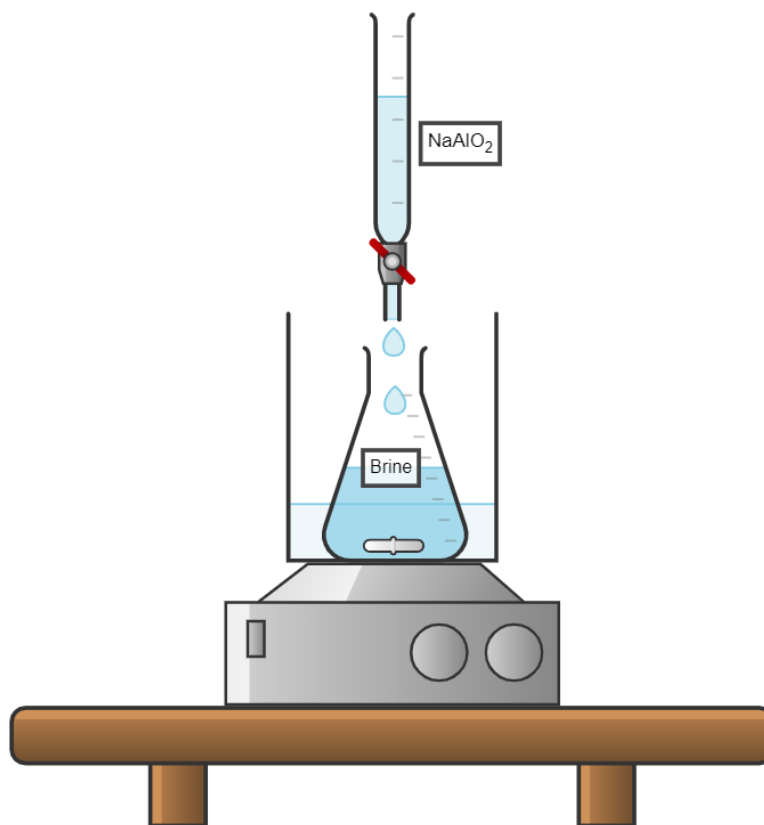


Figure A.2. Illustration of experimental set-up for treatment of simulated brine

A.3. Results and Discussion

Figure A.3 reports the TGA and DSC curves of the LDH samples synthesis using the simulated brines as the starting material. Comparing the DSC curves, it is observed that

SBL 1 and SBL 2 samples do not exhibit a double endotherm centered around 170 °C and 320 °C, as expected in a well-ordered FS sample. However, a double endotherm is visible in the DSC analysis of SBL 3 and it matches well with the two well-resolved mass loss steps. The total mass (Table A.2) for all the samples is also lower than the theoretical mass loss of an idealized FS structure (32.9%) (Vieille et al. 2003) and an idealized Br-LDH structure (27.7%). The mass loss between 100 – 250 °C, corresponding to the removal of the interlayer water, is comparable with the well-ordered FS sample for the three samples. Comparing the TGA and DSC curves (Figure A.3) and the values in Table A.2, it is observed that there is a higher percentage of mass loss at the 100 – 250 °C step for all the three protocols compared to the 250 – 400 °C, contrary to the theoretical mass loss. This suggests that a higher percentage of water molecules are present in the interlayer space instead of the main Ca-Al sheets.

Table A.2. Comparison of % mass lost recorded using TGA for LDH samples synthesized using simulated brine

Protocol	Loss of Sample Mass (%)			Total Mass Loss (%)
	100 °C < T < 250 °C	250 °C < T < 400 °C	T > 400 °C	
Well-ordered FS	12.8	19.2	0.9	32.9
Well-ordered Br-LDH	11.1	16.6	< 1%	27.7
SBL 1	11.7	7.6	4.4	24.3
SBL 2	9.9	10.4	4.8	25.4
SBL 3	10.6	6.5	3.6	21.5

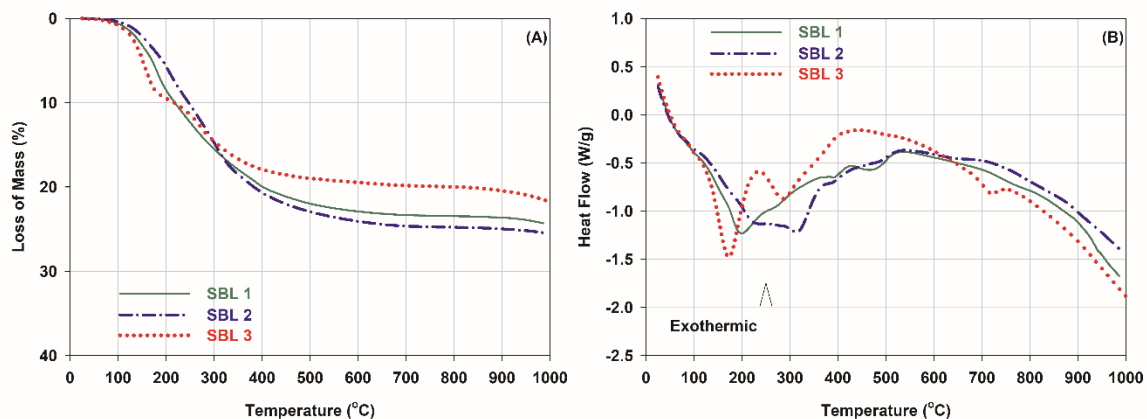


Figure A.3. Comparison of (A) TGA and (B) DSC analysis for LDH samples synthesized using simulated brine

The XRD patterns of the LDH samples (Figure A.4) show sharp and symmetric peaks characteristic of layered double hydroxide compounds. The reflections at 2θ around 11.15° and 22.57° corresponding to (002) and (004) planes, respectively, are typical Miller-Bravais indices of Friedel's salt. The basal spacing of the (002) reflection ($2\theta = 11.15^\circ$) is 0.791 nm is in agreement with the d-spacing reported for a FS with chloride ions in the interlayer (Grishchenko et al. 2013). No peaks were observed at $2\theta = 10.80^\circ$ (Rapin et al. 1999) which corresponds to a layered double hydroxide with bromide ions in the interlayer. In the case of SBL 3, no peaks were recorded at $2\theta = 9.01^\circ$ (Myneni et al. 1998) which ruled out the formation of ettringite to sequester sulfate ions. Several secondary phases were also identified in the XRD patterns of the synthesized samples.

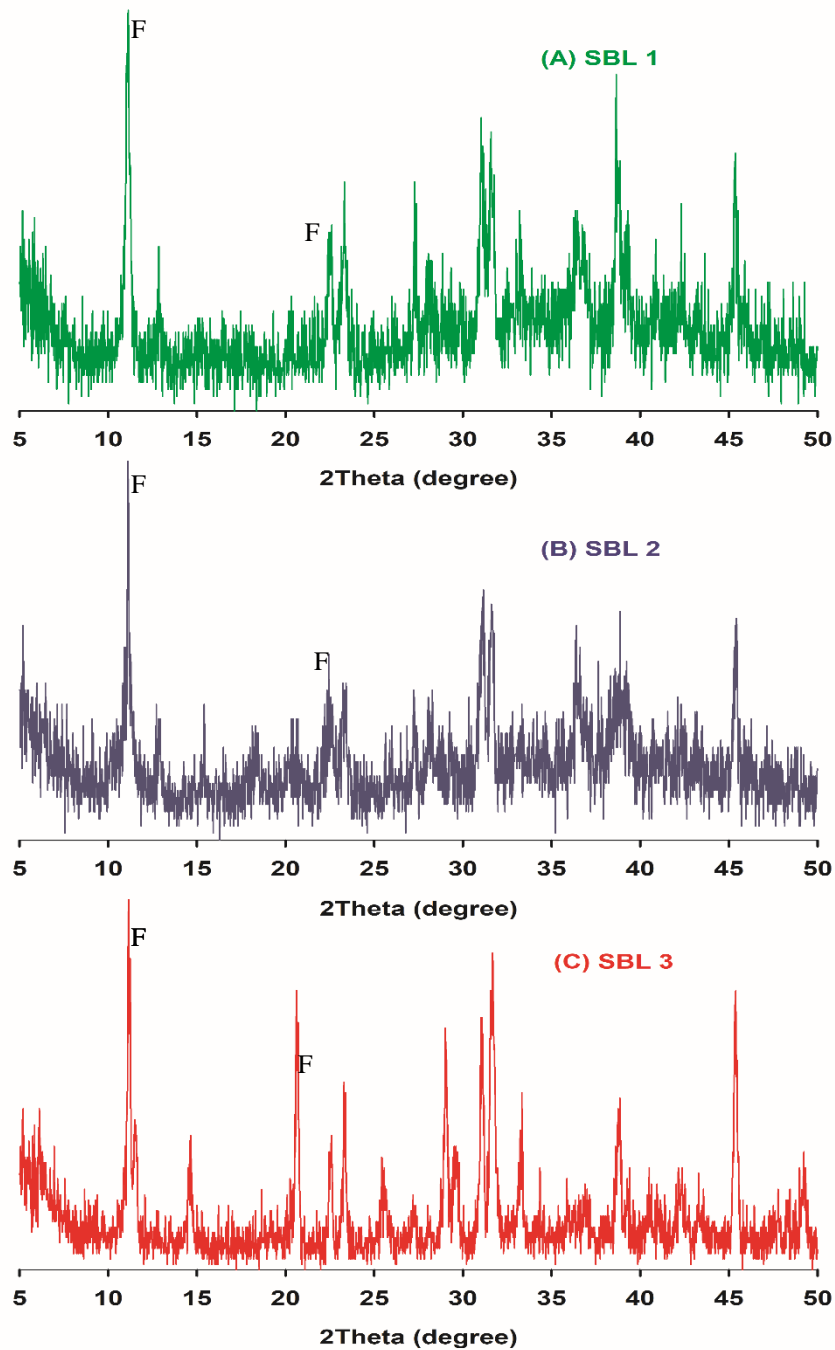


Figure A.4. Powder XRD patterns for LDH samples synthesized using simulated brine, where F denotes Friedel's salt

Figure A.5 summarizes the removal efficiency of the halides and sulfate ions from the three simulated brines through precipitation of layered double hydroxides. As discussed

in the previous chapters, the sequestration of the halides in the LDHs depends on the initial concentration of the halides, which can be observed in the removal efficiency. The removal efficiency increased from 53.7% in SBL 1 to 65.4% in SBL 2 as the initial concentration of chloride decreased from SBL 1 to SBL 2. Similarly, the removal efficiency of bromide increased from 30.9% to 39.8% as the initial concentration decreased SBL 1 to SBL 2. In the case of SBL 3, when sulfate was present in the solution, the removal efficiency of chloride and bromide decreased to 37.6% and 28.1%, respectively. Therefore, it could be assumed that the presence of sulfate inhibits the removal of the halides from the solution, similar to observations made by Fang et al. (2018). However, based on the results shown in Figure A.5, it can be concluded that precipitation of layered double hydroxides is a highly effective halides removal technology.

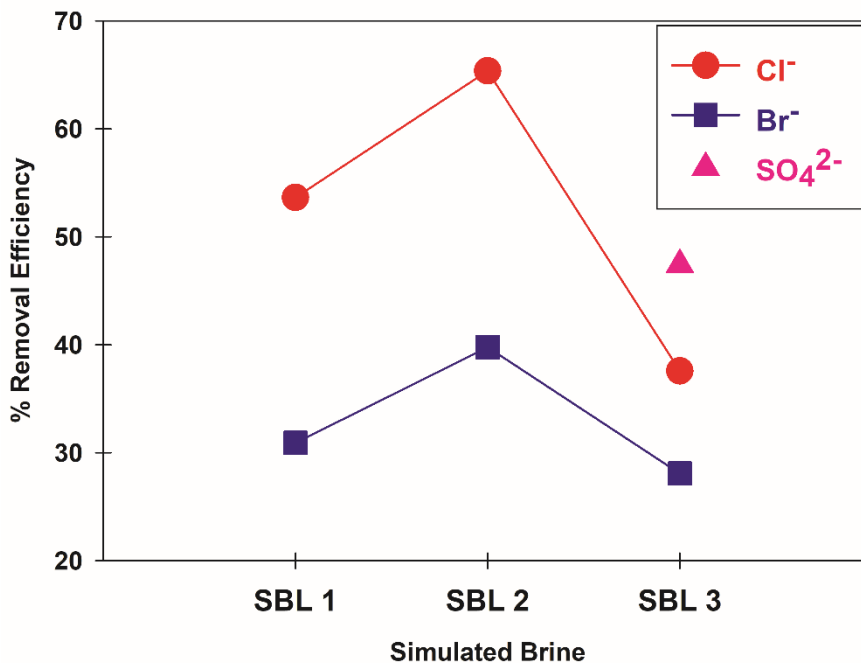


Figure A.5. Percentage removal efficiency of Cl⁻, Br⁻, and SO₄²⁻ ions from simulated brines

A.4. Conclusions

In this study, layered double hydroxide precipitation method was employed for the removal of halides from hypersaline solutions. Based on the results from previous experiments, it was established that a calcium to aluminum ratio of 3:1 would be an optimal condition for the formation of a well-ordered layered double hydroxide. Therefore, the Ca:Al ratio of 3:1 was employed to remove halides like chloride and bromide from three different simulated FGD wastewater brines. X-ray diffraction and thermogravimetric analysis showed that the structure of the precipitate after treatment of the simulated brine is similar to a layered double hydroxide, especially Friedel's salt, with chloride ions mainly in the interlayers. The chloride removal efficiency was between 53-65% and the bromide removal efficiency was between 30-40%. However, the removal efficiency decreased when sulfate is present in the solution, possibly indicating that sulfate inhibits the halide removal. In conclusion, the precipitation of layered double hydroxides is a highly effective halides removal technology.

The halide removal efficiency could be further improved by performing a second-stage treatment on the residual solution. The second stage treatment would be especially beneficial in the case of sulfate containing brines. The first stage will mainly remove the sulfate ions from the brines which will lower the inhibitory effect of the sulfate ions. The second stage could then remove the halides at a higher efficiency.

References

- Fang, P., Tang, Z., Chen, X., Huang, J., Tang, Z., and Cen, C. (2018). “Chloride Ion Removal from the Wet Flue Gas Desulfurization and Denitrification Wastewater Using Friedel’s Salt Precipitation Method.” *Journal of Chemistry*, 2018, 1–9.
- Grishchenko, R. O., Emelina, A. L., and Makarov, P. Y. (2013). “Thermodynamic properties and thermal behavior of Friedel’s salt.” *Thermochimica Acta*, 570, 74–79.
- Myneni, S. C. B., Traina, S. J., and Logan, T. J. (1998). “Ettringite solubility and geochemistry of the Ca(OH)₂-Al₂(SO₄)₃-H₂O system at 1 atm pressure and 298 K.” *Chemical Geology*, Elsevier, 148(1–2), 1–19.
- Rapin, J.-P., Noor, N. M., and François, M. (1999). “The double layered hydroxide 3CaO · Al₂O₃ · CaBr₂ · 10H₂O.” *Acta Crystallographica Section C Crystal Structure Communications*, International Union of Crystallography (IUCr), 55(8), IUC9900092.
- Renew, J. E., Huang, C.-H., Burns, S. E., Carrasquillo, M., Sun, W., and Ellison, K. M. (2016). “Immobilization of Heavy Metals by Solidification/Stabilization of Co-Disposed Flue Gas Desulfurization Brine and Coal Fly Ash.” *Energy & Fuels*, American Chemical Society, 30(6), 5042–5051.
- Vieille, L., Rousselot, I., Leroux, F., Besse, J. P., and Taviot-Guého, C. (2003). “Hydrocalumite and Its Polymer Derivatives. 1. Reversible Thermal Behavior of Friedel’s Salt: A Direct Observation by Means of High-Temperature in Situ Powder X-ray Diffraction.” *Chemistry of Materials*, American Chemical Society, 15(23), 4361–4368.